let. - vol. 48 (2002) št. - no. 12

STROJNIŠKI VESTNIK 12

JOURNAL OF MECHANICAL ENGINEERING

strani - pages 643 - 726

ISSN 0039-2480 . Stroj V . STJVAX

cena 800 SIT

9 770039 248001

© Strojniški vestnik 48(2002)12,643
Mesečnik
ISSN 0039-2480

© Journal of Mechanical Engineering 48(2002)12,643
Published monthly
ISSN 0039-2480

Vsebina
Contents

Strojniški vestnik - Journal of Mechanical Engineering
letnik - volume 48, (2002), številka - number 12

Uvodnik
Editorial

Josef Ressel - 175 let patenta ladijskega vijaka

Med najpomembnejše izume, ki so nastali na slovenskih tleh, štejemo ladijski vijak, ki ga je med službo v Pleterjah in Trstu preskusil in patentiral (dobil privilegij) leta 1827 češki gozdarski strokovnjak Josef Ressel. Razvoj zamisli za tako napravo sicer seže k Arhimedu in Leonardu da Vinci-ju, prvenstvo praktične uporabe in preskusov na Krki, Ljubljanici in Mirni pa pripada J.Resslu. Javno je vijačni pogon prikazal 1829 v Parizu (še na ročni pogon) in Trstu istega leta (že na parni pogon). Ladja Civetta je preplula pol morske milje, ko je po 5 minutah odpovedal parni batni stroj. Načrtovana ustanovitev delniške družbe za gradnjo ladij z vijačnim pogonom je propadla. Angleškemu izumitelju Smithu je to uspelo šele deset let pozneje, prva ladja z vijačnim pogonom pa je preplula Atlantik 1845. Resslovo zamisel vijačnega pogona zračnih balonov je do patentov razvil njegov sin Heinrich Ressel leta 1871.

Josef Ressel, rojen 1793 na Češkem, je bil šolan topničar (tako kakor naš Jurij Vega 1754-1802), nato pa je na dunajski univerzi študiral knjigovodstvo, kmetijstvo in farmacijo, mehaniko, hidravliko in gradbeno (civilno) arhitekturo ter končal dveletno gozdarsko akademijo. Kot gozdar je začel delati v Kostanjevici na Krki. Nato je bil gozdarski podmojster pri upravi državnih posestev v Ljubljani in kasneje primorski gozdarski mojster v Trstu. Delal je tudi v Istri, Dalmaciji, Benetkah in spet v Trstu. Pomembno delo je opravil tudi na Goriškem, saj je prvi izmeril in kartografiral Trnovski gozd. Čeprav uradno gozdarski tehnik, ki je uvajal napredno gozdarjenje, izsuševanje močvirij ter pogozditev Krasa, je izumil in patentiral tudi krogličnе in valjčne ležaje, kasneje pa še pnevmatsko pošto. Skušal je tudi izboljšati parni batni stroj in ga usposobiti za vodni promet. Iznajditeljsko je posegel skoraj v vsa področja tedanje tehnike, od rudarstva in metalurgije do kemije, gradbeništva, agroživilstva in vojne tehnike.Umrl je 1857 za tifusom v Ljubljani.

V spomin na Josefa Ressla imamo v Ljubljani pred Staro tehniko njegov spomenik, kakor tudi njegovo cesto med kolodvorom in zmajskim mostom. Pošta Slovenije je 15.novembra izdala spominsko znamko okrogle oblike, ki pa ima žal narobe obrnjeno sliko, bolj podobno sodobnim mešalom kot pa pravemu Resslovemu vijaku. Ker je voda zgoraj in trebuh ladje spodaj, so nekateri to poštno znamko že poimenovali "Titanic", ki leži potopljen na dnu morja s kobilico, vijakom in krmilom nad trupom. Sliko si lahko ogledate na naslovnici, model pravega Resslovega vijaka pa v domači literaturi (Sandi Sitar: Sto slovenskih znanstvenikov, Prešernova družba v Ljubljani 1987).

Prof.dr. Andro Alujevič
Odgovorni urednik SV

© Strojniški vestnik 48(2002)12,645-662
ISSN 0039-2480
UDK 519.61/.64:532.5
Izvirni znanstveni članek (1.01)

© Journal of Mechanical Engineering 48(2002)12,645-662
ISSN 0039-2480
UDC 519.61/.64:532.5
Original scientific paper (1.01)

Metoda robnih elementov za dinamiko viskoelastične Maxwellove tekočine

The Boundary-Element Method for the Dynamics of a Viscoelastic Maxwell Fluid

Leopold Škerget - Matej Požarnik

V prispevku je prikazan razvoj numerične sheme na osnovi metode robnih elementov (MRE) za modeliranje ravninskih tokov viskoelastične tekočine. Kot podlaga za razvoj je namenjena shema za modeliranje nestisljivih viskoznih tokov, ki smo jo razširili in ji dodali potrebne člene za zajemanje viskoelastičnosti nenewtonskih tekočin. Posebno pozornost smo namenili integraciji ohranitvenih zakonov in reoloških modelov. Shema je zapisana za hitrostno-vrtinčno formulacijo vodilnih enačb. Kot testni primeri so predstavljeni tokovi nenewtonske Maxwellove tekočine v kanalih različnih geometrijskih oblik.

(Ključne besede: modeli robnih elementov, dinamika tekočin, tekočine viskoelastične, modeli Maxwellovi)

In this paper we show a numerical scheme based on the boundary-element method (BEM) for the numerical modeling of planar, viscoelastic fluid flows. In particular, the singular-boundary-integral approach, which has been established for the viscous, incompressible flow problem, is modified and extended to include the viscoelastic fluid state. Special attention is given to a proper integration of the conservation and constitutive equations. A velocity-vorticity formulation of the governing equations is adopted. As test cases, non-Newtonian–Maxwell fluid flows in the channels of various geometries are studied.

(Keywords: boundary element methods, fluid dynamics, viscoelastic fluids, Maxwell models)

0 UVOD

V prispevku predstavljamo numerični model robnih elementov (MRE) za reševanje dinamike viskoelastične nestisljive tekočine. Sistem Navier-Stokesovih enačb ob upoštevanju Maxwellovih modelov tečenja viskoelastične tekočine smo zapisali za hitrostno-vrtinčno formulacijo. Ta ima v primeru robnoobmočne integralske predstavitve vodilnih enačb določene prednosti, saj smo iz računske sheme izločili tlak, kar pomeni, da se izognemo težavam pri predpisovanju robnih vrednosti tlaka. Posebna pozornost je posvečena spremembi diferencialnih vodilnih enačb v pripadajoče robnoobmočne integralske predstavitve, ki zadoščajo omejitvenemu kriteriju ohranitve mase oziroma pogoju solenoidnosti tokovnega polja.

Stabilnost in natančnost numeričnega algoritma dosežemo brez dodatnih stabilizacijskih tehnik z uporabo parabolične difuzijske osnovne rešitve, ki opisuje linearni del prenosnega pojava. Numerični model, predstavljen v prispevku, je mogoče nadgraditi

0 INTRODUCTION

This paper deals with a numerical scheme based on the boundary-element method (BEM) developed to numerically simulate viscoelastic, incompressible fluid flows. The method is based on a solution of the Navier–Stokes equations set in the velocity-vorticity formulation for different viscoelastic Maxwell fluids. This formulation has some advantages in the case of a boundary-domain integral representation of governing equations. It is simpler than a primitive variable formulation since the pressure does not appear explicitly in the field-function equations and thus the well-known difficulty connected with the computation of the pressure boundary values in incompressible flows is avoided. Particular attention is given to a proper transformation of the differential governing equations to the corresponding boundary-domain integral representations that satisfy the continuity equation or the solenoidality of the velocity field exactly.

The stability and the accuracy of the developed numerical scheme is achieved by employing the parabolic diffusion fundamental solution describing the linear part of transport phenomena without any additional stabilization techniques. The numerical model presented here is easy to upgrade in the sense of effectiveness,

v smislu učinkovitosti, stabilnosti in natančnosti z uporabo difuzivno-konvektivne osnovne rešitve, ki zajema večji del prenosnega pojava, in modela podobmočij [5].

1 VODILNE ENAČBE

1.1 Ohranitveni zakoni

Analitični opis gibanja zvezne snovi temelji na osnovnih ohranitvenih zakonih mase, gibalne količine, energije in kemijskih sestavin, pripadajočih reoloških modelih in enačbah stanja. V obravnavi se bomo omejili na laminarni tok nestisljive viskoelastične izotropne tekočine v območju rešitve Ω, ograjenim z ograjo Γ.

Opazovane funkcije polja so vektor hitrosti $v_i(r_j,t)$, tlak $p(r_j,t)$ in temperaturno polje $T(r_j,t)$, ki zadoščajo kontinuitetni, gibalni in energijski enačbi:

$$\frac{\partial v_j}{\partial x_j} = 0 \tag{1}$$

$$\rho_0 \frac{Dv_i}{Dt} = \frac{\partial \sigma_{ij}}{\partial x_j} + \rho g_i \tag{2}$$

$$c_{p0}\rho_0 \frac{DT}{Dt} = -\frac{\partial q_j}{\partial x_j} + I \tag{3}$$

ki so zapisane v obliki kartezičnega tenzorskega zapisa x_i in kjer so ρ_0 in c_{p0} nespremenljiva masna gostota oziroma izobarna specifična toplota, t čas, g_i težnostni pospešek, σ_{ij} napetostni tenzor, q_i gostota difuzijskega toplotnega toka in $D(.)/Dt = \partial(.)/\partial t + v_k\,\partial(.)/\partial x_k$ Stokesov oziroma snovski odvod spremenljivke (.). V gibalni enačbi (2) smo upoštevali nestisljivost tekočine v smislu Boussinesqove poenostavitve, pri kateri je vpliv spremenljive masne gostote zajet le v prostorninski sili ρg_i.

Zapisani sistem ohranitvenih enačb pomeni nedokončan sistem parcialnih diferencialnih enačb, ki ga moramo dopolniti z ustreznimi reološkimi modeli oziroma modeli tečenja za posamezno tekočino in znanimi robnimi ter začetnimi pogoji. Ti so v splošnem odvisni od zapisanega sistema enačb in so lahko podani za osnovne fizikalne ali izpeljane funkcije polja.

1.2 Reološki modeli

Cauchyjev napetostni tenzor σ_{ij} lahko v primeru toka nestisljive tekočine ločimo na prispevek tlaka in dodatnega deviatoričnega napetostnega tenzorja τ_{ij}:

$$\sigma_{ij} = -p\delta_{ij} + \tau_{ij} \tag{4}$$

kjer je δ_{ij} Kroneckerjeva funkcija delta. Bistveni del dinamike viskoelastičnih tekočin je izbira primernega reološkega modela, ki podaja soodvisnost dodatnih

stability and accuracy using a diffusion-convective fundamental solution where a larger part of the transport phenomena is taken into account. The subdomain technique can also be implemented [5].

1 GOVERNING EQUATIONS

1.1 Conservation laws

The analytical description of the motion of a continuous medium is based on the conservation of mass, momentum, energy and species concentration, with associated rheological models and equations of state. The present development will be focused on the laminar flow of an incompressible, viscoelastic, isotropic fluid in a solution domain Ω bounded by a boundary Γ.

The field functions of interest are the velocity vector field $v_i(r_j,t)$, the pressure field $p(r_j,t)$, and the temperature field $T(r_j,t)$, such that the mass, momentum, and energy equations:

written in the Cartesian frame x_i are satisfied, where ρ_0 and c_{p0} are the constant fluid mass density and the isobaric specific heat capacity, t is the time, g_i is the gravitational acceleration vector, σ_{ij} denotes the components of the total stress tensor, q_i stands for the specific heat flux, and $D(.)/Dt = \partial(.)/\partial t + v_k\,\partial(.)/\partial x_k$ represents the Stokes material derivative of the variable (.). The natural convection effect is considered in the momentum, Eq. (2), by using the Boussinesq approximation, where the temperature's influence on mass density is considered only with the body force ρg_i.

The set of field equations needs to be closed and solved in conjunction with the appropriate rheological equations of the fluid and the boundary, and the initial conditions of the flow problem. The boundary conditions in general depend on the dependent variables applied, i.e. the primitive or velocity-vorticity variables formulation.

1.2 Rheological models

For an incompressible fluid the Cauchy total stress σ_{ij} can be decomposed into a pressure contribution plus an extra deviatoric stress-tensor field function τ_{ij}:

where δ_{ij} is the Kronecker delta. The central problem in visco-elastic fluid dynamics is the selection of an appropriate rheological model that relates the extra

napetosti v en. (4) in kinematike toka. Obravnavo bomo omejili na razmeroma preproste diferencialne konstitutivne enačbe, znane kot implicitni Maxwellovi reološki modeli. Za širok spekter snovi, kakor so na primer tekočine s pojemajočim spominom, lahko konstitutivne enačbe zapišemo v obliki odvisnosti med napetostnim in deformacijskim tenzorjem ter njunimi odvodi po času.

Za Eulerjev postopek velja, da lahko snovske časovne odvode poljubnega simetričnega tenzorja drugega reda u_{ij}, ki ga lahko enačimo z dodatnim napetostnim tenzorjem τ_{ij} ali deformacijskim tenzorjem $\dot{\varepsilon}_{ij}$, podamo na različne načine. Z naslednjim izrazom definiramo Stokesov časovni snovski odvod tenzorja:

stress in Eq. (4) to the flow kinematics. The differential constitutive equations to be considered here are implicit, rate-type rheological models, generally associated with the name of Maxwell. For the broad class of materials, such as simple fluids with fading memory, the constitutive equation can be expressed using a relation between stress and the strain-rate tensor and their time derivatives.

For an Eulerian reference frame the material time derivative or convected derivative of an arbitrary symmetric, second-order tensor u_{ij}, which can be equated to the extra-stress tensor τ_{ij} or the strain-rate tensor $\dot{\varepsilon}_{ij}$, can be formulated in several ways. Let us first define the Stokes material time derivative with the expression:

$$\frac{Du_{ij}}{Dt} = \frac{\partial u_{ij}}{\partial t} + v_k \frac{\partial u_{ij}}{\partial x_k} \tag{5}$$

nato zgornje konvektivni oziroma sodeformabilni:

then the upper-convected or codeformation:

$$\overset{\nabla}{u}_{ij} = \frac{Du_{ij}}{Dt} - u_{ik}L_{jk} - u_{jk}L_{ik} \tag{6}$$

medtem ko je spodnje konvektivni odvod podan z izrazom:

while the lower-convected derivative is defined as:

$$\overset{\Delta}{u}_{ij} = \frac{Du_{ij}}{Dt} + u_{ik}L_{kj} + u_{jk}L_{ki} \tag{7}$$

kjer nadpisa ∇ in Δ označujeta zgornje oziroma spodnje konvektivni odvod. Hitrostni gradient L_{ij} je definiran kot:

where the superscripts ∇ and Δ stand for the upper- or lower-convected derivatives, respectively, and the velocity-gradient tensor L_{ij} is defined as:

$$L_{ij} = \frac{\partial v_i}{\partial x_j} = \dot{\varepsilon}_{ij} + \dot{\Omega}_{ij} \tag{8}$$

kjer je $\dot{\Omega}_{ij}$ tenzor vrtilnih hitrosti.

where $\dot{\Omega}_{ij}$ denotes the rotational velocity tensor.

Pri implicitnih Maxwellovih reoloških modelih podamo dodatni napetostni tenzor z vsoto viskoznih in elastičnih učinkov:

Using implicit Maxwell rheological models the extra-stress tensor is given as a sum of the viscosity and elasticity effects:

$$\tau_{ij} = \tau_{ij}^{v} + \tau_{ij}^{e} \tag{9}$$

Linearni Maxwellov konstitutivni model podamo z odvisnostjo:

The linear Maxwell constitutive model is given as follows:

$$\tau_{ij} = 2\eta_0 \dot{\varepsilon}_{ij} - \lambda_1 \frac{\partial \tau_{ij}}{\partial t} \tag{10}$$

kjer snovska stalnica tekočine λ_1 pomeni napetostni sprostitveni čas, medtem ko je η_0 dinamična viskoznost. Vpliv elastičnosti, ki je podan z lokalnim časovnim odvodom dodatnega napetostnega tenzorja, je pomemben le med prehodnim pojavom. Z razvojem hitrostnega polja lokalni časovni odvod izgublja pomembnost, tako da v ustaljenem stanju prevladujejo učinki viskoznosti.

where λ_1 is a material constant for the fluid and is called the stress-relaxation time, whereas η_0 stands for the dynamic viscosity. The elasticity is given by the local time derivative of the additional stress tensor, which is significant during transient conditions. As the flow develops, the local time derivative losses its influence to finally arrive at a steady state where the viscosity is dominant.

Najpreprostejši kvazilinearen Maxwellov model, podan v obliki:

The simplest quasilinear Maxwell model may be given in the following form:

$$\tau_{ij} = 2\eta_0 \dot{\varepsilon}_{ij} - \lambda_1 \frac{D\tau_{ij}}{Dt} \tag{11}$$

zajema nelinearnost zaradi lokalnega in konvektivnega odvoda napetostnega tenzorja.

where the nonlinearity of the model is due to the local and convective derivatives of the stress tensor.

Model predstavljen z en. (11), v praksi ni uporaben, kljub temu pa ga zaradi preprostosti lahko uporabimo pri študiju stabilnosti in natančnosti razvitega numeričnega algoritma.

V nadaljevanju sta prikazana oba konvektivna Maxwellova modela. Zgornje konvektivni Maxwellov model podamo z odvisnostjo:

The model (11) does not relate to practical problems, but it can be examined due to its simplicity as an appropriate model to study the stability and accuracy of the developed numerical solution algorithm.

In addition, both convected Maxwell models are studied. The upper-convected Maxwell model is governed by the following constitutive relation:

$$\tau_{ij} = 2\eta_0 \dot{\varepsilon}_{ij} - \lambda_1 \overset{\nabla}{\tau}_{ij} \tag{12}$$

medtem ko za spodnje konvektivni model velja zapis:

while for the lower-convected Maxwell model the following equation is valid:

$$\tau_{ij} = 2\eta_0 \dot{\varepsilon}_{ij} - \lambda_1 \overset{\Delta}{\tau}_{ij} \tag{13}$$

Zgornje konvektivni Maxwellov model je namenjen testiranju numeričnih modelov reševanja viskoelastičnih tokov, saj je gibanje nekaterih stvarnih tekočin, vsaj v omejenem obsegu, mogoče opisati z en. (12).

Preostane še, da zapišemo konstitutivni model difuzijskega toplotnega toka v en. (3). V primeru intenzivnega prehodnega pojava prenosa toplote moramo upoštevati končno hitrost širjenja motnje, tako da velja odvisnost:

The upper-convected Maxwell model (12) is used extensively in testing numerical solution models. Some real fluids behave qualitatively like Eq. (12), at least over a limited range of kinematics.

Let us write the constitutive model of diffusion heat flux in Eq. (3). In the case of intensive, unsteady heat transfer it is important to take into account the terminal velocity of a moving frontier:

$$q_i = -k_0 \frac{\partial T}{\partial x_i} - \lambda_0 \frac{\partial q_i}{\partial t} \tag{14}$$

kjer sta snovski stalnici k_0 in λ_0 toplotna prevodnost in toplotni sprostitveni čas. Za večino praktično pomembnih prenosnih pojavov zadošča poenostavitev, znana kot Fourierjev zakon difuzije toplote:

where the material constants k_0 and λ_0 stand for the heat conductivity and the heat relaxation time. For most heat-transfer problems of practical importance the simplification known as the Fourier law of heat diffusion is accurate enough:

$$q_i = -k \frac{\partial T}{\partial x_i} \tag{15}$$

1.3 Povzetek vodilnih enačb

Z upoštevanjem konstitutivnih modelov za napetostni tenzor (9) do (13) in gostoto toplotnega toka (15) v ohranitvenih zakonih (2) in (3) izpeljemo naslednji sistem nelinearnih enačb:

1.3 Summary of the governing equations

Combining the constitutive models for the stress tensor (9) to (13) and the specific heat flux (15) in the conservation equations (2) and (3), the following system of nonlinear equations is developed:

$$\frac{\partial v_j}{\partial x_j} = 0 \tag{16}$$

$$\rho_0 \frac{Dv_i}{Dt} = -\frac{\partial p}{\partial x_i} + \eta_0 \frac{\partial^2 v_i}{\partial x_j \partial x_j} + \rho g_i + \frac{\partial \tau_{ij}^e}{\partial x_j} \tag{17}$$

$$\tau_{ij} = 2\eta_0 \dot{\varepsilon}_{ij} + \tau_{ij}^e \tag{18}$$

$$\frac{\partial T}{\partial t} = a_0 \frac{\partial^2 T}{\partial x_j \partial x_j} + \frac{I}{c_{p0}\rho_0} \tag{19}$$

kjer je $a_0 = k_0 / c_{p0}\rho_0$ toplotna difuzivnost. Sklenjen sistem enačb (16) do (19) je formalno identičen enačbam, ki opisujejo tok newtonske viskozne tekočine z izjemo dodatnega člena, ki je posledica elastičnih učinkov tekočine in je v sistemu označen z nadpisom "e". Ta člen v enačbi ohranitve gibalne

where $a_0 = k_0 / c_{p0}\rho_0$ is the thermal diffusivity. The closed system of equations (16) to (19) is formally identical to the equations governing the motion of a Newtonian viscous fluid, except for the additional term describing the elasticity effects (denoted by the superscript "e"). The appearance of the additional terms

količine vpelje dodatno nelinearnost v dinamični sistem enačb.

Za tok v ravnini sistem enačb od (16) do (19) zagotavlja sedem enačb za sedem neznank, v_1, v_2, p, τ_{11}, τ_{12}, τ_{22}, in T. Enačbe razrešimo z upoštevanjem primernih robnih in začetnih pogojev. Če predpostavimo, da so vse funkcije polja, npr. $v_i^n = v_i^n(r_j,t)$, $\tau_{ij}^n = \tau_{ij}^n(r_j,t)$ itd., v časovnem koraku $t = t_n$ znane, je treba določiti vrednosti funkcij polja v naslednjem trenutku $t_{n+1} = t_n + \Delta t$.

2 HITROSTNO-VRTINČNA FORMULACIJA

Z vektorjem vrtinčnosti $\omega_i(r_j,t)$, ki pomeni rotor hitrostnega polja $v_i(r_j,t)$:

$$\omega_i = e_{ijk}\frac{\partial v_k}{\partial x_j}, \qquad \frac{\partial \omega_j}{\partial x_j} = 0 \tag{20}$$

računsko shemo gibanja tekočine razdelimo na kinematični in kinetični del [8]. Kinetiko toka podamo z nelinearno parabolično difuzivno-konvektivno prenosno enačbo vrtinčnosti, ki jo izpeljemo z delovanjem operatorja rotor na gibalno enačbo (17):

$$\frac{D\omega_i}{Dt} = \frac{\partial \omega_i}{\partial t} + v_j\frac{\partial \omega_i}{\partial x_j} = \nu_0\frac{\partial^2\omega_i}{\partial x_j\partial x_j} + \omega_j\frac{\partial v_i}{\partial x_j} + \frac{1}{\rho_0}e_{ijk}g_k\frac{\partial \rho}{\partial x_j} + \frac{1}{\rho_0}e_{ijk}\frac{\partial^2\tau_{km}^e}{\partial x_j\partial x_k} \tag{21}$$

za i,j,k,m = 1,2,3. V prenosni enačbi (21) je opazen dodatni prenosni člen $\omega_j L_{ij}$, ki ga ne zasledimo v gibalni enačbi (17). Z upoštevanjem odvisnosti:

$$\omega_j L_{ij} = \omega_j(\dot{\varepsilon}_{ij} + \dot{\Omega}_{ij}) = \omega_j\dot{\varepsilon}_{ij} \tag{22}$$

preprosto pokažemo, da del člena $\omega_j\dot{\varepsilon}_{ij}$, $\dot{\varepsilon}_{ij}$ za $i = j$, opravlja prenos vrtinčnosti z raztezanjem vrtinčne črte, preostali del, $\dot{\varepsilon}_{ij}$ za $i \neq j$, pa prenaša vrtinčnost z obračanjem vrtinčne črte. Prenosni pojav raztezanja in obračanja ne obstaja pri ravninskih tokovih, ko se vektorska enačba (21) poenostavi v skalarno:

$$\frac{D\omega}{Dt} = \frac{\partial \omega}{\partial t} + v_j\frac{\partial \omega}{\partial x_j} = \nu_0\frac{\partial^2\omega}{\partial x_j\partial x_j} + \frac{1}{\rho_0}e_{ij}g_j\frac{\partial \rho}{\partial x_i} + \frac{1}{\rho_0}e_{ij}\frac{\partial^2\tau_{jk}^e}{\partial x_i\partial x_k} \tag{23}$$

za i,j,k = 1,2. Enačba (21) podaja časovno spremembo vrtinčnosti delca tekočine zaradi viskozne difuzije, konvekcije, vzgona, učinkov deformacije in elastičnosti tekočine. V primerjavi z enačbo gibanja newtonske viskozne tekočine je enačba (21) močneje nelinearna, prav zaradi močno nelinearnega elastičnega izvirnega člena.

Z delovanjem operatorja rotor na vektor vrtinčnosti:

$$\vec{\nabla}\times\vec{\omega} = \vec{\nabla}\times(\vec{\nabla}\times\vec{v}) = \vec{\nabla}(\vec{\nabla}\cdot\vec{v}) - \Delta\vec{v} \tag{24}$$

in ob upoštevanju kontinuitetne enačbe (16), $div\ \vec{v} = 0$, izpeljemo naslednjo vektorsko eliptično Poissonovo enačbo:

2 THE VELOCITY-VORTICITY FORMULATION

Introducing the vorticity vector field function $\omega_i(r_j,t)$ as a curl of the corresponding velocity field $v_i(r_j,t)$:

which is a solenoidal vector by definition, the fluid-motion computation procedure is partitioned into its kinetics and kinematics [8] parts. The vorticity transport in the fluid domain is governed by a nonlinear parabolic diffusion-convection equation obtained as a curl of the momentum eq. (17):

for i,j,k,m = 1,2,3. In the transport eq. (21) an additional transport term $\omega_j L_{ij}$ is represented, whereas it cannot be found in eq. (17). Regarding the relation:

it is easy to understand the behaviour of $\omega_j\dot{\varepsilon}_{ij}$, $\dot{\varepsilon}_{ij}$ for $i = j$, representing vorticity transport due to the stretching of the vorticity line, while the other part, $\dot{\varepsilon}_{ij}$ for $i \neq j$, stands for the twisting of the vorticity line. Twisting and stretching transport phenomena do not exist during the planar flows when vector eq. (21) is reduced to the scalar one:

for i,j,k = 1,2. The vorticity equation (21) expresses time-dependent vorticity transport by viscous diffusion, convection, bouyancy forces, while the elasticity and deformation of the fluid acts as a highly nonlinear production term, making the nonlinearity of the equation even more severe, when compared to Newtonian viscous fluid flow.

By applying the curl operator to the vorticity definition:

and by using the continuity eq. (16), $div\ \vec{v} = 0$, the following vector elliptic Poisson equation is obtained:

$$\frac{\partial^2 v_i}{\partial x_j \partial x_j} + e_{ijk} \frac{\partial \omega_k}{\partial x_j} = 0 \tag{25}$$

Enačba podaja kinematiko toka nestisljive tekočine oziroma združljivosti in omejitveni pogoj med solenoidnima vektorskima poljema hitrosti in vrtinčnosti v dani točki prostora in časa. Z namenom, da bi povečali konvergenco in stabilnosti vezane hitrostno-vrtinčne iterativne sheme, en. (25) zapišemo v njeni nepravi prehodni obliki, kar se izraža v naslednji parabolični difuzijski enačbi za vektor hitrosti

The equation represents the kinematics of an incompressible fluid motion expressing the compatibility and restriction conditions between the solenoidal velocity and the vorticity vector field functions at a given point in space and time. To accelerate convergence of the coupled velocity-vorticity iterative scheme the false transient approach is used. Thus, in a solution scheme Eq. (25) is rewritten as parabolic diffusion equation for the velocity vector:

$$\frac{\partial^2 v_i}{\partial x_j \partial x_j} - \frac{1}{\alpha} \frac{\partial v_i}{\partial t} + e_{ijk} \frac{\partial \omega_k}{\partial x_j} = 0 \tag{26}$$

kjer je α sprostitveni parameter. Očitno je, da je vodilna hitrostna enačba (26) natančno izpolnjena v ustaljenem stanju ($t \to \infty$), ko umetni časovni odvod hitrosti odpade.

with α as a relaxation parameter. It is obvious that the governing velocity equation (26) is exactly satisfied only during the steady state ($t \to \infty$), when the time derivative vanishes.

3 TLAČNA ENAČBA

Za nestisljive tekočine velja ugotovitev, da je tlak le funkcija hitrostnega polja in nasprotno, medtem ko je gostota nespremenljiva. Tlak torej ni termodinamična veličina stanja. Zapišimo gibalno en. (17) z upoštevanjem vektorske enakosti (24) za tlačni gradient *grad p*:

3 PRESSURE EQUATION

In the case of incompressible fluid motion, pressure is only a function of the velocity field, and vice versa, while the fluid mass density is assumed to be invariant. Therefore, pressure is not a thermodynamic variable. Let us write momentum, Eq. (17), for the pressure gradient, *grad p*, by taking into account the vector relation (24):

$$\frac{\partial p}{\partial x_i} = f_i = -\rho_0 \frac{Dv_i}{Dt} - \eta_0 e_{ijk} \frac{\partial \omega_k}{\partial x_j} + \rho g_i + \frac{\partial \tau_{ij}^e}{\partial x_j} \tag{27}$$

ki se v primeru ravninskega toka poenostavi v odvisnost:

which simplifies in the case of planar flows in the following way:

$$\frac{\partial p}{\partial x_i} = f_i = -\rho_0 \frac{Dv_i}{Dt} - \eta_0 e_{ij} \frac{\partial \omega}{\partial x_j} + \rho g_i + \frac{\partial \tau_{ij}^e}{\partial x_j} \tag{28}$$

V vektorski funkciji f_i smo združili vztrajnostne, difuzijske, težnostne in elastične učinke. Pri izpeljavi tlačne enačbe v odvisnosti od hitrosti poiščemo divergenco členov en. (27), kar se kaže v naslednji eliptični Poissonovi enačbi za tlak:

Inertia, diffusion, gravitational and elasticity effects are incorporated in vector function f_i. To derive the pressure equation dependent on velocity the divergence of Eq. (27) should be calculated, resulting in the elliptic Poisson pressure equation

$$\frac{\partial p}{\partial x_i \partial x_i} - \frac{\partial f_i}{\partial x_i} = 0 \tag{29}$$

4 METODA ROBNIH ELEMENTOV

Uporaba Greenovih osnovnih rešitev kot utežnih funkcij v numeričnem modelu pomeni eno izmed osnovnih lastnosti in prednosti metode robnih elementov (MRE). Ker osnovne rešitve opisujejo le linearni del prenosnega pojava, je izbira primernega linearnega operatorja $L[.]$ ključnega pomena za zapis integralskih enačb, ki ustrezajo prvotnemu sistemu ohranitvenih diferencialnih enačb.

Znane diferencialne modele prenosnih pojavov v toku tekočine lahko zapišemo v obliki naslednjega splošnega stavka:

4 THE BOUNDARY-ELEMENT METHOD

The unique advantage of the boundary-element method (BEM) originates from the application of Green fundamental solutions as particular weighting functions. Since they only consider the linear transport phenomenon, the appropriate selection of a linear differential operator $L[.]$ is of vital importance in establishing stable and accurate singular integral representations corresponding to original differential conservation equations.

All the various conservation models can be written in the following general form

$$L[u] + b = 0 \tag{30}$$

kjer je $L[.]$ eliptični ali parabolični linearni diferencialni operator, $u(r_j,t)$ je poljubna funkcija polja in $b(r_j,t)$ pomeni nehomogeni del nelinearnih vplivov oziroma prostorninskih virov.

where the operator $L[.]$ can be either elliptic or parabolic, $u(r_j,t)$ is an arbitrary field function, and the nonhomogenous term $b(r_j,t)$ is applied for nonlinear transport effects or pseudo body forces.

4.1 Integralska predstavitev kinematike

Hitrostno en. (26) lahko prepoznamo kot parabolično difuzijsko enačbo, zato uporabimo linearni parabolični difuzijski operator:

4.1 Integral representation of flow kinematics

The velocity Eq. (26) can be recognized as a parabolic diffusion equation. Employing the linear parabolic diffusion operator as follows:

$$L[\cdot]=\alpha\frac{\partial^2(\cdot)}{\partial x_j\partial x_j}-\frac{\partial(\cdot)}{\partial t} \tag{31}$$

tako, da lahko zapišemo:

the following can be stated:

$$L[v_i]+b_i=\alpha\frac{\partial^2 v_i}{\partial x_j\partial x_j}-\frac{\partial v_i}{\partial t}+b_i=0 \tag{32}$$

Pri izpeljavi singularne robne integralske enačbe izhajamo iz Greenovih teoremov za skalarna polja ali iz integrala utežnega ostanka, kar se kaže v naslednji obliki vektorske integralske formulacije:

The singular boundary integral representation for the velocity vector can be formulated by using the Green theorems for scalar functions or weighting residuals technique rendering the following vector integral formulation:

$$c(\xi)v_i(\xi,t_F)+\alpha\int_\Gamma\int_{t_{F-1}}^{t_F}v_i\frac{\partial u^\star}{\partial n}dtd\Gamma=\alpha\int_\Gamma\int_{t_{F-1}}^{t_F}\frac{\partial v_i}{\partial n}u^\star dtd\Gamma+\int_\Omega\int_{t_{F-1}}^{t_F}bu^\star dtd\Omega+\int_\Omega v_{i,F-1}u^\star_{F-1}d\Omega \tag{33}$$

kjer je u^* parabolična difuzijska osnovna rešitev, npr. rešitev enačbe:

with u^* the parabolic diffusion fundamental solution as the solution of the equation:

$$a\frac{\partial^2 u^\star}{\partial x_j\partial x_j}+\frac{\partial u^\star}{\partial t}+\delta(\xi,s)\delta(t_F,t)=0 \tag{34}$$

in podana z izrazom:

and given by the expression:

$$u^\star=\frac{1}{(4\pi a\tau)^{d/2}}\exp\left(-\frac{r^2}{4a\tau}\right) \tag{35}$$

kjer sta (ξ,t_F) in (s,t) izvirna točka in referenčna točka polja, d pomeni izmero problema in $\tau = t_F - t$. Če izenačimo prostorninske sile z enakostjo:

where (ξ,t_F) and (s,t) are the source point and the reference field point, d is the dimension of the problem and $\tau = t_F - t$. The pseudo-body force vector includes the vortical fluid flow part:

$$b=\alpha e_{ijk}\frac{\partial\omega_k}{\partial x_j} \tag{36}$$

velja končna oblika integralske predstavitve kinematike toka, npr. v vektorski obliki:

rendering the following final integral formulation of flow kinematics, in vector form:

$$\begin{aligned}c(\xi)\vec{v}(\xi,t_F)+\alpha\int_\Gamma\int_{t_{F-1}}^{t_F}\vec{v}\frac{\partial u^\star}{\partial n}dtd\Gamma&=\alpha\int_\Gamma\int_{t_{F-1}}^{t_F}\frac{\partial\vec{v}}{\partial n}u^\star dtd\Gamma-\alpha\int_\Gamma\int_{t_{F-1}}^{t_F}\vec{\omega}\times\vec{n}u^\star dtd\Gamma\\&+\alpha\int_\Omega\int_{t_{F-1}}^{t_F}\vec{\omega}\times\vec{\nabla}u^\star dtd\Omega+\int_\Omega\vec{v}_{F-1}u^\star_{F-1}d\Omega\end{aligned} \tag{37}$$

oziroma v tenzorskem simbolnem zapisu:

or in tensor symbolic notation:

$$\begin{aligned}c(\xi)v_i(\xi,t_F)+\alpha\int_\Gamma\int_{t_{F-1}}^{t_F}v_i\frac{\partial u^\star}{\partial n}dtd\Gamma&=\alpha\int_\Gamma\int_{t_{F-1}}^{t_F}\frac{\partial v_i}{\partial n}u^\star dtd\Gamma\\-\alpha e_{ijk}\int_\Gamma\int_{t_{F-1}}^{t_F}\omega_j n_k u^\star dtd\Gamma+\alpha e_{ijk}\int_\Omega\int_{t_{F-1}}^{t_F}\omega_j\frac{\partial u^\star}{\partial x_k}dtd\Omega&+\int_\Omega v_{i,F-1}u^\star_{F-1}d\Omega\end{aligned} \tag{38}$$

Kinematika ravninskega toka je podana z dvema skalarnima enačbama:

The kinematics of plane motion is given by two scalar equations as follows:

$$\begin{aligned}c(\xi)v_i(\xi,t_F)+\alpha\int_\Gamma\int_{t_{F-1}}^{t_F}v_i\frac{\partial u^\star}{\partial n}dtd\Gamma&=\alpha\int_\Gamma\int_{t_{F-1}}^{t_F}\frac{\partial v_i}{\partial n}u^\star dtd\Gamma\\+\alpha e_{ij}\int_\Gamma\int_{t_{F-1}}^{t_F}\omega n_j u^\star dtd\Gamma-\alpha e_{ij}\int_\Omega\int_{t_{F-1}}^{t_F}\omega\frac{\partial u^\star}{\partial x_j}dtd\Omega&+\int_\Omega v_{i,F-1}u^\star_{F-1}d\Omega\end{aligned} \tag{39}$$

Eno osnovnih izhodišč numeričnega modela toka nestisljive tekočine je divergence prosta oziroma solenoidna rešitev za hitrostno in vrtinčno polje. Za en. (36) oziroma (38) lahko preprosto pokažemo, da sta enačbi izpolnjeni tudi v primeru, ko nobena od divergenc ni enaka nič [9]. Povzamemo lahko, da en. (38) v splošnem ne predstavlja kinematike toka nestisljive tekočine. S ponovno zahtevo po združljivosti in omejitvi hitrostnega ter vrtinčnega polja, $\vec{\omega} = rot\,\vec{v}$ in $div\,\vec{v} = 0$, robna integrala na desni strani en. (38) preoblikujemo, kar se kaže v končni obliki singularne robne integralske predstavitve kinematike prostorskega toka:

One of the most important issues in the numerical modeling of incompressible flow phenomena is to obtain a divergence-free final solution both for the velocity field and for the vorticity conservation. In the case of equations (36) or (38) it can be easily shown that solutions where none of the divergences are zero are permitted [9]. Thus, it is possible to conclude that Eq. (38) does not generally represent the kinematics of incompressible fluid flow. By using additional compatibility and restriction conditions for the velocity and vorticiy fields, $\vec{\omega} = rot\,\vec{v}$ and $div\,\vec{v} = 0$, boundary integrals on the right-hand side of Eq. (38) are rewritten, resulting in the final singular boundary integral statement of the kinematics of spatial flow:

$$c(\xi)\vec{v}(\xi,t_F)+\alpha\int_\Gamma\int_{t_{F-1}}^{t_F}\left(\vec{\nabla}u^\star\cdot\vec{n}\right)\vec{v}dtd\Gamma=\alpha\int_\Gamma\int_{t_{F-1}}^{t_F}\left(\vec{\nabla}u^\star\times\vec{n}\right)\times\vec{v}dtd\Gamma+\alpha\int_\Omega\int_{t_{F-1}}^{t_F}\left(\vec{\omega}\times\vec{\nabla}u^\star\right)dtd\Omega+\int_\Omega\vec{v}_{F-1}u^\star_{F-1}d\Omega \quad (40)$$

ali tudi v zgoščenem simbolnem zapisu za krožno kombinacijo indeksov *ijkij* = 12312:

or in the compact symbol notation for the cyclic combination of: *ijkij* = 12312:

$$c(\xi)v_i(\xi,t_F)+\alpha\int_\Gamma\int_{t_{F-1}}^{t_F}v_i\frac{\partial u^\star}{\partial n}dtd\Gamma=\alpha\int_\Gamma\int_{t_{F-1}}^{t_F}v_k\left(\frac{\partial u^\star}{\partial x_k}n_i-\frac{\partial u^\star}{\partial x_i}n_k\right)dtd\Gamma$$
$$-\alpha\int_\Gamma\int_{t_{F-1}}^{t_F}v_j\left(\frac{\partial u^\star}{\partial x_i}n_j-\frac{\partial u^\star}{\partial x_j}n_i\right)dtd\Gamma+\alpha\int_\Omega\int_{t_{F-1}}^{t_F}\omega_j\frac{\partial u^\star}{\partial x_k}dtd\Omega-\alpha\int_\Omega\int_{t_{F-1}}^{t_F}\omega_k\frac{\partial u^\star}{\partial x_j}dtd\Omega+\int_\Omega v_{i,F-1}u^\star_{F-1}d\Omega \quad (41)$$

Kinematika ravninskega toka je podana z:

The kinematics of planar fluid motion is given by:

$$c(\xi)v_i(\xi,t_F)+\alpha\int_\Gamma\int_{t_{F-1}}^{t_F}v_i\frac{\partial u^\star}{\partial n}dtd\Gamma=\alpha\int_\Gamma\int_{t_{F-1}}^{t_F}v_j\frac{\partial u^\star}{\partial t}dtd\Gamma-\alpha e_{ij}\int_\Omega\int_{t_{F-1}}^{t_F}\omega\frac{\partial u^\star}{\partial x_j}dtd\Omega+\int_\Omega v_{i,F-1}u^\star_{F-1}d\Omega \quad (42)$$

Enačba (41) je popolnoma ustrezna kontinuitetni oziroma omejitveni enačbi in definiciji vrtinčnosti ter podaja kinematiko nestisljive tekočine v integralski obliki. Hitrostni robni pogoji so vključeni v robnih integralih, medtem ko je z območnim integralom zajet vpliv vrtinčnega polja na razvoj hitrostnega polja. Zadnji območni integral upošteva vpliv začetnih hitrostnih pogojev nepravega prehodnega pojava. V en. (42) se pojavljata normalni in tangentni odvod osnovne rešitve $\partial u^*/\partial n$ in $\partial u^*/\partial t$, kar je pomembna razlika proti en. (39), kjer sta osnovna rešitev in njen normalni odvod, u^* in $\partial u^*/\partial n$. Pri izračunu robnih vrednosti funkcij polja moramo uporabiti normalno oziroma tangentno obliko vektorske enačbe (40), [7].

Robne vrednosti vrtinčnosti so v integralski obliki zajete v območnem integralu. Izračun robnih vrednosti vrtinčnosti zaradi zapisa nesingularnega implicitnega sistema terja tangentno obliko vektorske enačbe (40).

Equation (41) is equivalent to the continuity equation, also recognized as the restriction equation and the vorticity definition expressing the kinematics of general incompressible fluid flow in the integral form. Velocity boundary conditions are incorporated into boundary integrals, while in domain integrals the influence of the vorticity field on the developing velocity field is given. The last domain integral takes into account the influence of the initial velocity conditions of false transient phenomena. In Eq. (42) the normal and tangential derivatives of the fundamental solution, $\partial u^*/\partial n$ and $\partial u^*/\partial t$, are employed, an important difference in comparison to Eq. (39), where the fundamental solution and the normal derivative of the fundamental solution, u^* and $\partial u^*/\partial n$, are used. To compute the boundary values of the field functions, the normal or tangential form of vector Eq. (40), [7], is required.

The boundary vorticity values are expressed in integral form within the domain integral. When the unknows are the boundary vorticities one has to use the tangential component of vector Eq. (40) because of the nonsingular implicit system of equations

$$c(\xi)\vec{n}(\xi)\times\vec{v}(\xi,t_F)+\vec{n}(\xi)\times\alpha\int_\Gamma\int_{t_{F-1}}^{t_F}\left(\vec{\nabla}u^\star\cdot\vec{n}\right)\vec{v}dtd\Gamma=$$
$$\vec{n}(\xi)\times\alpha\int_\Gamma\int_{t_{F-1}}^{t_F}\left(\vec{\nabla}u^\star\times\vec{n}\right)\times\vec{v}dtd\Gamma+\vec{n}(\xi)\times\alpha\int_\Omega\int_{t_{F-1}}^{t_F}\left(\vec{\omega}\times\vec{\nabla}u^\star\right)dtd\Omega+\vec{n}(\xi)\times\alpha\int_\Omega\vec{v}_{F-1}u^\star_{F-1}d\Omega \quad (43)$$

4.2 Integralska predstavitev kinetike

Za zapis kinetike toka viskoelastične tekočine v integralski obliki moramo upoštevati parabolično

4.2 Integral representation of flow kinetics

Considering the kinetics of viscoelastic fluid flow in an integral representation one has to take into

difuzivno-konvektivno naravo prenosne enačbe vrtinčnosti. Z uporabo linearnega paraboličnega difuzivnega diferencialnega operatorja:

account the parabolic diffusion-convection character of the vorticity transport equation. Since only the linear parabolic diffusion differential operator is employed, i.e.:

$$L[\cdot] = \nu_0 \frac{\partial^2(\cdot)}{\partial x_j \partial x_j} - \frac{\partial(\cdot)}{\partial t} \tag{44}$$

prenosno enačbo vrtinčnosti (33) zapišemo v obliki nehomogene parabolične difuzivne enačbe:

the vorticity equation (33) can be formulated as a nonhomogenous parabolic diffusion equation as follows:

$$L[\omega] + b = \nu_0 \frac{\partial^2 \omega}{\partial x_j \partial x_j} - \frac{\partial \omega}{\partial t} + b = 0 \tag{45}$$

z naslednjim pripadajočim integralskim stavkom, zapisanim za časovni korak $\Delta t = t_F - t_{F-1}$:

with the following corresponding integral representation written in a time-increment form for a time step $\Delta t = t_F - t_{F-1}$:

$$c(\xi)\omega(\xi,t_F) + \nu_0 \int_\Gamma \int_{t_{F-1}}^{t_F} \omega \frac{\partial u^\star}{\partial n} dt d\Gamma = \nu_0 \int_\Gamma \int_{t_{F-1}}^{t_F} \frac{\partial \omega}{\partial n} u^\star dt d\Gamma + \int_\Omega \int_{t_{F-1}}^{t_F} b u^\star dt d\Omega + \int_\Omega \omega_{F-1} u^\star_{F-1} d\Omega \tag{46}$$

kjer je u^* difuzivna osnovna rešitev, podana z en. (35). Območni integral nehomogenega nelinearnega prispevka b:

where u^* is the parabolic diffusion fundamental solution given by Eq. (35). The domain integral of the non-homogenous nonlinear contribution b, represented as:

$$b = -\frac{\partial v_j \omega}{\partial x_j} + \frac{1}{\rho_0} e_{ij} g_j \frac{\partial \rho}{\partial x_i} + \frac{1}{\rho_0} e_{ij} \frac{\partial^2 \tau^e_{jk}}{\partial x_i \partial x_k} \tag{47}$$

vsebuje konvekcijo, vzgonske in elastične učinke, tako da velja naslednji zapis kinetike vrtinčnosti v integralski obliki:

includes the convection, the bouyancy force effects, and the viscoelastic effects. Thus the final integral statement reads as:

$$\begin{aligned} c(\xi)\omega(\xi,t_F) + \nu_0 \int_\Gamma \int_{t_{F-1}}^{t_F} \omega \frac{\partial u^\star}{\partial n} dt d\Gamma &= \nu_0 \int_\Gamma \int_{t_{F-1}}^{t_F} \frac{\partial \omega}{\partial n} u^\star dt d\Gamma - \int_\Gamma \int_{t_{F-1}}^{t_F} \omega v_n u^\star dt d\Gamma + \int_\Omega \int_{t_{F-1}}^{t_F} \omega v_j \frac{\partial u^\star}{\partial x_j} dt d\Omega \\ &+ e_{ij} \frac{1}{\rho_0} \int_\Gamma \int_{t_{F-1}}^{t_F} n_i g_j \rho u^\star dt d\Gamma - e_{ij} \frac{1}{\rho_0} \int_\Omega \int_{t_{F-1}}^{t_F} g_j \rho \frac{\partial u^\star}{\partial x_i} dt d\Omega + e_{ij} \frac{1}{\rho_0} \int_\Gamma \int_{t_{F-1}}^{t_F} \frac{\partial \tau^e_{jk}}{\partial x_k} n_i u^\star dt d\Gamma \\ &- e_{ij} \frac{1}{\rho_0} \int_\Omega \int_{t_{F-1}}^{t_F} \frac{\partial \tau^e_{jk}}{\partial x_k} \frac{\partial u^\star}{\partial x_i} dt d\Omega + \int_\Omega \omega_{F-1} u^\star_{F-1} d\Omega \end{aligned} \tag{48}$$

Iz en. (48) je razvidna popolna podobnost med prenosom vrtinčnosti v viskoelastični tekočini in prenosom vrtinčnosti v toku newtonske viskozne tekočine z izjemo dodatnega elastičnega prispevka, ki deluje kot močno nelinearni izvirni člen.

Singularno robno integralsko predstavitev toplotne prenosne enačbe izpeljemo enako kakor izpeljavo vrtinčne enačbe, tako da velja integralski stavek:

Eq. (48) shows the analogy between the vorticity transport in the viscoelastic fluid and the vorticity transport in viscous, Newtonian motion, with the only difference in the extra viscoelastic contribution acting as a highly nonlinear source term.

By applying a similar procedure to the heat-transport equation, one derives the following integral statement:

$$\begin{aligned} c(\xi)T(\xi,t_F) + a_0 \int_\Gamma \int_{t_{F-1}}^{t_F} T \frac{\partial u^\star}{\partial n} dt d\Gamma &= a_0 \int_\Gamma \int_{t_{F-1}}^{t_F} \frac{\partial T}{\partial n} u^\star dt d\Gamma - \int_\Gamma \int_{t_{F-1}}^{t_F} T v_n u^\star dt d\Gamma \\ &+ \int_\Omega \int_{t_{F-1}}^{t_F} T v_j \frac{\partial u^\star}{\partial x_j} dt d\Omega + \int_\Omega T_{F-1} u^\star_{F-1} d\Omega \end{aligned} \tag{49}$$

4.3 Integralska predstavitev tlačne enačbe

Tlačna en. (29) je eliptična Poissonova enačba, tako da uporabimo linearni eliptični Laplacev diferencialni operator:

4.3 Integral representation of the pressure equation

The pressure Eq. (29) is recognized as an elliptic Poisson equation, thus employing the linear elliptic Laplace differential operator:

$$L[\cdot] = \frac{\partial^2(\cdot)}{\partial x_i \partial x_i} \tag{50}$$

kar se izraža v zapisu:

the following can be stated:

$$L[p] + b = \frac{\partial^2 p}{\partial x_i \partial x_i} + b = 0 \tag{51}$$

medtem ko je pripadajoča singularna robna integralska tlačna predstavitev podana s stavkom:

$$c(\xi)\,p(\xi)+\int_\Gamma p\frac{\partial u^\star}{\partial n}d\Gamma=\int_\Gamma \frac{\partial p}{\partial n}u^\star d\Gamma+\int_\Omega bu^\star d\Omega \tag{52}$$

kjer je u^* Laplaceova osnovna rešitev, npr. rešitev enačbe:

$$\frac{\partial^2 u^\star}{\partial x_i \partial x_i}+\delta(\xi,s)=0 \tag{53}$$

Za ravninsko geometrijo velja rešitev:

$$u^\star=\frac{1}{2\pi}\ln\left(\frac{1}{r}\right) \tag{54}$$

Z izenačitvijo navidezno prostorninskih sil:

$$b=-\frac{\partial f_i}{\partial x_i} \tag{55}$$

izpeljemo integralsko odvisnost:

$$c(\xi)\,p(\xi)+\int_\Gamma p\frac{\partial u^\star}{\partial n}d\Gamma=\int_\Gamma \frac{\partial p}{\partial n}u^\star d\Gamma-\int_\Omega \frac{\partial f_i}{\partial x_i}u^\star d\Omega \tag{56}$$

Z Gaussovim divergenčnim stavkom območni integral v en. (56) preoblikujemo kot:

$$\int_\Omega \frac{\partial f_i}{\partial x_i}u^\star d\Omega=\int_\Gamma f_i n_i u^\star d\Gamma-\int_\Omega f_i\frac{\partial u^\star}{\partial x_i}d\Omega \tag{57}$$

ker pa je $\partial p/\partial n=\vec{f}\cdot\vec{n}$, velja končna oblika tlačnega integralskega stavka:

$$c(\xi)\,p(\xi)+\int_\Gamma p\frac{\partial u^\star}{\partial n}d\Gamma=\int_\Omega f_i\frac{\partial u^\star}{\partial x_i}d\Omega \tag{58}$$

kjer je vektor f_i podan za prostorski tok z en. (27) in za ravninsko gibanje z en. (29).

5 RAČUNSKA SHEMA

Singularne robnoobmočne integralske enačbe lahko rešimo za neznane funkcije polja le približno v smislu ustreznega numeričnega modela, s katerim integralske enačbe predelamo v pripadajoči sistem algebrajskih enačb. Osnova modela robnih elementov je diskretizacija roba z robnimi elementi in območja rešitve z notranjimi celicami [10]. Ker je za utežno funkcijo izbrana Greenova osnovna rešitev, z robno diskretizacijo v celoti zajamemo linearni del rešitve (difuzijo), medtem ko z notranjo delitvijo na celice upoštevamo nelinearne prispevke prenosnega pojava. V prispevku so uporabljeni daljični kvadratni zvezni robni elementi in četverokotne kvadratne zvezne notranje celice.

V računskem postopku iskanja približne rešitve predstavljata kinematika in kinetika prenosnega pojava vezan nelinearni sistem. V primeru splošnega časovno odvisnega pojava izračunamo najprej na temelju znanih začetnih vrednosti funkcij polja nove približke vrtinčnega polja z rešitvijo en. (48). Z novimi območnimi

while the corresponding singular integral pressure representation is given by:

where u^* is the Laplace fundamental solution, being the solution of the equation:

For planar geometry the following solution is suitable:

By equating pseudo-body forces with the expression:

the integral statement is derived:

Using the Gauss divergence theorem the domain integral in eq. (56) is rewritten as:

because the relation $\partial p/\partial n=\vec{f}\cdot\vec{n}$, the final form of the pressure integral statement is obtained:

where vector f_i for the spatial flow is given by eq. (27) and for planar flow by Eq. (29).

5 COMPUTATIONAL SCHEME

If one wants to solve singular, boundary-domain, integral equations to obtain values of field functions in the computational domain one first has to transform the derived integral equations into their discrete algebraic forms. The key to this is the partitioning of the computational external boundary into boundary elements and the interior domain into domain cells [10]. Use of the Green fundamental solution results in boundary discretization of the linear part of the solution (diffusion), while internal cells take care of the nonlinear contribution of the transport phenomena. In this paper, quadratic interpolation functions were used in the case of boundary elements and internal cells in the case of domain.

The kinematics and kinetics of the fluid-flow motion can be seen as two intertwined problems in a nonlinear system of equations. For general time-dependent flows using known information about the motion at an instant time level, new vorticity values for a subsequent time level are determined by solving eq. (48). With this new domain, vorticity values corresponding to

vrednostmi vrtinčnosti kinetike toka izračunamo nove robne vrednosti vrtinčnosti z rešitvijo kinematike en. (43). Ta izračun je ključnega pomena za ohranitev solenoidnosti hitrostnega in vrtinčnega polja. Sledi izrecen izračun hitrosti v območju. Če obravnavamo neizotermne tokove, pri katerih so vzgonski učinki pomembni, so vse tri enačbe, tj. kontinuitetna, vrtinčna in energijska, vezane v močno nelinearen sistem, ki ga lahko razrešimo le iterativno. Za viskoelastične tekočine velja, da moramo v nelinearno shemo vključiti še izračun napetostnega tenzorja, skladno z reološkim modelom. Tlačno polje določimo zunaj nelinearne sheme na podlagi vseh znanih funkcij polja z rešitvijo en. (58).

boundary vorticity values are determined by solving the flow kinematics Eq. (43). This part of the computation is of crucial importance for preserving the solenoidality of the velocity and vorticity fields, which is followed by an explicit computation of domain velocities. In the case of nonisothermal flows, where the bouyance forces are important, all three equations, such as the continutity, vorticity and energy equations, are coupled into a highly nonlinear system, which can be solved only iteratively. For viscoelastic fluids, an additional nonlinearity is introduced by computing the components of the stress tensor in accordance with the rheological model employed. The pressure field is determined outside the nonlinear scheme on the basis of all known field functions by solving Eq. (58).

6 NUMERIČNI REZULTATI

6.1 Naravna konvekcija

V prvem numeričnem primeru smo preučili naravno konvekcijo viskoelastične tekočine v zaprti kotanji. Kot standardni testni primer CFD je problem gibanja newtonske tekočine zaradi vzgonskih sil predložil že De Vahl Davis s sodelavci ([2] in [3]).

6 NUMERICAL SOLUTION

6.1 Natural convection

As a first numerical example, the natural convection of a viscoelastic fluid in a closed cavity is examined. The problem has been analyzed by De Vahl Davis et al. ([2] and [3]) as one of the standard test cases of Newtonian viscous fluid flows in CFD.

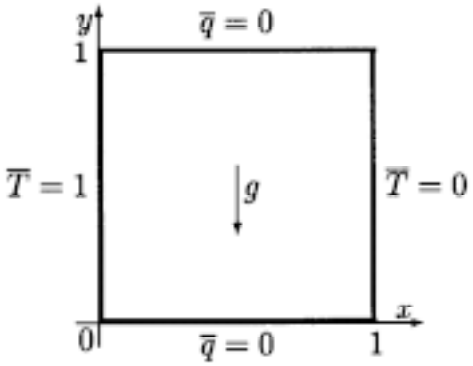

Sl. 1. *Naravna konvekcija v zaprti kotanji. Geometrija in robni pogoji.*
Fig. 1. *Natural convection in a closed cavity. Geometry and boundary conditions.*

Kotanja je popolnoma napolnjena z nestisljivo viskoelastično tekočino. Uporabljena konstitutivna modela sta v prvem primeru kvazilinearni Maxwellov model (model A) in v drugem premeru zgornje konvektivni Maxwellov model (model B), ki sta podrobno opisana v poglavju 3.

Zgornja in spodnja stena kotanje sta izolirani, medtem ko sta leva in desna stena ogreti na različno temperaturo. Zaradi temperaturne razlike obstaja toplotni tok v tekočini. Ker je gostota tekočine odvisna od temperature, se pojavijo vzgonske sile, ki poganjajo tekočino. Ob topli steni se tekočina dviguje, ob hladni spušča. Hitrost gibanja newtonske tekočine je funkcija Rayleighevega števila $Ra = g\beta(T_t\text{-}T_k)L^3/a_0\upsilon$. V našem primeru smo izbrali $Ra = 10^3$. Tok newtonske tekočine ($\lambda_1 = 0$) smo primerjali z nenewtonskimi tokovi za vrednosti napetostnega sprostitvenega časa $\lambda_1 = 0{,}06$, 0,07 in 0,08. Masna

A cavity is filled with an incompressible viscoelastic fluid. Two different rheological models are employed: the quasilinear Maxwell model in case A and the upper-convected Maxwell model in case B. Both are described in detail in section 3.

The top and bottom walls are insulated, while the left-hand and right-hand walls are heated to different temperatures. Due to the temperature difference a heat flow occurs through the fluid. Because the density of the fluid depends on the temperature, the fluid starts moving upward at the hot wall due to buoyancy, and downward at the cold wall. The velocity of the fluid depends on the Rayleigh number $Ra = g\beta(T_t\text{-}T_k)L^3/a_0\upsilon$. In our case $Ra = 10^3$ was selected. The Newtonian fluid flow ($\lambda_1 = 0$) was compared to the non-Newtonian flow for different values of the relaxation time parameter $\lambda_1 =$

gostota je podana z enačbo stanja $\rho = \rho_0(1+\beta T)$ idealnega plina.

0.06, 0.07 and 0.08. The mass density is given by the equation of state $\rho = \rho_0(1+\beta T)$.

Sl. 2. *Naravna konvekcija nenewtonske viskoelastične tekočine modelirana z zgornje konvektivnim Maxwellovim reološkim modelom (λ_1=0,07); vektorji hitrosti (levo), tokovnice (sredina) in izolinije vrtinčnosti (desno)*

Fig. 2. *Natural convection of non-Newtonian viscoelastic fluid modeled with upper-convected Maxwell rheological model (λ_1=0.07); velocity vectors (left), streamlines (middle), and vorticity lines (right)*

Preglednica 1. *Primerjava vrednosti $\overline{Nu}$ števila med newtonsko tekočino in različnimi modeli nenewtonske tekočine*

Table 1. *Comparison of $\overline{Nu}$ number for Newtonian fluid flow and different models of non-Newtonian fluid flow*

	Davis	MRE - A			MRE - B		
λ_1	0	0,6	0,7	0,8	0,6	0,7	0,8
$\overline{Nu}$	1,117	1,136	1,134	1,132	1,176	1,162	/

Geometrija problema in robni pogoji so prikazani na sliki 1. Računska mreža je sestavljena iz 80 robnih elementov in 400 notranjih celic, kar pomeni mrežo 20×20 celic z razmerjem 6 med najdaljšim in najkrajšim elementom. Vse izračune smo izvedli kot ustaljene, pri čemer smo prehodni pojav simulirali z zelo velikim časovnim korakom ($\Delta t = 10^{16}$). Podsprostitev smo definirali s podsprostitvenim parametrom ϑ, ki je znašal v primeru simulacije newtonskega toka $\vartheta = 0{,}001$ in v primeru izračuna nenewtonskih tokov $\vartheta = 0{,}0001$. Konvergenčni kriterij je vedno predstavljala napaka v velikosti $= 10^{-6}$.

Slika 2 prikazuje vektorsko polje hitrosti, tokovnice in izočrte vrtinčnosti za zgornje konvektivni Maxwellov reološki model (B) pri vrednosti parametra $\lambda_1 = 0{,}07$. Slike 3, 4, 5 in 6 prikazujejo hitrostne profile v_y vzdolž vodoravne črte in hitrostne profile v_x vzdolž navpične črte skozi geometrijsko središče kotanje. Izvedena je primerjava newtonske primerjalne rešitve MRE na gostoti mreže 32×32, ki se odlično ujema z rešitvijo Davisa ([2] in [3]), z nenewtonskimi rešitvami MRE na že omenjeni računski mreži 20×20.

Na slikah 3 in 4 je nenewtonska tekočina modelirana kot navidezlinearna (A), na slikah 5 in 6 pa so prikazani rezultati zgornje konvektivnega Maxwellovega modela viskoelastične tekočine (B). Opazimo razmeroma velik vpliv elastičnosti tekočine

The geometry and boundary conditions of the problem are shown in Fig. 1. The computational mesh is composed of 80 boundary elements and 400 internal cells, i.e. 20×20 cells with a ratio of 6 between the longest and the shortest element. All the simulations were performed as steady with the transient phenomenon simulated using an extremely large time step ($\Delta t = 10^{16}$). The underrelaxation parameter ϑ (in the case of a temperature computation defined by $T^{i+1} = \vartheta T^{i+1} + (1-\vartheta)T^i$ and analogous for other field functions) was set to $\vartheta = 0.001$ in the case of Newtonian flow and $\vartheta = 0.0001$ in case of non-Newtonian flows. The convergence criterion was selected as $\varepsilon = 10^{-6}$.

Fig. 2 shows the velocity vectors, the streamlines, and the vorticity lines for the upper-convected Maxwell rheological model (B) for the relaxation-time parameter being fixed at $\lambda_1 = 0.07$. Figs. 3, 4, 5, and 6 show velocity profiles v_y along a horizontal line and velocity profiles v_x along a vertical line, through the geometric center of the cavity. The comparison between a BEM reference solution obtained on mesh density 32×32, which is in excellent agreement with the Davis solution ([2] and [3]), and BEM non-Newtonian solutions obtained on mesh density 20×20 is performed.

On Figs. 3 and 4 the non-Newtonian fluid is modeled as quasilinear (A), while in Figs. 5 and 6 the upper-convected Maxwell model (B) is used. It is easy to see a relatively strong influence of the

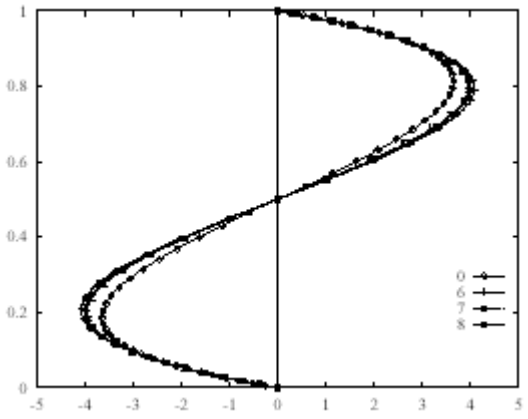

Sl. 3. *Nenewtonska tekočina kot Maxwellova navidezlinearna viskoelastična tekočina (A). Hitrostni profili v_x vzdolž navpične črte skozi geometrijsko središče kotanje.*

Fig. 3. *Non-Newtonian fluid as Maxwell quasilinear viscoelastic fluid (A). Velocity profiles v_x along a vertical line through the center of cavity.*

(0 : λ_1=0; 6 : λ_1=0,06; 7 : λ_1=0,07 in/and 8 : λ_1=0,08)

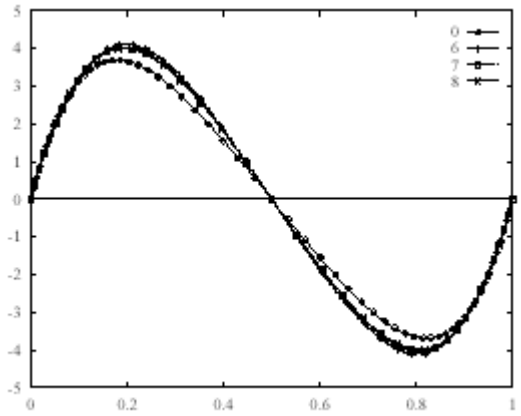

Sl. 4. *Nenewtonska tekočina kot Maxwellova navidezlinearna viskoelastična tekočina (A). Hitrostni profili v_y vzdolž vodoravne črte skozi geometrijsko središče kotanje.*

Fig. 4. *Non-Newtonian fluid as Maxwell quasilinear viscoelastic fluid (A). Velocity profiles v_y along a horizontal line through the center of cavity.*

(0 : λ_1=0; 6 : λ_1=0,06; 7 : λ_1=0,07 in/and 8 : λ_1=0,08)

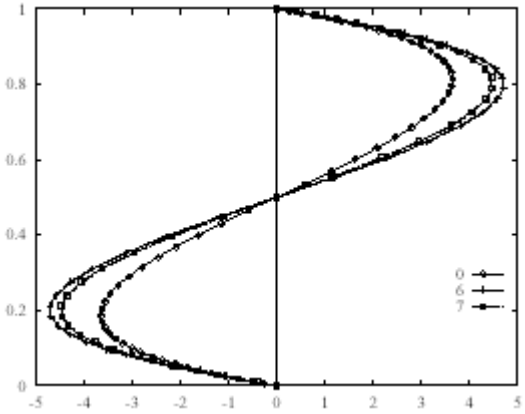

Sl. 5. *Nenewtonska tekočina kot Maxwellova zgornje konvektivna viskoelastična tekočina (B). Hitrostni profili v_x vzdolž navpične črte skozi geometrijsko središče kotanje.*

Fig. 5. *Non-Newtonian fluid as Maxwell upper-convected viscoelastic fluid (B). Velocity profiles v_x along a vertical line through the center of cavity.*

(0 : λ_1=0; 6 : λ_1=0,06 in/and 7 : λ_1=0,07)

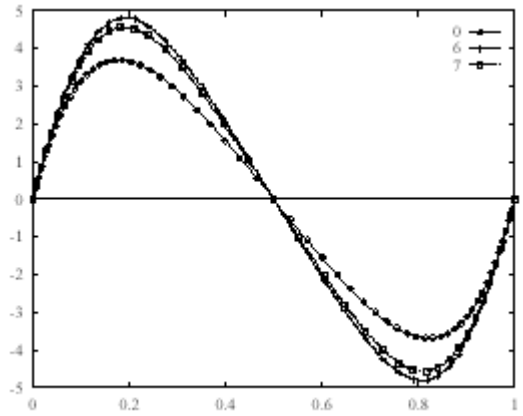

Sl. 6. *Nenewtonska tekočina kot Maxwellova zgornje konvektivna viskoelastična tekočina (B). Hitrostni profili v_y vzdolž vodoravne črte skozi geometrijsko središče kotanje.*

Fig. 6. *Non-Newtonian fluid as Maxwell upper-convected viscoelastic fluid (B). Velocity profiles v_y along a horizontal line through the center of cavity.*

(0 : λ_1=0; 6 : λ_1=0,06 in/and 7 : λ_1=0,07)

v primeru zgornje konvektivnega reološkega modela. V reološkem modelu (12) se ob Stokesovem odvodu dodatnega napetostnega tenzorja oziroma tenzorja gostote toka gibalne količine pojavi dodaten člen, ki opravlja prenos gibalne količine na način, ki ga lahko enačimo z raztezno - obračalnim mehanizmom v prenosni enačbi vrtinčnosti (21).

V preglednici 1 je prikazana primerjava vrednosti povprečnega Nusseltovega števila $\overline{Nu}$ za

viscoelasticity in the case of the upper-convected rheological model. For the rheological model (12), not only the Stokes derivative of the extra-stress tensor is acting, but also an extra term is employed, adding the momentum transport similar to the twisting and stretching mechanism of exchange in the vorticity transport equation (21).

Table 1 shows the comparison of the values of the average Nusselt number $\overline{Nu}$ for the Newtonian

newtonsko tekočino in za različne vrednosti napetostnega relaksacijskega časa (λ_1) pri izbranih Maxwellovih reoloških modelih nenewtonske tekočine.

6.2 Tok v kanalu oblike Z

Kot drugi numerični primer smo preučili tok viskoelastične tekočine v zavitem kanalu oblike Z. Uporabljeni reološki model je Maxwellov zgornje konvektivni model (B). Izbran testni primer je zapletena kombinacija vstopno - izstopnega problema, ostrih robov in dodatnih nelinearnosti zaradi modeliranja toka nenewtonske tekočine. Slika 7 prikazuje geometrijsko obliko kanala z robnimi pogoji. Pri vstopu v kanal smo predpisali razviti profil laminarnega toka s povprečno hitrostjo 1,0 m/s $\left(\bar{v}_{in}=1{,}0 \;\; m/s\right)$. Pri izstopu smo definirali izstopne robne pogoje. Trdne stene zaznamujejo brezzdrsni robni pogoji neprepustnega roba.

fluid and for different values of the relaxation time (λ_1) in the case of the Maxwell non-Newtonian rheological models.

6.2 Flow in Z channel

As a second numerical example, the flow of a viscoelastic fluid in a bent channel with a Z shape is examined. The Maxwell upper-convected rheological model (B) was selected. Flow in a bent channel represents a complicated combination of the inlet-outlet problem, sharp edges, and extra nonlinearities as result of viscoelastic non-Newtonian fluid flow. The geometry of the channel with the boundary conditions prescribed is shown in Fig. 7. At the inlet to the channel, a laminar parabolic velocity profile with an average velocity of 1.0 m/s $\left(\bar{v}_{in}=1.0 \;\; m/s\right)$ was prescribed. At the outlet, outlet velocity conditions were given. At the solid walls a no-slip velocity condition was specified.

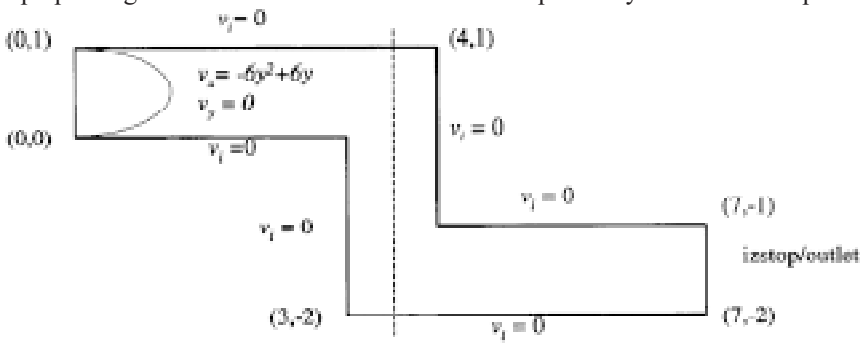

Sl. 7. *Kanal oblike Z. Geometrija in robni pogoji*
Fig. 7. *Flow in Z channel. Geometry and boundary conditions*

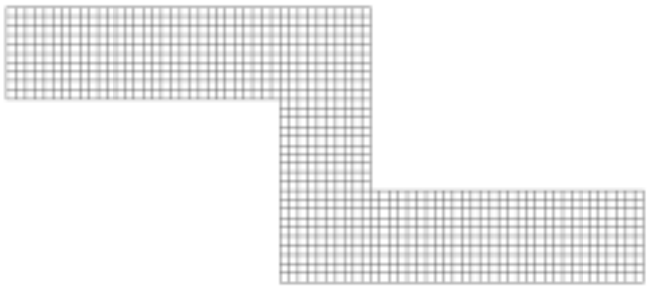

Sl. 8. *Računska mreža pri modeliranju toka viskoelastične tekočine v kanalu oblike Z*
Fig. 8. *Computational mesh for simulation of viscoelastic fluid in Z channel*

Sl. 9. *Tok nenewtonske viskoelastične tekočine v kanalu oblike Z modelirane z zgornje konvektivnim Maxwellovim reološkim modelom (λ_1=0,06); tokovnice (levo) in izočrte vrtinčnosti (desno)*
Fig. 9. *Non-Newtonian viscoelastic fluid flow in Z channel. Upper-convected Maxwell rheological model with (λ_1=0.06); streamlines (left) and vorticity lines (right)*

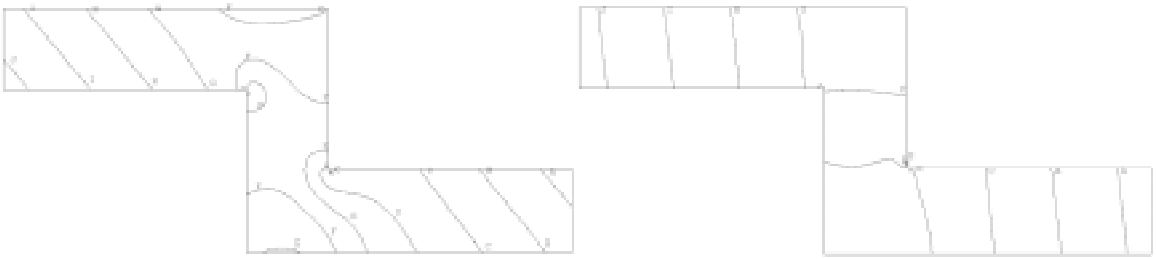

Sl. 10. *Primerjava tlačnih polj v kanalu oblike Z. 0 : λ_1=0 (desno) in 6 : λ_1=0,06 (levo)*
Fig. 10. *Comparison of pressure fields in Z channel. 0 : λ_1=0 (right) and 6 : λ_1=0.06 (left)*

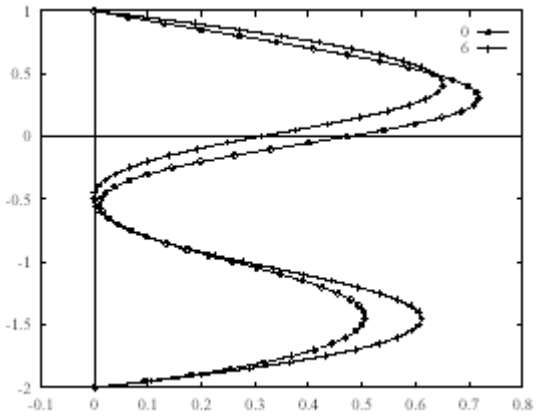

Sl. 11. *Profil hitrosti v_x vzdolž navpičnice skozi središčno točko geometrije kanala*
Fig. 11. *Velocity profile v_x along a vertical line through the center of the channel (0 : λ_1=0 in/and 6 : λ_1=0,06)*

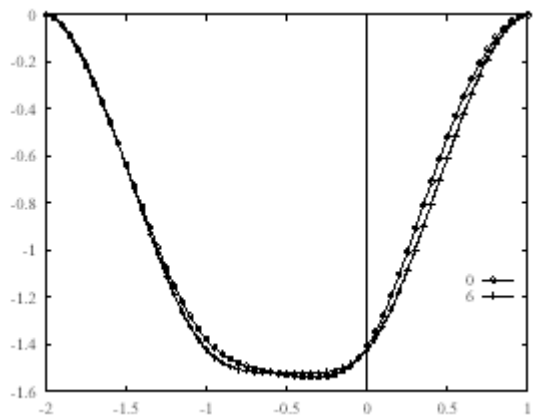

Sl. 12. *Profil hitrosti v_y vzdolž navpičnice skozi središčno točko geometrije kanala*
Fig. 12. *Velocity profile v_y along a vertical line through the center of the channel (0 : λ_1=0 in/and 6 : λ_1=0,06)*

Enakomerno računsko mrežo je sestavljalo 200 robnih elementov in 900 notranjih celic. Prikazana je na sliki 8.

Reynoldsovo število in Weissenbergovo število sta definirani kot:

$$Re = \frac{\bar{v}_{out} L}{\nu} \tag{59}$$

$$We = \frac{\lambda_1 \bar{v}_{out}}{L} \tag{60}$$

kjer sta ν in λ_1 kinematična viskoznost tekočine in napetostni sprostitveni čas ter je $(\bar{v}_{out})$ karakteristična hitrost (povprečna izstopna). Karakteristična linearna izmera L pomeni polovico višine izstopne odprtine. V skladu z navedenimi definicijami je tok v kanalu blizu Stokesovemu z vrednostjo Reynoldsovega števila Re = 0,7. Vrednost Weissenbergovega števila, odločilnega za konvergenco numeričnega algoritma, je znašala We = 0,12. Vse izračune smo ponovno izvedli kot ustaljene, pri čemer smo prehodni pojav simulirali z zelo velikim časovnim korakom ($\Delta t = 10^{16}$). Podsprostitev smo definirali s podsprostitvenim parametrom ϑ, ki je znašal v primeru simulacije newtonskega toka ϑ = 0,01 in v primeru nenewtonskega toka ϑ = 0,001. Konvergenčni kriterij je bila kot vedno napaka v velikosti $\varepsilon = 10^{-6}$.

Sliki 11 in 12 prikazujeta profile hitrosti v_x in v_y vzdolž navpičnice skozi središčno točko geometrijske

A uniform computational mesh consists of 200 boundary elements and 900 internal cells. It is shown in Fig. 8.

The Reynolds and Weissenberg numbers were defined according to convention as:

where ν and λ_1 are the fluid kinematic viscosity and the relaxation time, respectively, and $(\bar{v}_{out})$ is a characteristic velocity (average at the outlet). A characteristic linear dimension L is defined as half of the outlet opening. Throughout the channel, creeping flow was assumed with Re = 0.7. The value of the Weissenberg number, which is crucial for achieving the stability of the numerical alghoritm according to the literature, was chosen to be We = 0.12. All the simulations were again performed as steady with a large time step ($\Delta t = 10^{16}$). Underrelaxation was defined with the underrelaxation parameter ϑ set to ϑ = 0.01 in the case of Newtonian flow and ϑ = 0.001 in the case of non-Newtonian flow. The convergence criterion was selected as $\varepsilon = 10^{-6}$.

Figs. 11 and 12 show the velocity profiles v_x and v_y along a vertical line through the center of the

oblike kanala. Primerjamo tok newtonske tekočine ($\lambda_1 = 0$) s tokom viskoelastične tekočine (Maxwellov zgornje konvektivni model) pri vrednosti ($\lambda_1 = 0{,}06$). Slika 10 kaže primerjavo tlačnih polj omenjenih tokov.

6.3 Tok v simetričnem kanalu z nenadno zožitvijo 4:1

Predstavljeni numerični algoritem smo testirali tudi na vstopno-izstopnem problemu toka viskoelastične tekočine v simetričnem kanalu z nenadno zožitvijo 4:1, katerega geometrijska oblika je predstavljena na sliki 13.

channel. A comparison of the Newtonian fluid flow ($\lambda_1 = 0$) and the non-Newtonian viscoelastic fluid flow (Maxwell upper-convected model) at ($\lambda_1 = 0.06$) is shown. Fig. 10 presents the pressure fields in both cases.

6.3 Flow in a 4:1 planar sudden-contracted channel

The developed numerical alghoritm was tested for the test case of analysing the inflow-outflow viscoelastic fluid problem in a planar channel with a 4:1 sudden contraction. A detailed presentation of the flow geometry is given in fig. 13.

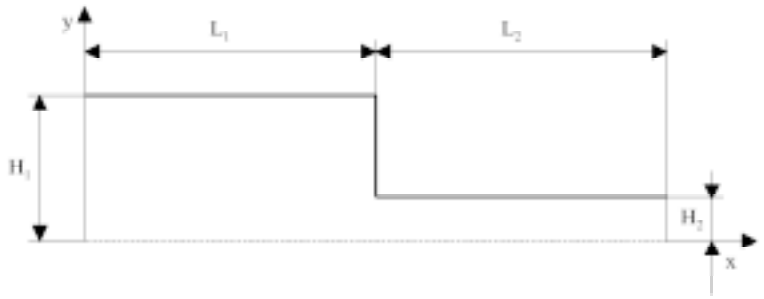

Sl. 13. *Kanal z nenadno 4:1 zožitvijo*
Fig. 13. *Channel with a 4:1 abrupt contraction*

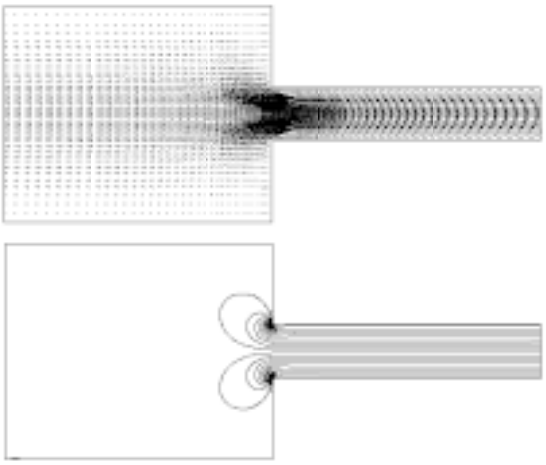

Sl. 14. *Kanal z nenadno 4:1 zožitvijo. Vektorji hitrosti (zgoraj) in vrtinčno polje (spodaj)*
Fig. 14. *Channel with a 4:1 abrupt contraction. Velocity vectors (above) and vorticity field (below)*

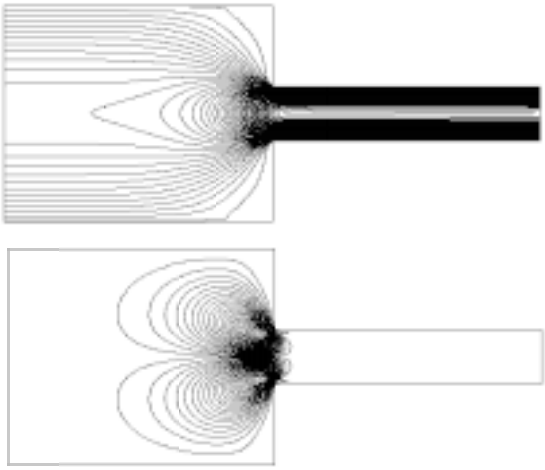

Sl. 15. *Kanal z nenadno 4:1 zožitvijo. Izočrte hitrosti v smeri koordinatne osi x (zgoraj) in izočrte hitrosti v smeri koordinatne osi y (spodaj)*
Fig. 15. *Channel with a 4:1 abrupt contraction. Velocity lines in coordinate direction x (above) and velocity lines in coordinate direction y (below)*

Oba dela kanala (vstopni in izstopni) merita v dolžino $L_1 = L_2 = 10H_2$, kar zadošča za popolno razvitje hitrostnega profila. Tokovne razmere v kanalu podobne geometrijske oblike so podrobno predstavljene v [6]. Izmera H_2 je določena kot polovica višine izstopnega kanala ($H_2 = 0{,}125$). Reynoldsovo število in Weissenbergovo število sta definirani enako kakor v prejšnjem primeru. Tok v kanalu je zelo blizu Stokesovemu z vrednostjo Reynoldsovega števila *Re*

The inlet and outlet lengths were both $L_1 = L_2 = 10H_2$ to ensure fully developed flows in these regions. The flow field in a channel of similar geometry is described in detail in [6]. The dimension H_2 is defined as the half-width of the downstream channel ($H_2 = 0.125$). The Reynolds and Weissenberg numbers are defined as in the previous case. Throughout the channel, almost creeping flow was assumed with $Re = 0.001$. The

= 0,001. Vrednosti Weisenbergovega števila smo spreminjali od $We = 6{,}4\times10^{-3}$ ($\lambda_1 = 0{,}1$) do $We = 51{,}2\times10^{-3}$ ($\lambda_1 = 0{,}8$), kar je podobno navedenemu v [1].

Za numerično modeliranje smo uporabili diskretizacijo, sestavljeno iz 560 neenakih notranjih celic, zgoščenih okoli ostrih vogalov pri zožitvi kanala. Pri vstopu v kanal smo predpisali razviti parabolični profil laminarnega toka s povprečno hitrostjo 0,002 m/s $\left(\overline{v}_{in} = 0{,}002\ \ m/s\right)$. Ta vrednost ustreza izstopnemu paraboličnemu profilu z $\left(\overline{v}_{out} = 0{,}008\ \ m/s\right)$. Na trdnih stenah smo predpisali brezzdrsne hitrostne robne pogoje. Na začetku modeliranja (t = 0) je bilo računsko območje popolnoma napolnjeno z mirujočo tekočino. Ustaljeno stanje smo modelirali s časovnim korakom ($\Delta t = 10^{16}$), medtem ko je vrednost podsprostitvenega parametra znašala $\vartheta = 0{,}01$. Konvergenčni kriterij smo nastavili na $\varepsilon = 10^{-6}$.

Sliki 14 in 15 prikazujeta vektorsko polje hitrosti, polje vrtinčnosti ter izočrte hitrosti v koordinatnih smereh x in y v ustaljenem stanju viskoelastičnega toka λ_1 = 0,8 za Re = 0,001 in $We = 51{,}2\times10^{-3}$.

7 SKLEP

V prispevku je predstavljena metoda robnih elementov za modeliranje toka viskoelastične tekočine. Različni Maxwellovi modeli prikazujejo široko uporabnost MRE. Kljub dodatnim nelinearnim izvirnim členom razvita shema ohranja vse prednosti modeliranja nestisljivih viskoznih tokov z MRE [5]. Kot testni primer rabijo naravna konvekcija viskoelastične tekočine v zaprti kotanji, tok v kanalu oblike Z in tok v kanalu z nenadno zožitvijo 4 : 1. Na podlagi rezultatov ugotavljamo, da je razvita shema stabilna in natančna.

Weissenberg number varied from $We = 6.4\times10^{-3}$ ($\lambda_1 = 0.1$) to $We = 51.2\times10^{-3}$ ($\lambda_1 = 0.8$), similar to [1].

The computational mesh used for the simulations consisted of 560 non-uniform internal cells refined around the sharp corner of the inlet to the exit channel. At the inlet to the main channel the laminar parabolic velocity profile with an average velocity of 0.002 m/s $\left(\overline{v}_{in} = 0.002\ \ m/s\right)$ was prescribed corresponding to the outlet parabolic velocity profile with $\left(\overline{v}_{out} = 0.008\ \ m/s\right)$. At the solid walls a no-slip velocity condition was specified. At the beginning of the simulation (t = 0) the computational domain was filled with quiescent fluid. The steady state was modeled with the time step ($\Delta t = 10^{16}$), and with the underrelaxation parameter set to ϑ = 0.01. The convergence criterion was selected as $\varepsilon = 10^{-6}$.

Figs. 14 and 15 show the velocity vector field, the vorticity field and the velocity isolines in both coordinate directions x and y in the steady state of the viscoelastic non-Newtonian upper-convected Maxwell fluid flow $\lambda_1 = 0.8$ for $Re = 0.001$ and $We = 51.2\times10^{-3}$.

7 CONCLUSIONS

The boundary-domain integral approach to the solution of viscoelastic fluid motion problems is presented. Different Maxwell fluid models are used to show the applicability of the proposed BEM model. All the attractive features of the BEM model, based on the application of different fundamental solutions already established in viscous fluid dynamics, are preserved [5]. The numerical scheme is verified using test cases of a viscoelastic fluid's natural convection flow, viscoelastic flow through the Z channel, and a 4 : 1 abrupt-contraction-channel viscoelastic flow. The computational results show that the scheme is stable and accurate.

8 LITERATURA
8 REFERENCES

[1] Aboubacar, M., M.F. Webster (2001) A cell-vertex finite volume/element method on triangles for abrupt contraction viscoelastic flows. *J. Non-Newtonian Fluid Mech.*, 98, 83-106.

[2] Davis, G.D.V., I.P. Jones (1983) Natural convection in a square cavity: A comparison exercise. *Int. Jou. for Num. Meth. in Fluids*., 3, 227-248.

[3] Davis, G.D.V. (1983) Natural convection of air in a square cavity: A bench mark numerical solution. *Int. Jou. for Num. Meth. in Fluids*., 3, 249-264.

[4] Dou, H., N.P. Thien (1999) The flow of an Oldroyd-B fluid past a cylinder in a channel: adaptive viscosity vorticity (DAVSS-ω) formulation*; J. Non-Newtonian Fluid Mech*., 87, 47-73.

[5] Hriberšek, M., L. Škerget (1999) Fast boundary-domain integral algorithm for computation of incomprešible fluid flow problems. *Int. J. Num. Meth. Fluids*., 31, 891-907.

[6] Oliveira, P.J., F.T. Pinho (1999) Plane contraction flows of upper convected Maxwell and Phan-Thien-Tanner fluids as predicted by a finite-volume method; *J. Non-Newtonian Fluid Mech.,* 88, 63-88.

[7] Škerget, L., A. Alujevič, C.A. Brebbia, G. Kuhn (1989) Natural and forced convection simulation using the velocity-vorticity approach. *Topics in Boundary Element Research*., 5(4), 49-86.

[8] Škerget, L., M. Hriberšek, G. Kuhn (1999) Computational fluid dynamics by boundary-domain integral method. *Int. J. Numer. Meth. Engng.*, 46, 1291-1311.
[9] Wu, J.C. (1982) Problems of general viscous flow. Developments in BEM. *Elsevier Appl. Sci. Publ.,* 2(2).
[10] Wrobel, L.C. (2002) The boundary element method. Vol. 1., Applications in thermo-fluids and acoustics. *Wiley*.

Naslov avtorjev: prof.dr. Leopold Škerget
dr. Matej Požarnik
Fakulteta za strojništvo
Univerza v Mariboru
Smetanova 17
2000 Maribor
leo@uni-mb.si
matej.pozarnik@uni-mb.si

Author's Address: Prof.Dr. Leopold Škerget
Dr. Matej Požarnik
Faculty of Mechnical Eng.
University of Maribor
Smetanova 17
2000 Maribor, Slovenia
leo@uni-mb.si
matej.pozarnik@uni-mb.si

Prejeto: 20.12.2002
Received:

Sprejeto: 31.1.2003
Accepted:

© Strojniški vestnik 48(2002)12,663-676
ISSN 0039-2480
UDK 66.063:66.069.82
Izvirni znanstveni članek (1.01)

© Journal of Mechanical Engineering 48(2002)12,663-676
ISSN 0039-2480
UDC 66.063:66.069.82
Original scientific paper (1.01)

Metode prepoznave poplavnega stanja pri aeraciji v posodi s turbinskim mešalom

Flooding-Recognition Methods in a Turbine-Stirred Vessel

Andrej Bombač - Iztok Žun

V prispevku so obravnavane nekatere metode, s katerimi lahko na različne načine zaznamo poplavno stanje pri dispergiranju plina v kapljevino v posodi z enojnim Rushtonovim mešalom. To so metode merjenja splošnih veličin, npr. najmanjša moč mešala in največji prirastek plinaste faze ter metoda zaznave lokalnih karakteristik faznega stika. Preskus je potekal pri dispergiranju zraka v vodo ter delno pri dispergiranju zraka v vodno raztopino karboksi-metil-celuloze (KMC) različnih koncentracij. Prikazani sta medsebojna primerjava rezultatov ter primerjava z rezultati kriterijev drugih avtorjev.

(Ključne besede: mešala turbinska, stanja poplavna, metode prepoznavanja, dispergiranje zraka)

This article paper presents some appropriate methods for flooding detection by the dispersion of gases into liquids in a stirred vessel equipped with a single Rushton turbine. These methods are based on measurements of global properties, such as mixing-power minimum and gas-holdup maximum, and a method based on the local interfacial characteristics of two-phase systems. The experiments were performed by dispersing air into water and air partly into water-carboxy-methyl cellulose (CMC) solutions of different concentrations. A comparison of the results of the different methods is shown, as well as a comparison with the results from criteria found in the literature.

(Keywords: turbine-stirred vessel, flooding, recognition methods, air dispersion)

0 UVOD

Pri dispergiranju plina v kapljevino v posodi z mešalom nastajajo na lopaticah mešala plinske votline, ki so osnovni mehanizem dispergiranja. V odvisnosti od količine dovedenega plina (q) in vrtilne frekvence mešala (n) ter od prenosnih lastnosti kapljevine nastajajo na lopaticah mešala različne strukture plinskih votlin. Z večanjem pretoka zraka pri stalni vrtilni frekvenci mešala lahko nastanejo naslednje strukture plinskih votlin [4]: struktura vrtinčno oprijemajočih se plinskih votlin (*VC*), struktura z eno veliko plinsko votlino (*1L*), struktura z dvema velikima plinskima votlinama (*2L*), struktura s tremi velikimi plinskimi votlinami (*S33*), struktura s tremi majhnimi in tremi velikimi plinskimi votlinami (*L33*) ter struktura raztrganih plinskih votlin (*RC*). Po viru [9] poteka dispergiranje na industrijskih napravah večinoma v režimu velikih plinskih votlin, tako da je pomembno poznavanje hidrodinamičnega režima, pri katerem lahko napovemo poplavno stanje. Po splošni definiciji poplavnega stanja, ki jo zasledimo v literaturi, je poplavno stanje predstavljeno kot prehod v neučinkovito delovanje mešala pri dispergiranju plina. Tako se z vidika struktur plinskih voltin pojavi poplavno stanje takrat, ko je na

0 INTRODUCTION

In the dispersing of air into water using stirrers in a mixing vessel, gas-filled cavities are formed behind each blade of the impeller, which represents the basic mechanism of dispersal. Depending on the air flow rate (q) and impeller rotational frequency (n), as well as liquid transport properties, various different gas-filled cavity structures are formed. By increasing the air flow rate at a constant impeller speed the following structures [4] can be formed: a vortex-clinging (*VC*) structure, a structure with one large cavity (*1L*), a structure with two large cavities (*2L*), a small '3-3' (*S33*) structure, a large '3-3' (*L33*) structure and ragged cavities (*RC*). According to Smith [9], dispersal with industrial-scale reactors mostly takes place in the large cavity regime, so the prediction of hydrodynamic regimes at which flooding occurs is of great importance. The general definition of flooding is often described in the literature as a transition to the unsatisfactory operation of an impeller in a gas-liquid system. Flooding occurred when an *RC* structure was detected in a particular location. Otherwise, flooding corresponded to the

opazovanem mestu zabeležena struktura raztrganih plinskih votlin, poplavno stanje pa je označeno z ustreznim hidrodinamičnim režimom (n_F, q_F).

Prispevek obravnava tri različne najpogosteje uporabljene eksperimentalne metode zaznave poplavnega stanja mešala pri dispergiranju zraka v posodi z Rushtonovim mešalom v vodi in v navidezplastični tekočini (karakteristike faznega stika). To so: metoda največjega prirastka deleža plinaste faze ([8] in [12]), metoda najmanjše moči mešala [7] in metoda zaznave karakteristik faznega stika ([6], [2], [4] in [5]). Iz medsebojne primerjave rezultatov teh metod je ugotovljeno, da je pri enostopenjskem mešalu poplavno stanje moč prepoznati z vsemi tremi metodami, rezultati se dobro ujemajo tudi z napovedanimi vrednostmi kriterijev drugih avtorjev.

1 POSKUS

1.1 Poskusna naprava

Poskus je bil izveden v pokončni valjasti posodi notranjega premera $T = 450$ mm z zaobljenimi robovi in ravnim dnom. V posodi, narejeni iz pleksi stekla, so bili osno simetrično nameščeni štirje motilniki toka, uporabljeno je bilo Rushtonovo mešalo s šestimi lopaticami. Shematski prikaz je podan na sliki 1. Uporabljeni so bili: demineralizirana voda, vodna raztopina KMC ter stisnjen zrak iz pnevmatskega voda pri sobni temperaturi. Podrobnejši opis geometrijskih parametrov mešalne posode in mešala je prikazan v delih [3] in [4].

hydrodynamic regimes marked with n_F and q_F, where the impeller was no longer capable of dispersing all of the introduced air.

The purpose of this article is to present three different experimental methods of impeller-flooding recognition by air dispersing into water and air dispersing into a pseudoplastic fluid (interfacial characteristics) in a stirred vessel with a single Rushton turbine. These methods are: maximal gas holdup ([8] and [12]), minimal mixing power [7] and local detection of interfacial characteristics ([6], [2], [4] and [5]). Based on a comparison of the results of the given methods with single-impeller stirring it was found that the flooding state was easily recognized with all three methods. The results were in good agreement with the predicted data from the literature.

1 EXPERIMENT

1.1 Experimental setup

An experiment was performed in a cylindrical flat-bottomed Perspex vessel of diameter 450 mm with rounded edges and four baffles mounted perpendicularly to the vessel wall. A Rushton disk impeller with six blades was used. Demineralized water, a water solution of CMC and compressed air at room temperature were used in all experiments. The geometric details of the vessel and the impeller can be found elsewhere [3] and [4].

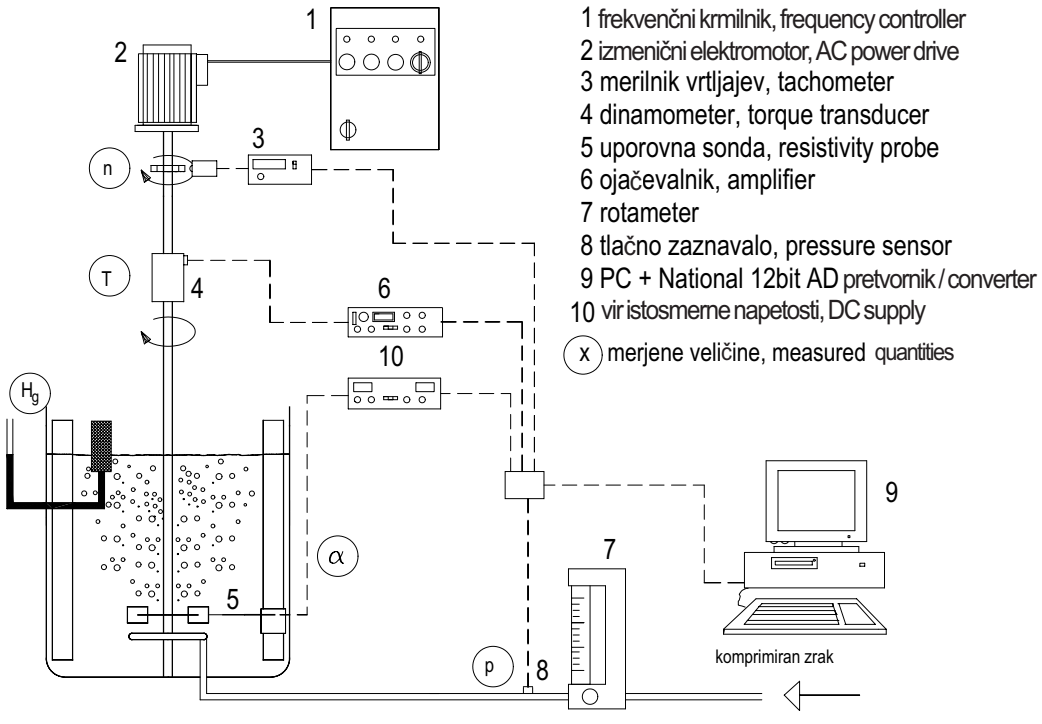

Sl. 1. *Merilna proga*
Fig. 1. *Experimental setup*

1.2 Merilna proga

Merilna proga je prikazana na sliki 1. Pogonski elektromotor je bil krmiljen s frekvenčnim krmilnikom, vrtilna frekvenca mešala je bila merjena s števnikom impulzov, ki deluje na načelu odboja lastnega signala z razredom točnosti 0,1. Vrtilni moment gredi je bil merjen z dinamometrom razreda točnosti 1, prostorninski pretok zraka z rotametrom razreda točnosti 2, z upoštevanjem poprave tlaka. Za omogočanje meritev večjih pretokov zraka sta bila vzporedno vezana dva rotametra. Celotni prirastek plinaste faze (α_g) je bil merjen po načelu, opisanem v delu [8], prikazano na sliki 1. Zaznavalo gladine je bil nameščen na 2/3 radija posode.

Za obratovalne pogoje preskusne naprave so pri danih omejitvenih pogojih in točnosti merilne opreme izračunane tudi relativne napake naslednjih veličin [10]: največja merilna napaka momenta 16,1% (pri najnižjih vrtljajih), merilna napaka merjenja vrtilne frekvence 0,5%, relativna napaka merjenja temperature 0,5 %, relativna napaka merjenja tlaka s tlačnim zaznavalom 2%, relativna napaka Froudovega števila 1%, relativna napaka pretočnega števila 1,1% in relativna napaka globalnega deleža plinaste faze, manjša od 5%.

1.3 Metode zaznave poplavnega stanja

Za vse v nadaljevanju opisane metode je veljal enoten kriterij izvajanja meritev, po katerem so bile iskane veličine izmerjene pri nespremenljivi vrtilni frekvenci mešala (n_i = konst) in postopnim majhnim povečevanjem pretoka zraka (q_1, q_2, q_3,...q_{k-1}, q_k). Pri vsaki nastavitvi (n_i, q_j), potem ko se je popolnoma razvil tok, so bile izmerjene višina gladine v posodi ($H_{g,i}$), moč mešala pri dispergiranju ($P_{g,i}$) ter strukturna funkcija ($M_{p,i}$). Pri nastavitvi na višjo vrtilno frekvenco mešala n_2, je bil postopek ponovljen.

1.3.1 Metoda zmanjšanja moči

Moč je bila izračunana iz izmerkov vrtilne frekvence in zaviralnega momenta mešalne osi. Na splošno se z večanjem pretoka plina pri dispergiranju moč mešala zmanjšuje in doseže najnižjo vrednost tik pred nastankom poplavnega stanja. Pri nastanku poplavnega stanja se moč mešala poveča, (sl. 2), kar so v svojih delih opisali ([7] ter [6]). Tako lahko poplavno stanje prepoznamo iz odvisnosti razmerja moči π (P_g/P), ki se ob nastanku poplavnega stanja izrazito poveča. Tedaj plin mešalo obteka, mešalo pa zajema skoraj v celoti kapljevino, ki rotira znotraj dvigajočega se obročnega dvofaznega toka. Posledično se to kaže s povečanjem moči mešala. Takšen hidrodinamičen režim, pri katerem je zaznano poplavno stanje »označimo« kot (q_F, n_F), določeno posredno pri tisti vrednosti $(\pi_i)_F$, ko je bilo zadoščeno pogoju:

1.2 Measurements

The experimental setup is shown in Figure 1. The AC motor drive was controlled by a frequency controller, the impeller speed was measured with an infrared reflection counter of accuracy class 0.1. The impeller torque was measured using an in-line, precisely calibrated, HBM torque transducer of accuracy class 1. The volumetric air flow rates were measured by calibrated rotameters of accuracy class 2 , corrected for actual pressure. To enable measurements of larger air flow rates two rotameters were connected in parallel. The measurements of gas holdup (α_g) were based on the change of the liquid height in the vessel using the method described in work of [8], see Figure 1. A level sensor was located at 2/3 of the tank radius.

The relative errors of the measured quantities were calculated for the working conditions of the experimental setup as follows [10]: maximum relative error of the torque at the lowest impeller speed was 16.1%, the relative error of the rotational speed was 0.5%, the relative error of temperature was 0.5%, the relative error of pressure was 2%, the relative error of the Froude number was 1%, the relative error of the Flow number was 1.1% and the relative error of the global gas holdup was less than 5%.

1.3 Flooding-recognition methods

For all the experimental methods described below the properties being investigated were always measured using the same principle. At a constant rotational impeller speed (n_i = const) the surface level ($H_{g,i}$), the gassing mixing power ($P_{g,i}$) and the structural function ($M_{p,i}$) with successive small increases in air flow rate (q_1, q_2, q_3,...q_{k-1}, q_k) were taken. At each setting of (n_i, q_j) after a fully-developed regime was achieved, $H_{g,i}$ and $P_{g,i}$ were measured or $M_{p,i}$ recorded. After increasing the impeller speed to n_2, the procedure was repeated.

1.3.1 Minimum mixing power

The mixing power was calculated based on the rotational impeller speed and the mixing torque. In general, increasing the gas flow rate during dispersion reduces the mixing power and achieves the lowest value just before flooding occurs. When the impeller is flooded the mixing power increases, as shown in Figure 2, and described elsewhere [7], [6]. With this principle the power ratio curve described as $\pi = P_g/P$ can be used for flooding recognition. In such a regime the gas remains undistributed, the impeller is filled with liquid rotating inside an annular two-phase flow, which rises around the mixing shaft towards the free surface. Consequently, an increase in the mixing power takes place. The flooding regime (q_F, n_F) was determined indirectly by such a value of $(\pi_i)_F$ that fits the given condition:

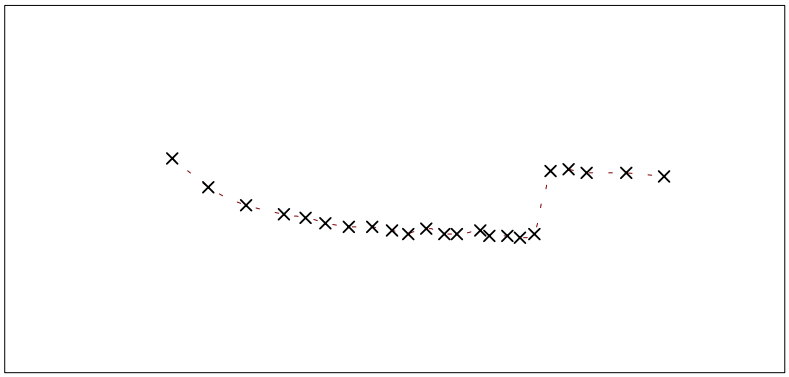

Sl. 2. *Odvisnost razmerja moči od vrtilne frekvence mešala pri nastanku poplavnega stanja*
Fig. 2. *Power ratio vs. impeller rotational frequency*

$$\frac{\pi_i - \pi_{i-1}}{Fl_i - Fl_{i-1}} \geq c_F \quad (1),$$

kjer so bile predhodno izmerjene vrednosti razmerij moči ($\pi_1, \pi_2, \pi_3, \ldots \pi_i \ldots \pi_{k-1}, \pi_k$), pri čemer je $c_F = 2$.

where ($\pi_1, \pi_2, \pi_3, \ldots \pi_i \ldots \pi_{k-1}, \pi_k$) were previously measured power ratios, and $c_F = 2$.

1.3.2 Celotni delež plinaste faze

Celotni delež plinaste faze je bil podan z razmerjem med prirastkom prostornine zaradi vnesene plinaste faze in celotno prostornino dvofaznega sistema, kar je lahko za posodo nespremenljivega prereza prevedeno v razmerje višin:

1.3.2 Maximum gas holdup

Global gas holdup was defined by the ratio between the gas phase and the liquid phase volume that can be transformed into a ratio of heights as follows:

$$\alpha_g = \frac{H_g - H}{H_g} \quad (2),$$

kjer pomenijo: H_g – višino gladine dvofaznega sistema pri dispergiranju in H – višino gladine vode pri mešanju brez dovajanja zraka. S povečevanjem vnosa plina v posodo se viša tudi gladina dvofaznega sistema do neke mejne vrednosti, ki je povzročena z nastankom poplavnega stanja. Pri prehodu iz dispergirnega v poplavno stanje se pojavi opazno znižanje gladine, kakor je prikazano na sliki 3. Do te spremembe pride zaradi izrazito nehomogene porazdelitve plinaste faze po prostornini kapljevine, tako v kapljevini pod mešalom ni obtekanja dvofaznega toka. Za določitev hidrodinamičnega režima poplavnega stanja (q_F, n_F) je bil uporabljen kriterij, ko je bilo pri vrednosti $(\alpha_i)_F$ zadoščeno pogoju:

where H_g means the height of the two-phase free surface during dispersion and H is the liquid height in single-phase mixing. Increasing the air flow rate during dispersion increases the gas holdup correspondingly, until flooding occurs. In the flooding transition a remarkable reduction of gas holdup can be seen, as depicted in Figure 3. This change can be explained by the extremely non-uniform distribution of gas in the liquid bulk, where, especially below the impeller, there was no two-phase circulation. The flooding regime (q_F, n_F) was determined indirectly by such a value of $(\alpha_i)_F$ that fits the given condition:

$$\frac{\alpha_i - \alpha_{i-1}}{Fl_i - Fl_{i-1}} \geq \left| c_F \right| \quad (3),$$

vrednosti celotnih deležev plinaste faze ($\alpha_{g,1}, \alpha_{g,2}, \ldots \alpha_i, \ldots \alpha_{g,k-1}, \alpha_{g,k}$) so bile predhodno izmerjene.

where the values ($\alpha_{g,1}, \alpha_{g,2}, \ldots \alpha_i, \ldots \alpha_{g,k-1}, \alpha_{g,k}$) were previously measured.

1.3.3 Metoda karakteristik faznega stika

Mehanizem dispergiranja je tesno povezan s strukturami plinskih votlin na lopaticah mešala [4]. S povečevanjem pretoka zraka se povprečna gostota izstopajočega dvofaznega toka iz mešala manjša, kakor tudi moč mešala, vse dokler se ne pojavi poplavno stanje [13]. Za lokalno zaznavo plinskih votlin za lopaticami mešala je bila že

1.3.3 Interfacial characteristic method

The dispersing mechanism is closely connected with the different structures of gas-filled cavities that are present at the impeller blades, as described in [4]. With increasing the air flow rate the average density of the discharge two-phase flow decreases (as well as the impeller power) until flooding occurs [13]. For local detection of the gas-filled cavity behind the impeller blade a previously

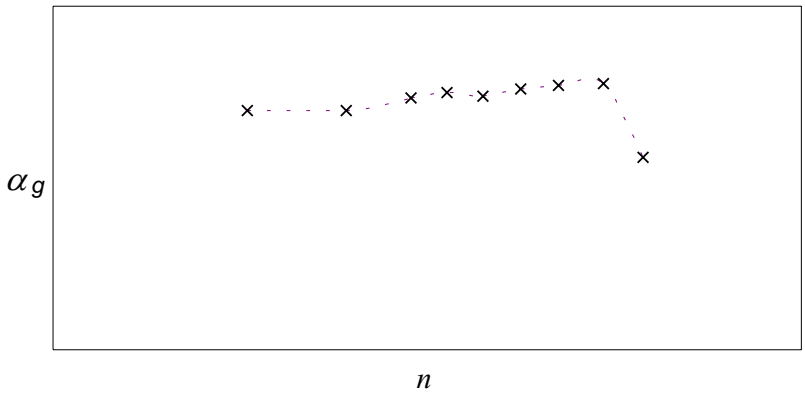

Sl. 3. *Odvisnost celotnega deleža plinaste faze od vrtilne frekvence mešala*
Fig. 3. *Global gas holdup vs. impeller rotational frequency*

poprej razvita preskusna metoda karakteristik faznega stika. Velika razlika v električni upornosti vode in zraka je osnovna lastnost, ki jo z uporovno sondo zaznamo in pomeni odziv sonde v obliki električne napetosti, oziroma ustrezno strukturno funkcijo:

developed experimental method based on local interfacial characteristics was used. A remarkable difference in the electrical resistance of the water and the air is a basic property, which can be detected using a resistivity probe and presented as a probe voltage response or corresponding structural function M_p defined as:

$$M_p(x,t) = \begin{cases} 1, & x \text{ je v fazi / is in phase } p \\ 0, & x \text{ ni v fazi / is not in phase } p \end{cases} \qquad p = \{L, G, S\} \tag{4}$$

kjer so v področju dvofaznega toka na mestu x ter v času t mogoča tri stanja p: L kapljevita faza , G plinasta faza in S stična površina.

Frekvenčna analiza strukturne funkcije M_p z diskretno Fourierjevo preslikavo omogoča prikaz značilnih frekvenc pojavljajoče se plinaste faze. Fourierjevi koeficienti so bili določeni iz:

where in a two-phase flow field three states p are possible at a particular point x at any time t: the liquid phase L, the gas phase G or the phase interface S.

A frequency analysis of the structural function M_p with a discrete Fourier transformation enabled the presentation of the significant frequencies of an appearing gas phase. The Fourier coefficients X_k were obtained from:

$$X_k = \Delta t \sum_{k=0}^{N-1} M_p(t_k) e^{-\frac{j2\pi ik}{N}} \tag{5},$$

kjer pomeni Δt časovni korak med vzorcema diskretne funkcije. Med Fourierjevimi koeficienti X_k, ki se ujemajo s frekvenco $k/(N\Delta t)$, so veljavni le koeficienti med $k = 0$ to $k = N/2 - 1$. Kriterij prepoznave struktur plinskih votlin je podrobneje opisan v delu [4], ter omogoča pri mešanju z Rushtonovim mešalom prepoznavo naslednjih struktur: vrtinčno oprijemajoča struktura plinskih votlin (*VC*), struktura z eno veliko plinsko votlino (*1L*), struktura z dvema velikima plinskima votlinama (*2L*), struktura s tremi velikimi plinskimi votlinami (*S33*), struktura s tremi majhnimi in tremi velikimi plinskimi votlinami (*L33*) ter struktura raztrganih plinskih votlin (*RC*). Značilni vzorci struktur v frekvenčnem prostoru so prikazani na sliki 4. Kakor je videti iz razvoja struktur, je zadnja značilna struktura, struktura raztrganih plinskih votlin, ki pripada poplavnemu stanju. Po viru [11] se stabilna struktura L33 vrne v strukturo šestih simetričnih oprijemajočih se plinskih voltin, pri višjih vrtilnih frekvencah mešala pa se prehod naredi prek strukture s šestimi velikimi plinskimi votlinami enake velikosti, ki so opisane kot silovito vibrirajoče votline oziroma raztrgane votline [7].

where Δt denotes the time interval between successive instants t_i. Among the Fourier coefficients X_k that correspond to the frequency $k/(N\Delta t)$, only the coefficients from $k = 0$ to $k = N/2 - 1$ are meaningful. The criterion for gas-filled cavity-structure recognition was described in detail in [4], as were the recognized structures: a vortex-clinging (*VC*) structure, a structure with one large cavity (*1L*), a structure with two large cavities (*2L*), a small '3-3' (*S33*) structure, a large '3-3' (*L33*) structure and ragged cavities (*RC*). A significant pattern of the structures in a frequency domain is depicted in Figure 4. The last evident structure, as can be seen from the evolution of the frequency domain, is the ragged cavities structure, and corresponds to the flooding state. According to the literature [11] the stable L33 structure reverts to six symmetrical clinging cavities; at higher impeller speeds the transition occurs through a regime with six large cavities of identical size, which are described as violently vibrating, i.e. ragged cavities [7].

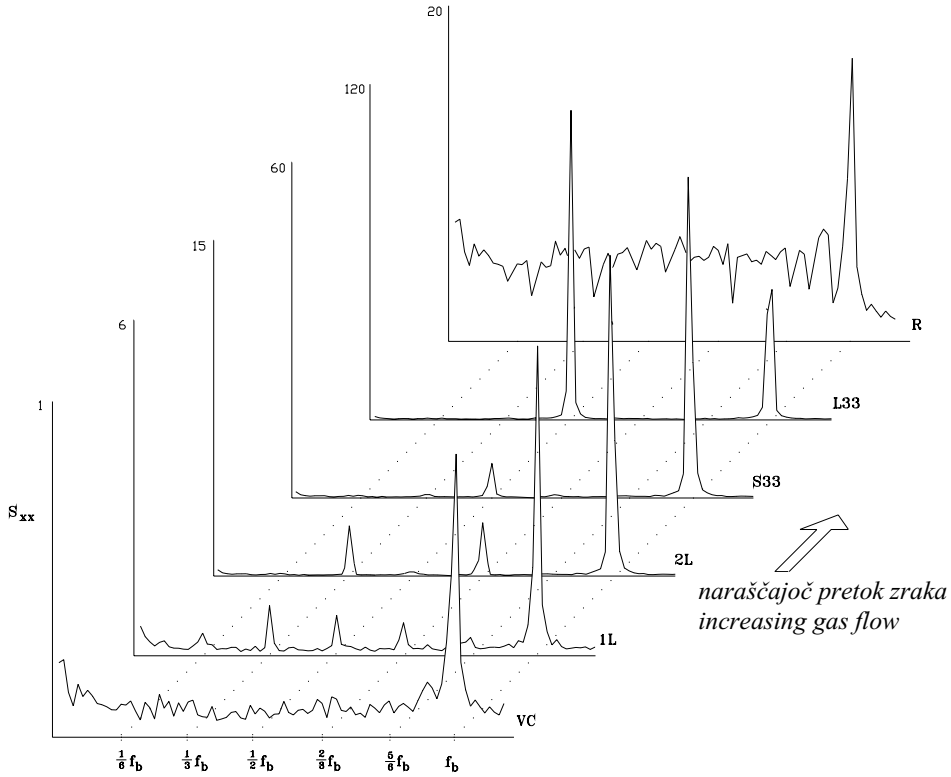

Sl. 4. *Razvoj struktur plinskih votlin ob postopnem večanju pretoka zraka. Poplavno stanje je določeno s pojavom strukture raztrganih plinskih votlin.*
Fig. 4. *Gas-filled cavity structure development with incremental increase of gas flow. Flooding is determined with the appearance of ragged cavity structure.*

2 ANALIZA REZULTATOV IN PRIMERJAVA

2.1 Nastanek poplavnega stanja pri dispergiranju zraka v vodi

2.1.1 Metoda celotnega deleža plinaste faze

Nastanek poplavnega staja je opažen pri tisti vrednosti pretočnega števila, pri kateri se pojavi opazno znižanje gladine dvofaznega sistema, oziroma celotnega deleža plinaste faze. Na podlagi spremembe gladine lahko prepoznamo poplavna stanja le za vrednosti *Fr* od 0,05 do 0,6. Na sliki 5 so prikazane vrednosti α_g pri *Fr* = 0,05 do 0,13 v odvisnosti od *Fl*. Vidno je enakomerno zvečanje deleža plina pri povečevanju vnosa zraka, sledi močno zmanjšanje vrednosti v točki poplavnega stanja. Pri nadaljnjem večanju pretoka zraka se zaradi večjih mehurčkov in večje količine plina v stebru plina okoli mešalne osi gladina lahko znova rahlo zviša, kar pa je z vidika učinkovitosti zaradi zrazito nehomogene porazdelitve plinaste faze neučinkovita operacija. Na sliki 6 so prikazane vrednosti α_g pri *Fr* = 0,2 do 0,6 v odvisnosti od *Fl*. Tudi tu so lepo vidna zmanjšanja vrednosti v točkah poplavnega stanja. Pri večjih vrednostih *Fr*>0,7 je vnesena količina zraka že tako velika, da se pojavlja močno nihanje gladine s 'pljuskanjem' vode, kar je za odbiranje višine gladine nezanesljivo. Tudi

2 RESULTS ANALYSIS AND COMPARISON

2.1 Flooding in air dispersing into water

2.1.1 Maximum gas holdup method

In this method the flooding is detected by the particular flow number, where there is a rapid decrease of surface level or gas holdup. Based on the free-surface level change only flooding states at Froude numbers between 0.05 and 0.6 can be recognized. In Figure 5 the dependence of α_g on *Fl* at given *Fr* = 0.05 to 0.13 is depicted. A reasonable increase of α_g can be seen, with its dependence on the increasing flow number, followed by a rapid reduction of α_g in the flooding regime. With further enlargement of the air input the surface level can be a little higher than that in the flooding state, probably due to large air bubbles that rise upwards to the surface around the mixing shaft like a slug flow. Such an extreme non-homogeneous distribution can be described from the efficiency aspect as an unsatisfactory operation. Depicted in Figure 6 is the dependence of α_g on *Fl* at *Fr* = 0.05 to 0.13. Again a decrease of α_g can be seen in the flooding state. At higher values, at *Fr*>0.7, a waving of the free surface occurred so the relevant readings were no longer possible. Otherwise,

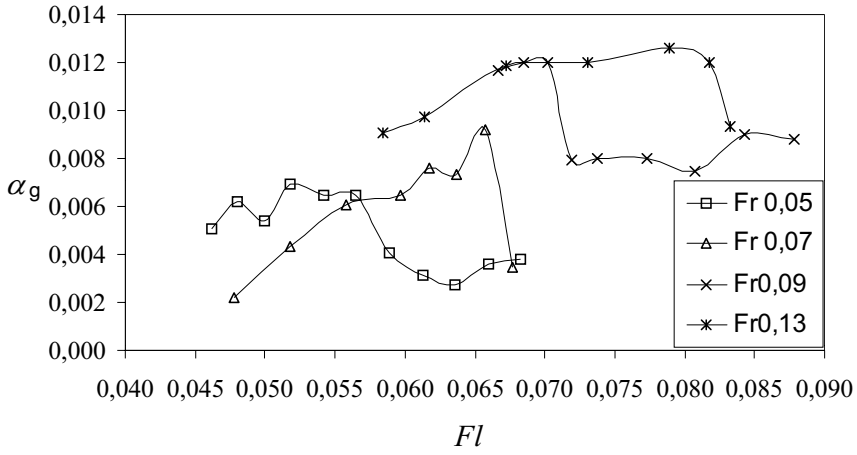

Sl. 5. *Prirastek celotnega deleža plinaste faze v odvisnosti od Froudovega in pretočnega števila*
Fig. 5. *Global gas holdup vs. Froude and Flow number*

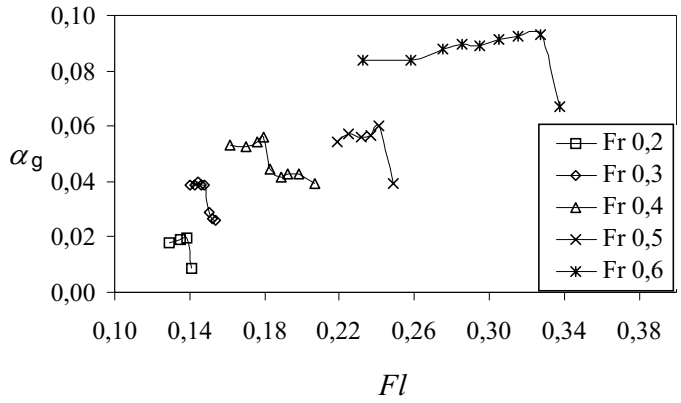

Sl. 6. *Prirastek celotnega deleža plinaste faze v odvisnosti od Froudovega in pretočnega števila*
Fig. 6. *Global gas holdup vs. Froude and Flow number*

sicer pri nastanku poplavnega stanja v mešalniku težko zaznamo gladino dvofaznega sistema, kar se kaže tudi z večjo napako izmerka.

V literaturi [11] in [7] so razmejitvene črte različnih struktur dvofaznih tokov običajno prikazane v tokovni mapi, diagramu, izraženem z brezizmernimi števili *Fr* in *Fl*. V diagramu 7 so vnesene vrednosti, ki ustrezajo prepoznavnim poplavnim stanjem. Razmejitvena črta poplavnega stanja je podana z ustrezno poenostavitveno premico, katere koeficienti so prikazani v preglednici 1.

readings of H_g in all flooding states were difficult to detect precisely, which was reflected in a higher relative error of α_g.

Usually the delineation line between the dispersing and flooding regimes is depicted in a flow regime map expressed with dimensionless *Fr* and *Fl* numbers, such as the one found in the literature [11] and [7]. In Figure 7 all the recognized flooding regimes (n_F, q_F) given by this method are indirectly shown through *Fr* an *Fl* numbers. Based on this data the flooding line is approximated by Equation 6, coefficients k_1 and k_2, and the regression coefficient *r*; all are given in Table 1.

Preglednica 1. *Pripadajoči koeficienti k enačbi [6]*
Table 1: *Corresponding coefficients to Eq. [6]*

metoda method	k_1	k_2	r
celotni prirastek plinaste faze global gas holdup	-0,54	2,1	0,96
najmanjši porast moči minimal mixing power	0,05	1,5	0,97
značilnica faznega stika interfacial characteristics	0,33	1,4	0,96

2.1.2 Metoda zmanjšanja moči

S to metodo so potekale meritve poplavnega stanja pri vrednostih *Fr* od 0,05 do 1,13. Na slikah 8 in 9 so podane tipične krivulje razmerja moči P/P_0, pri katerem je v poplavnem stanju opazno zvečanje razmerja moči. Pri manjših vrednostih *Fr* (0,05, 0,06, 0,07 in 0,09 na sliki

2.1.2 Minimum mixing power

According to this method the measurements were taken at *Fr* numbers from 0.05 to 1.13. Typical curves of the power ratio P/P_0 are depicted in Figures 8 and 9, where a steep increase of the power ratio during the flooding state can be seen. On the other

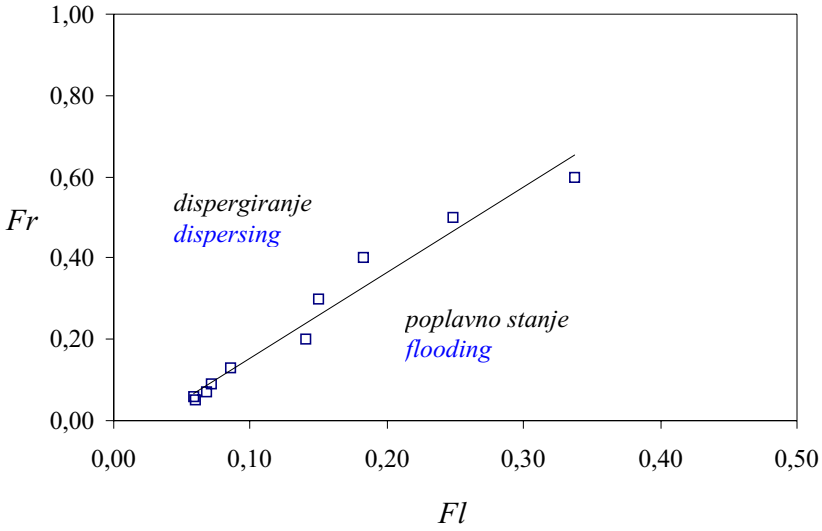

Sl. 7. *Točke poplavnega stanja določene z metodo celotnega deleža plinaste faze v tokovnem diagramu z mejo poplavnega stanja*

Fig. 7. *Flooding points determined by global gas holdup method on a flow chart with approximated flooding limit*

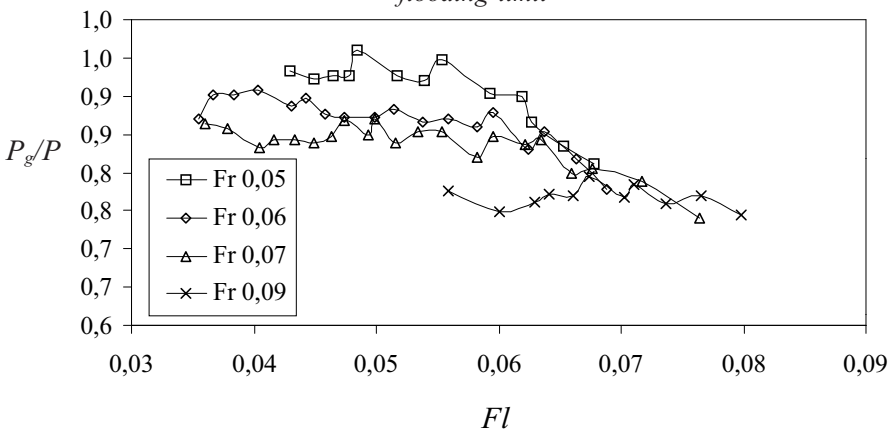

Sl. 8. *Odvisnost razmerja moči od pretočnega števila pri različnih vrednosti Froudovega števila*

Fig. 8. *Power ratio vs. Flow number at different Froude number values*

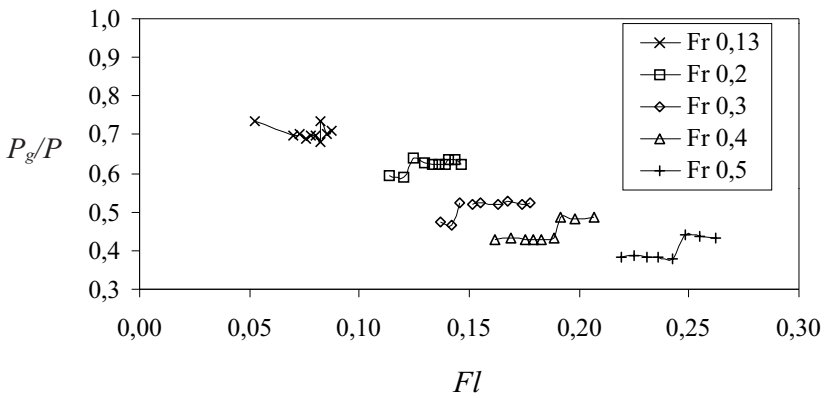

Sl. 9. *Odvisnost razmerja moči od pretočnega števila pri različnih vrednosti Froudovega števila*

Fig. 9. *Power ratio vs. Flow number at different Froude number values*

8) metoda ni dala pomembnih rezultatov. Razlog je lahko v premajhni moči mešala, saj so izmerki vrtilnega momenta mešala enakega velikostnega razreda kakor odstopki merilnika vrtilnega momenta. V diagramu, prikazanem na sliki 11, so podane vse z metodo zmanjšanja moči prepoznane točke poplavnega stanja. Podana je tudi ustrezna razmejitvena premica, katere koeficienta k_1 in k_2 in poenostavitveni koeficient r so prikazani v preglednici 1.

2.1.3 Metoda karakteristik faznega stika

Iz postopnega razvoja značilnih vzorcev struktur plinskih votlin v frekvenčnem prostoru (sl. 4) za vsako nastavitev parametrov hidrodinamičnega režima (n=*konst,* q_j), je lepo razviden nastanek strukture raztrganih plinskih votlin, ki ustreza poplavnemu stanju. Režimi (n_F, q_F), prepoznani kot poplavno stanje, so bili v obliki brezizmernih števil *Fl* in *Fr* vneseni v diagram na sliki 12. Izmerjene vrednosti so predstavljene z ustrezno razmejitveno premico, katere koeficienti so prikazani v preglednici 1.

2.1.4 Medsebojna primerjava rezultatov različnih metod

Pri meritvah so se glede na uporabljeno metodo in merilna oprema pojavile nekatere omejitve. Tako z metodo prirastka deleža plinaste faze ni bilo mogoče določiti poplavnega stanja predvsem pri večjih pretokih zraka, medtem ko z metodo zmanjšanja moči predvsem pri nižjih pretočnih številih. Z metodo karakteristik faznega stika je bilo mogoče prepoznati poplavno stanje v celotnem območju merjenih režimov. Za prepoznavna poplavna stanja, določena z vsemi tremi metodami, so bile izdelane ustrezne razmejitvene premice, podane z enačbo:

hand, this method did not give any relevant results for smaller *Fr* numbers (0.05, 0.06, 0.07 and 0.09 in Figure 8), which can be explained with the very small values of the impeller power and are of the same scale as the dynamometer´s accuracy class. All the recognized flooding regimes are depicted in Figure 11, together with the corresponding correlated delineation line; the appropriate coefficients k_1 and k_2 and the regression coefficient r are given in Table 1.

2.1.3 Interfacial characteristic method

From the coherent development of the structure patterns in a frequency domain, as shown in Figure 4, the appearance of the ragged cavities structure can be found for each hydrodynamic regime set (n=*const,* q_j). The corresponding flooding regimes (n_F, q_F) were collected and are shown in the form of dimensionless *Fr* and *Fl* numbers in a flow regime map, see Figure 12, as well as a flooding line approximated in the form of eq. 2. The corresponding coefficients are given in Table 1.

2.1.4 Comparison of results of different methods

According to the methods used and the measuring instrumentation, some restrictions appeared. Flooding could not be recognized at higher air flow rates with the global-gas-holdup method and at lower gas flow rates with the minimum-mixing-power method. Using the interfacial characteristics method gave relevant recognition of the flooding in all the measured regimes. For all the recognized flooding states with the given methods, the corresponding regression lines were approximated by the equation:

$$Fr_F = k_1 + k_2 \cdot Fl_F \qquad (6).$$

Vrednosti posameznih koeficientov so prikazane v preglednici 1.

Individual values of the coefficients are given in Table 1.

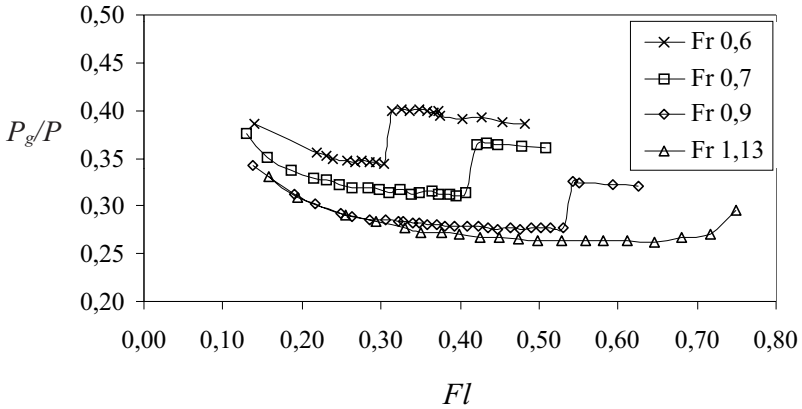

Sl. 10. *Odvisnost razmerja moči od pretočnega števila pri različnih vrednosti Froudovega števila*
Fig. 10. *Power ratio vs. Flow number at different Froude number values*

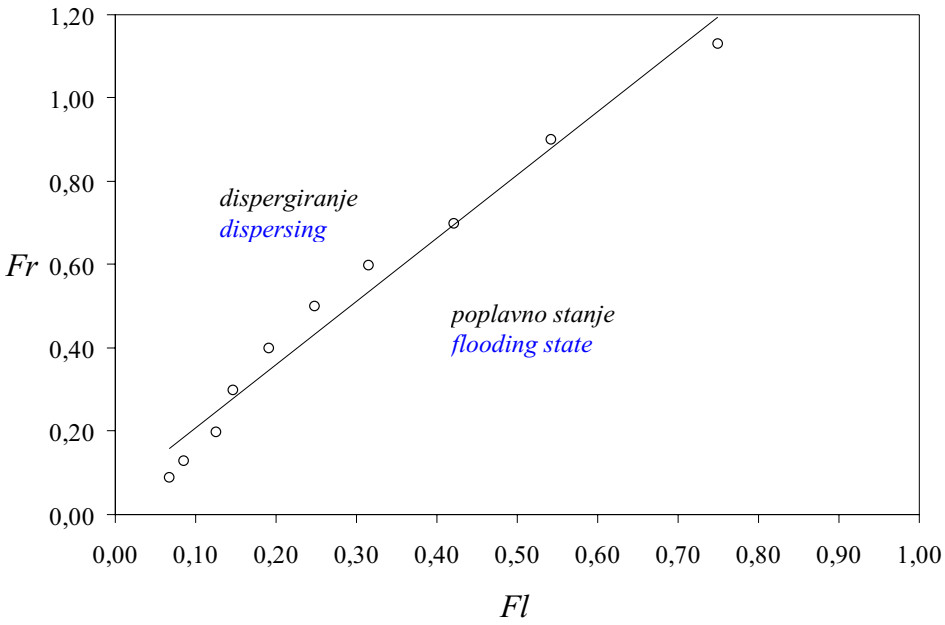

Sl. 11. *Točke poplavnega stanja določene z metodo razmerja moči v tokovnem diagramu z mejo poplavnega stanja*

Fig. 11. *Flooding points determined by power ratio method on a flow chart with approximated flooding limit*

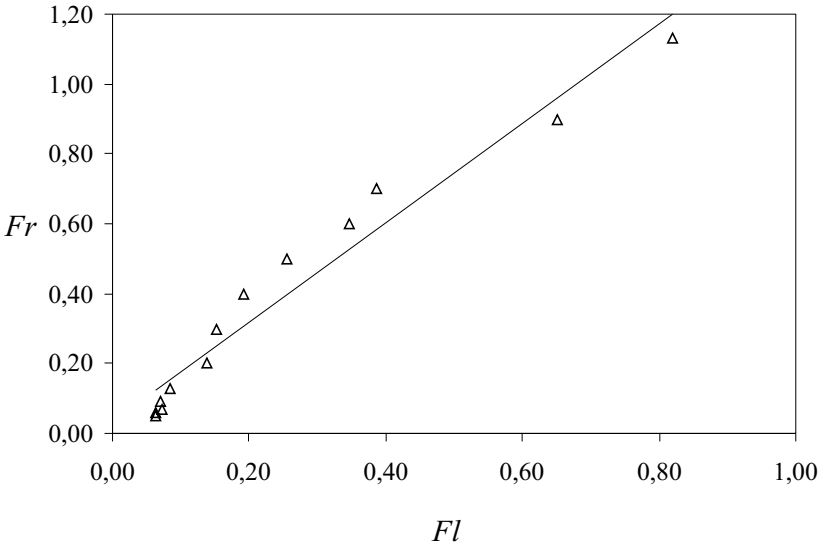

Sl. 12. *Točke poplavnega stanja določene z metodo karakteristik struktur faznega stika v tokovnem diagramu z mejo poplavnega stanja*

Fig. 12. *Flooding points determined by local characteristics method on a flow chart with approximated flooding limit*

Primerjava rezultatov kaže, da so vse tri metode primerne za določitev poplavnega stanja mešala. Pri nižjih vrednosti *Fr* in *Fl* je medsebojno razhajanje manjše med metodami celotnega prirastka deleža plinaste faze in karakteristikami faznega stika. Glede na strmino pripadajočih poenostavitvenih premic je boljše ujemanje med metodama karakteristik faznega stika in najmanjše moči mešanja.

Pri dispergiranju plina z enim mešalom se lokalne spremembe na lopaticah mešala in v neposredni okolici mešala kažejo enoznačno tudi na celotni ravni. Pri poplavnem stanju mešala se torej

A comparison of the results showed that all three methods are suitable for flooding detection. The smallest differences can be seen at the smaller values of *Fr* and *Fl* between the global-gas-holdup method and the interfacial characteristics method. According to the trend, better agreement can be found between the minimum mixing-power and the interfacial characteristics methods.

In gas dispersing with one impeller, the local changes at the impeller blades and in the close vicinity of the impeller affect the global level directly. In impeller flooding the global change is expressed

celotna sprememba izraža kot zmanjšanje celotnega deleža plina oziroma kot povečanje moči mešala. Poraja se vprašanje, ali je mogoče zaznati poplavno stanje pri dispergiranju z dvema mešaloma ali tremi mešali s katerokoli celotno metodo, kar ostaja odprto vprašanje za nadaljnje raziskave.

2.1.5 Primerjava rezultatov z napovedanimi po virih iz literature

Rezultati naših raziskav so bili primerjani tudi z rezultati kriterijev drugih avtorjev, kar je prikazano na sliki 13. Primerjani so le kriteriji, ki obsegajo tudi geometrijska razmerja in velikostni razred reaktorja kakor v naši raziskavi pri dispergiranju z enim Rushtonovim mešalom. Po [12], kriterij izhaja iz meritev prirastka deleža plinaste faze, je meja poplavnega stanja v reaktorju pri D/T = 1/3 definirana z vrtilno frekvneco mešala ter pretokom plina v obliki:

through a reduction of the gas holdup or an increase of the minimum mixing power. The question appears, whether it is possible to detect flooding by dispersing with dual or triple impellers using any of the mentioned global methods? This remains open for further research.

2.1.5 Comparison of the results with those quoted from the literature

The results of our experiments were compared with those based on the correlations of other researchers, as can be seen in Figure 13. Only the criteria including the geometrical ratios between the impeller and the tank diameter and reactor-size scale were taken for a comparison with the experimental results during dispersion with a single Rushton turbine. According to [12], these criteria are derived from global-gas-holdup measurements, a flooding regime at a D/T ratio equal to 1/3 is defined with impeller speed and gas flow rate in the form:

$$n_F = 2{,}694 \cdot q_F^{\,0{,}283} \cdot T^{-1{,}207} \quad (7).$$

Nienow [7] je postavil povezavo, ki zajema tudi različna geometrijska razmerja med mešalom in posodo ($1/3 \le D/T \le 2/3$) ter velikostni razred posode ($0{,}29 \le T \le 1{,}2$ v m):

Nienow [7] postulated a correlation including different geometrical ratios ($1/3 \le D/T \le 2/3$) as well as reactor scale size ($0{,}29 \le T \le 1{,}2$ [m]):

$$Fl_F = 30\,(D/T)^{3,5}\,Fr_F \quad (8).$$

S slike 13 je razvidno dobro ujemanje vrednosti napovedi naših meritev po metodi najmanjše moči mešnja in metodi karakteristik faznega stika z napovedjo po [7]. Glede na to, da so njihove vrednosti v pasu znotraj naših, to potrjuje Nienowo kombinacijo kriterijev porasta moči mešanja ter opazovanja tokovnih struktur, ko je bil postavljen omenjeni kriterij (en. 8). Iz primerjave metod na temelju celotnega prirastka plinaste faze se težnja naših vrednosti v izmerjenem področju dobro ujema z vrednostmi po [12], sicer pa je poplavno stanje v našem primeru doseženo pri nekoliko višjih vrednostih pretočnega števila.

In Figure 13, good agreement can be seen between our predicted values, based on the minimum-mixing-power method and the interfacial characteristics method with those predicted by Nienow. Regarding the fact that the values given with Eq. 8. appear in between ours, the assumption of their criterion postulated on the combination of the minimum-mixing-power and flow-structure methods can be confirmed. From the comparison of the results based on the global-gas-holdup method, the trend of our values is in a good agreement with those of [12] in the measured range, otherwise the flooding was achieved at slightly higher values of *Fl* number.

2.2 Nastanek poplavnega stanja pri dispergiranju zraka v raztopini KMC

Dispergiranje zraka v vodni raztopini KMC je potekalo z Rushtonovim mešalom. Ta preskus je bil izveden na isti merilni progi, izsledki obravnavani v tem prispevku pa izhajajo iz študije struktur plinskih votlin objavljene v delu [3].

Strukture plinskih votlin so bile predstavljene v diagramu struktur, izraženem z brezrazsežnimi števili *Fr-Fl*. Plinske votline so v navidezplastični kapljevini večje od teh v vodi in imajo drugačno obliko, opazen je bil tudi pojav, pri katerem ostanejo plinske votline na lopaticah mešala še po zaprtju dovoda zraka. Pri navidezno

2.2 Flooding in air dispersing into pseudoplastic fluid CMC

Dispersing of air into a pseudoplastic fluid of water-diluted CMC was performed with a single Rushton impeller using the same experimental setup. The results discussed here are derived from a gas-filled-cavity-structure study published elsewhere [3].

The structures were classified in a flow-regime map given with *Fr-Fl* dependency. The gas-filled cavities in a CMC solution are larger than those in water, and have a rather different shape. A phenomenon was also found whereby gas-filled cavities were present at the impeller blades for a longer time of observation, even after the air inflow was closed.

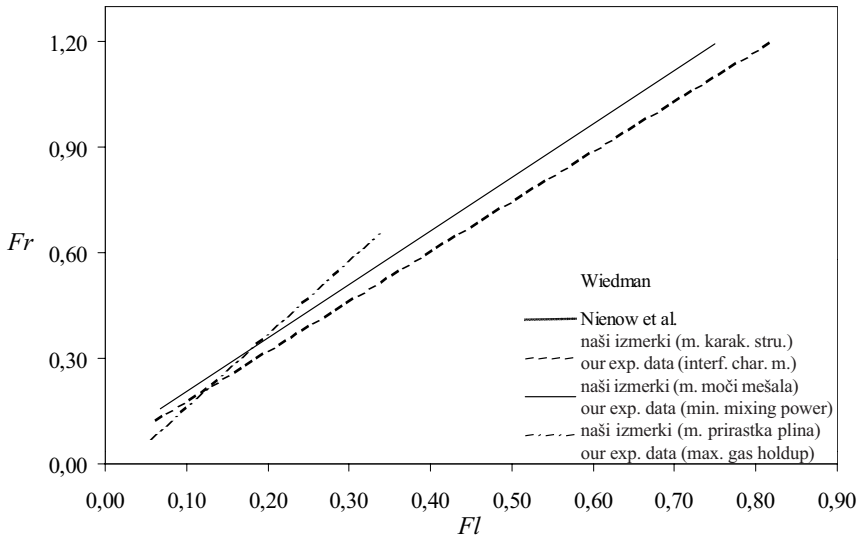

Sl. 13. *Primerjava meja poplavnega stanja z rezultati drugih avtorjev*
Fig. 13. *Comparision between our results and calculated values by other authors*

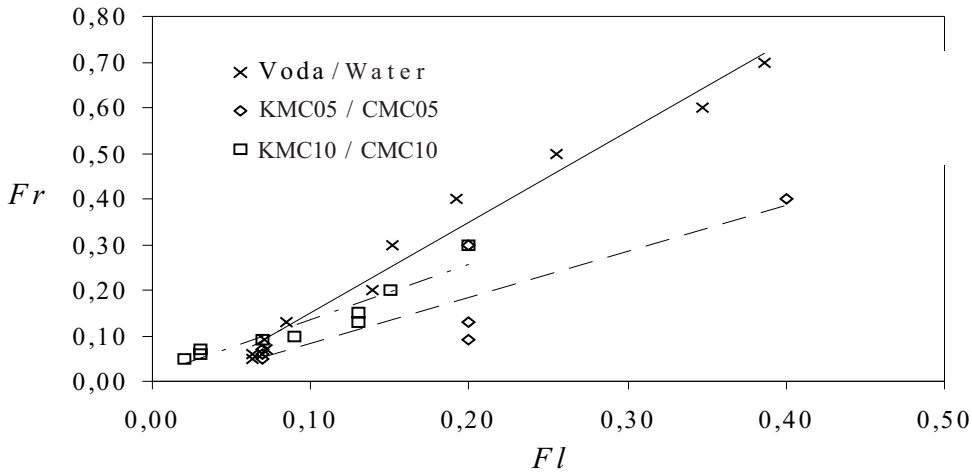

Sl. 14. *Nastanek poplavnega stanja pri dispergiranju zraka v vodo in 0,5% in 1,0% raztopino KMC*
Fig. 14. *Flooding transition in air dispersing into water and into CMC of 0.5 and 1.0 % mass concentration of CMC*

plastični tekočini poteka prehod iz dispergirnega v poplavno stanje prek strukture L6, kar se kaže z nastankom poplavnega stanja pri precej večjih vrednostih pretočnega števila (sl. 14). Primerjave z vrednostmi po virih iz literature zaradi očitnega pomanjkanja tovrstnih podatkov ni bilo mogoče izvesti. Pomembna je ugotovitev, da je porazdelitev plinaste faze po prostornini kapljevine pri 0,5% raztopini KMC še dokaj zadovoljivo, medtem ko dispergiranje v 1% raztopini verjetno že meji na neučinkovito delovanje.

3 SKLEP

Obravnavana je bila zaznava poplavnega stanja v posodi z enojnim Rushtonovim mešalom pri dispergiranju zraka v vodi s tremi različnimi metodami, to so: metoda celotnega prirastka plinaste faze, metoda najmanjše moči mešanja in metoda karakteristik faznega stika ter pri dispergiranju zraka

Transition from the dispersing to the flooding state was performed via a structure of six identical large cavities, which was reflected in much higher values of flow number, shown in Figure 14. A comparison with values from literature sources could not be made due to the obvious lack of such data. Another significant finding was that the impeller was capable of dispersing air into fluid at 0.5% of the mass concentration, whereas at 1% of the mass concentration dispersing was seen to be an unsatisfactory operation, in other words, any other impeller suitable for higher viscosities should be used.

3 CONCLUSION

In a mixing vessel equipped with a Rushton turbine, the recognition of the flooding state during the dispersion of air into water was detected with three different methods: the global-gas-holdup method, minimum-mixing-power method and the interfacial characteristics method, while for the

v vodni raztopini karboksi – metil celuloze z metodo karakteristik faznega stika.

Narejena je bila primerjava rezultatov posameznih metod in ocena primernosti uporabe posamezne metode za določitev poplavnega stanja. Poplavno stanje mešala je bilo zaznano z vsemi tremi metodami. Glede na to, da je na gredi le eno mešalo, se krajevne spremembe na mešalu kažejo neposredno tudi na celotni ravni. Rezultati vseh treh metod se med seboj dokaj dobro ujemajo, za industrijsko uporabo lahko uporabimo katerokoli od omenjenih metod.

dispersing of air into a CMC solution the interfacial characteristics method was used.

An estimation of the individual method's adequacy, as well as a comparison of the results of the given methods was performed. Impeller flooding was detected by using all three methods. The results of the discussed methods were in good agreement among themselves, as well as with the given criteria and results of other researchers. Any of the mentioned methods can be applied to industrial use. Given the fact that air-dispersing was performed with a single Rushton impeller, all the changes at the local level are reflected directly in the global one.

ZAHVALA

To delo je del večjega projekta J2-7517, ki ga financira Ministrstvo za šolstvo, znanost in šport Republike Slovenije.

ACKNOWLEDGMENT

The authors wish to acknowledge the Slovenian Ministry of Education, Science and Sport for financial support under the current project No. J2-7517.

3 OZNAKE
3 SYMBOLS

premer mešala	D	m	impeller diameter
zemeljski pospešek	g	m/s^2	gravity
vrtilna frekvenca mešala	n	s^{-1}	impeller rotational frequency
moč pri mešanju kapljevine	P	W	impeller power
prostorninski pretok zraka	q	m^3/s	volumetric air flow
premer posode	T	m	tank diameter
pretočno število	Fl	$q/(n \cdot D^3)$	flow number
Froudeovo število	Fr	$D \cdot n^2/g$	Froude number
celotni delež plinaste faze	α	%	global gas holdup
razmerje moči	π_i	$P_{g,i}/P$	power ratio
Indeksi:			**Indexes:**
tekoči indeks	i, j		current index
poplavno stanje	F		flooding state
dispergiranje plina v kapljevino	g		dispersing state

4 LITERATURA
4 REFERENCES

[1] Bombač, A. (1998) Vpliv geometrijskih parametrov na Newtonovo število pri aeraciji v posodi z mešali, *Strojniški vestnik* (44) 3-4.

[2] Bombač, A. and I. Žun (1992) Detection of loading-flooding transition in an aerated stirred vessel, in Proc. Kuhljevi dnevi, (in Slovene), Portorož, *Slovene Society of Mechanics*, 123.

[3] Bombač, A., I. Žun, M. Žumer, J. Turk (1996) Strukture plinskih votlin pri dispergiranju zraka v psevdoplastično tekočino s turbinskim mešalom, Kuhljevi dnevi, Gozd-Martuljek, *Slovensko društvo za mehaniko*.

[4] Bombač, A., I. Žun, B. Filipič, M. Žumer (1997) Gas-filled cavity structures and local void fraction distribution in aerated stirred vessel, *AIChE J.*

[5] Bombač, A., I. Žun (2000) Gas-filled cavity structures and local void fraction distribution in vessel with dual-impellers. *ChemEngSci*, (55), 15.

[6] Lu, W., H. Chen (1986) Flooding and critical impeller speed for gas dispersion in aerated turbine-agitated vessels, *Chem. Eng. Jour.*, 33.

[7] Nienow, A. W., M. M .C. G. Warmoskerken, J. M. Smith, M. Konno ((1985) On flooding/loading transition and the complete dispersal condition in aerated vessels agitated by a Rushton-turbine, Proc 5th European Conference on Mixing, Wuerzburk, *BHRA Fluid Enginireeng Cranfield*, 143-154.

[8] Rushton, J. H., J.J. Bimbinet (1964) Hold-up and flooding in air-water mixing, *Can J. Chem. Eng.*, 46.
[9] Smith, J. M. (1991) Simple performance correlations for agitated vessels, in fluid mechanics of mixing, ed. R. King, *Kluwer Academic Publisher*, Dordrecht, 55.
[10] Turk, J. (1999) Poplavno stanje pri večstopenjskem turbinskem mešalu, Diplomsko delo, *Univerza v Ljubljani*, FS, Ljubljana.
[11] Warmoeskerken, M. M. C. G. and J. M. Smith (1985) Flooding of disk turbines in gas-liquid dispersions: A new description of the phenomenon, *Chem. Eng. Sci*., 40, No. 11, 2063.
[12] Wiedmann, J.A. (1983) Zum Überflutungsverhalten zwei- und dreiphasig betriebener Rührreaktoren. *Chem.Ing.Tech*., 55, 9.
[13] Žun, I., A. Bombač (1997) An application of local void fraction measurements in discharge flow of single and dual Rushton turbine, *Proc. 9th European Conference on Mixing/Mixing 97/Mutiphase systems*, Paris, 153.

Naslov avtorjev: doc.dr. Andrej Bombač
prof.dr. Iztok Žun
Fakulteta za strojništvo
Univerza v Ljubljani
Aškerčeva 6
1000 Ljubljana
andrej.bombac@fs.uni-lj.si
iztok.zun@fs.uni-lj.si

Authors' Address: Doc.Dr. Andrej Bombač
Prof.Dr. Iztok Žun
Faculty of Mechanical Eng.
University of Ljubljana
Aškerčeva 6
1000 Ljubljana, Slovenia
andrej.bombac@fs.uni-lj.si
iztok.zun@fs.uni-lj.si

Prejeto: 20.12.2002
Received:

Sprejeto: 31.1.2003
Accepted:

© Strojniški vestnik 48(2002)12,677-686
ISSN 0039-2480
UDK 532.7:533.6.08
Izvirni znanstveni članek (1.01)

© Journal of Mechanical Engineering 48(2002)12,677-686
ISSN 0039-2480
UDC 532.7:533.6.08
Original scientific paper (1.01)

Analiza kinematike toka v rotirajočem difuzorju

An Analysis of the Flow Kinematics in a Rotating Diffuser

Tom Bajcar - Brane Širok - Ferdinand Trenc - Dragica Jošt

V prispevku so predstavljene raziskave hitrostnega polja toka zraka v rotirajočem vzdolžnem difuzorju okroglega prereza. Meritve hitrostnih komponent toka so potekale z uporabo laser-Dopplerjeve anemometrije (LDA). Z meritvami je bila potrjena delitev toka na zunanji vrtilni del ob vrteči se steni in notranji nevrtilni del v vzdolžni osi difuzorja. Ugotovljeno je bilo pomembno povečanje vseh treh komponent hitrosti v ozkem pasu ob vrteči se steni difuzorja. Poleg tega je bil izveden tudi numerični izračun hitrostnega polja v difuzorju s tremi različnimi turbulentnimi modeli.

(Ključne besede: difuzorji rotirajoči, kinematika toka, polja hitrostna, anemometrija Dopplerjeva, anemometrija laserska)

This paper describes a study of the flow-velocity field inside a rotating axial diffuser with a circular cross-section. The flow-velocity components were measured with an LDA system. The velocity-component measurements confirmed the existence of two types of flow: a rotating region near the rotating wall and a non-rotating region near the longitudinal axis of the diffuser. A significant increase in all three velocity components was observed in a thin layer at the rotating-diffuser wall. In addition, three different turbulence-closure models were applied for the velocity-field prediction inside the rotating diffuser.

(Keywords: rotating diffusers, flow kinematics, velocity fields, laser-Doppler anemometry)

0 UVOD

Analiza hitrostnega polja turbulentnega toka tekočine v vrtečem se vzdolžnem difuzorju ima svoje osnove v raziskavah toka tekočine skozi difuzor in preučevanju vrtinčnih tokov. Začetek pomembnejših raziskav toka v difuzorju sega nekako v prva desetletja 20. stoletja, predvsem z namenom preučiti dogajanje v mejni plasti difuzorja pri različnih kotih razširitve difuzorja [1]. Preveliki koti razširitve namreč povzročijo, da se mejna plast ob steni difuzorja na določenem mestu odlepi od stene, kar je posledica vzdolžnih tlačnih gradientov.

Ena izmed glavnih značilnosti vrtinčnih tokov je pojav centrifugalne sile kot posledice radialnega tlačnega gradienta, ki se pojavi v vrtinčnih tokovih [2]. V najpreprostejši obliki z zanemaritvijo strižnih sil ima radialni tlačni gradient $\partial p/\partial r$ obliko:

$$\frac{\partial p}{\partial r} = \rho \cdot \frac{u_t^2}{r} \qquad (1),$$

kjer so: ρ gostota tekočine, u_t njegova obodna hitrost, r pa radij. Centrifugalna sila pospešuje širjenje curka vrtinčnega toka radialno navzven.

0 INTRODUCTION

Analyses of the velocity field of the turbulent fluid flow in an axially rotating diffuser are based on studies of the fluid flowing through a stationary diffuser and on investigations of the swirl flow. Studies of flow inside the diffuser were initiated in the first decades of the 20th century, mainly to investigate the fluid behaviour inside the diffuser's boundary layer at different diffuser cone angles [1]. Diffuser cone angles that are too large cause the boundary layer at a particular point of the diffuser to separate from the wall. This separation is a consequence of the axial pressure gradients.

One of the main properties of the swirl flow is the presence of a centrifugal force, which is a consequence of the radial pressure gradient in swirl flows [2]. The simplest form of the radial pressure gradient $\partial p/\partial r$, where the shear forces are negligible, can be expressed as:

$$\frac{\partial p}{\partial r} = \rho \cdot \frac{u_t^2}{r} \qquad (1),$$

where ρ, u_t and r denote fluid density, fluid tangential velocity and radius, respectively. The centrifugal force enhances the swirling flow jet to spread radially outwards.

Raziskave turbulentnih vrtinčnih tokov, ki nastanejo v osno rotirajočih ravnih ceveh [3], so pokazale predvsem povečanje obodnih in radialnih komponent hitrosti tekočine v bližini vrteče se stene cevi, profili vzdolžne komponente hitrosti tekočine pa so po obliki postali bolj podobni laminarnim kakor turbulentnim (t.i. laminarizacija). Poleg tega je bilo ugotovljeno tudi zmanjšanje hidravličnih izgub v primerjavi z mirujočo cevjo.

Očitno je, da toka skozi vrtečo se cev ni mogoče povsem primerjati s tokom skozi vrteči se difuzor, saj je treba pri slednjem upoštevati geometrijsko obliko difuzorja, ki povzroči mnoge kakovostne in količinske spremembe v toku, še posebej v njegovi mejni plasti oz. v plasteh tekočine tik ob steni difuzorja. Raziskave vrtinčnega toka v vzdolžnih difuzorjih okroglega prereza so redke; ena izmed izčrpnejših je študija Clausena in sod. [4], ki predstavlja raziskavo vrtinčnega toka iz vrteče se cevi, katerega vrtinec prepreči odlepljanje mejne plasti od stene mirujočega difuzorja s kotom razširitve 20°.

Rezultati tu predstavljenega preskusa so v nadaljevanju pogosto primerjani z ugotovitvami zgoraj navedenih raziskav.

1 OPIS PRESKUSA

Analiza hitrostnega polja v difuzorju je bila izvedena na merilni postaji, ki jo prikazuje slika 1. Postavljena je bila v Laboratoriju za toplotne batne stroje na Fakulteti za strojništvo v Ljubljani. Difuzor, katerega shema je na sliki 2, je bil izdelan iz pleksi stekla in je bil prek jeklene zunanje cevi in ležajev povezan z notranjo mirujočo cevjo. Geometrijske karakteristike difuzorja so naslednje: dolžina stožčastega dela $L = 165$ mm, kot razširitve oz. razširitve $\theta = 18°$, vstopni premer $d_v = 60$ mm, razmerje izstopnega in vstopnega prereza $A_{iz}/A_v = 3{,}5$.

Studies of swirl flows in axially rotating straight pipes [3] reported increased tangential and radial velocity components in the vicinity of the rotating-pipe wall, whereas the shape of the axial velocity-component profiles of the fluid became closer to the laminar profiles rather than the turbulent ones (the so-called "laminarization"). The reduction of hydraulic losses in comparison with a stationary pipe was revealed as well.

It is obvious that the swirl flow in an axially rotating straight pipe cannot be simply approximated by the swirl flow in a rotating diffuser; the geometrical properties of the latter cause many qualitative and quantitative changes in the flow, particularly in its boundary layer, that is in the fluid layers directly at the diffuser wall. There are only a few studies of the turbulent swirl flow in axial diffusers with a circular transverse section; one of the most comprehensive was published by Clausen et al. [4], who investigated the swirl flow (originating from an axially rotating pipe), which prevented the separation of the flow from the wall of a stationary axial diffuser with a cone angle of 20°.

The results of the experimental investigations presented in this paper were compared to appropriate results from other authors.

1 EXPERIMENTAL SET-UP

The analysis of the velocity field in the rotating diffuser was carried out on the experimental set-up shown in Fig. 1. The experimental set-up was located in the Laboratory for Reciprocating Engines at the Faculty of Mechanical Engineering in Ljubljana. The diffuser, shown in schematic view in Fig. 2, was made of Plexiglas and was fastened through the steel connection outer pipe and bearings to the non-rotating inner pipe. The diffuser has the following geometric characteristics: length of the conical part of the diffuser $L = 165$ mm, cone angle $\theta = 18°$, inlet diffuser diameter $d_v = 60$ mm, diffuser outlet-to-inlet area ratio $A_{iz}/A_v = 3.5$.

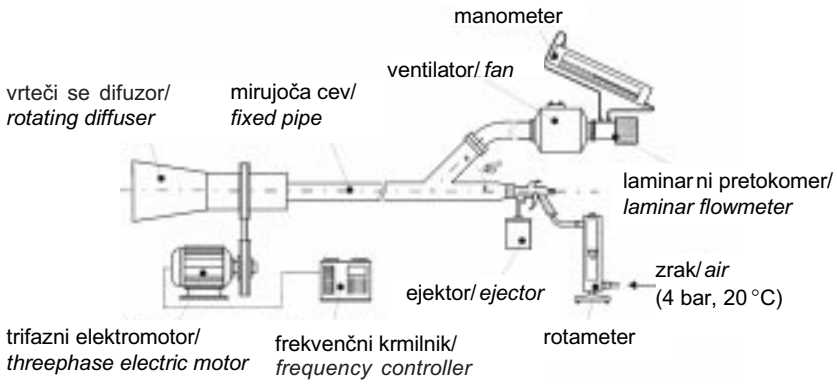

Sl. 1. *Shema merilne postaje*
Fig. 1. *Schematic view of the experimental station*

Difuzor se je vrtel okrog svoje vzdolžne osi prek jermenice z uporabo dvopolnega trofaznega elektromotorja SEVER z močjo 1,5 kW pri 2810 min^{-1}. Elektromotor je bil krmiljen z vektorskim frekvenčnim pretvornikom MITSUBISHI FREQROL-A024, s katerim se je lahko spreminjala vrtilna frekvenca elektromotorja in s tem tudi difuzorja. Na koncu mirujoče cevi dolžine 1900 mm, ki je vodila k difuzorju, je bil pritrjen ejektor, ki je služil kot generator delcev oziroma vir pasivnega onesnaževala, potrebnega za vizualizacijo toka ter merjenje hitrostnih profilov z metodo LDA. Kemična sestava kapljic onesnaževala je bila 80 prostorninskih % vode in 20 prostorninskih % zelo goste tekočine za meglo (tip E) proizvajalca Conrad Electronic. Ejekcija kapljic je bila izvedena s stisnjenim zrakom z nadtlakom 4 bar, ki je tekel skozi rotameter HEINRICHS 237929, kar je v mirujoči cevi vzpostavilo prostorninski tok $\dot{V}$ = 4 l/s. Z uporabo vzdolžnega ventilatorja in njegovega napetostnega krmilnika se je prostorninski tok v mirujoči cevi lahko povečal. Prostorninski tok zraka skozi ventilator je bil merjen z laminarnim pretokomerom MERIAM Instruments – Laminar Flow Element Model 50MC2-2f. Tok zraka je iz ventilatorja vstopal v mirujočo cev pod kotom 45°. Difuzor je deloval pri treh različnih vrtilnih frekvencah *f* in treh različnih prostorninskih tokovih zraka $\dot{V}$ oziroma vrednostih Reynoldsovega števila na vstopu v difuzor *Re* (preglednica 1).

Smer vrtenja difuzorja je bila pri obeh vrtilnih frekvencah enaka, in sicer v nasprotni smeri urnega kazalca, opazovano od izstopa iz difuzorja proti njegovemu vstopu. Vse navedene vrednosti Reynoldsovega števila predstavljajo vrednosti Reynoldsovega števila na vstopu v difuzor.

The diffuser rotated around its longitudinal axis via a belt-pulley and was driven by a SEVER triphase electric motor with a power output of 1.5 kW at 2810 min^{-1}. A MITSUBISHI FREQROL-A024 vector frequency inverter was applied to alternate the rotating speed of the motor and thus the rotating frequency of the diffuser. An ejector was placed at the end of a 1900-mm-long fixed (non-rotating) pipe that led to the diffuser. The ejector was used as a particle generator that provided passive pollutant to the airflow for LDA measurements. The pollutant droplets consisted of 80 vol% of water and 20 vol% of very thick fog fluid (type E), distributed by Conrad Electronic. The droplets were ejected by pressurized air at 4 bar, flowing through a HEINRICHS 237929 rotameter. Thus, an axial airflow of $\dot{V}$ = 4 l/s entered the non-rotating pipe through the particle generator. The axial airflow through the diffuser could be increased by introducing additional airflow to the non-rotating pipe from a controlled fan. The volumetric airflow through the fan was measured with a MERIAM Instruments Laminar Flow Element, Model 50MC2-2f. The airflow from the fan entered the non-rotating pipe at an angle of 45°. The diffuser operated at three different rotating frequencies, *f*, as well as at three different volumetric airflows, $\dot{V}$, with the appropriate values of a diffuser-inlet Reynolds number *Re* (Table 1).

The direction of the diffuser rotation at both rotating frequencies was anti-clockwise when observed from the diffuser outlet towards its inlet. All reported values of the Reynolds number, *Re*, in the following text denote values of the diffuser-inlet Reynolds number.

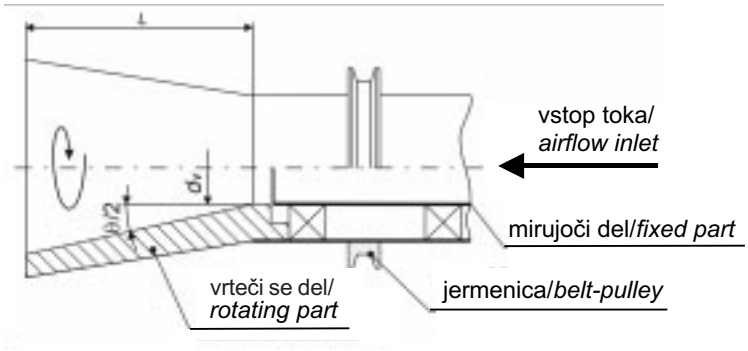

Sl. 2. *Shema zgradbe rotirajočega difuzorja*
Fig. 2. *Schematic view of the rotating diffuser*

Preglednica 1. *Vrtilne frekvence difuzorja, prostorninski tokovi in vrednosti vstopnega Reynoldsovega števila*
Table 1. *Rotating frequencies of the diffuser, airflows and values of the inlet Reynolds number*

f Hz	$\dot{V}$ l/s	*Re* -
0	4	$5{,}84 \cdot 10^3$
30	8	$1{,}17 \cdot 10^4$
52,8	13,8	$2{,}01 \cdot 10^4$

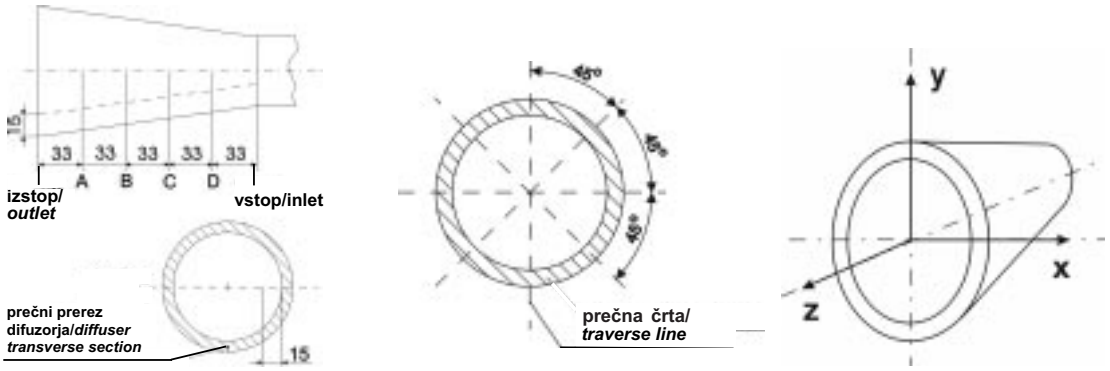

a) **b)** **c)**

Sl. 3. *a) – Merilna mesta znotraj difuzorja (mere v milimetrih); b) – Prečne črte na vstopnem in izstopnem prečnem prerezu difuzorja; c) – Uporabljeni koordinatni sistem*

Fig. 3. *a) – Positions of the measurement points inside the diffuser cone (all dimensions in millimetres); b) – Traverse lines in the diffuser inlet and outlet transverse section; c) - Coordinate system applied for measurements of velocity components*

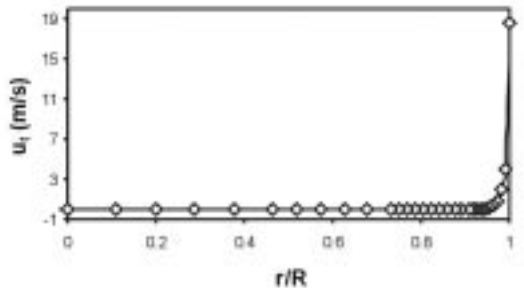

Sl. 4. *Časovno povprečene srednje vrednosti obodne hitrosti u_t na izstopu iz difuzorja na x-osi koordinatnega sistema ($f = 52,8$ Hz, $Re = 5,84 \times 10^3$)*

Fig. 4. *Distribution of the time-averaged mean tangential velocity u_t at the diffuser outlet on the x-axis of the coordinate system ($f = 52.8$ Hz, $Re = 5.84 \times 10^3$)*

Merjenje hitrostnih profilov s sistemom LDA je potekalo v vseh obratovalnih razmerah, in sicer v pasu 15 mm ob steni na štirih enako oddaljenih prečnih prerezih (A, B, C in D) v notranjosti difuzorja (sl. 3a), poleg tega pa tudi na vstopnem in izstopnem prerezu difuzorja na štirih prečnih črtah (sl. 3b). Slika 3c prikazuje uporabljeni koordinatni sistem. Razmerje r/R na diagramih predstavlja razmerje oddaljenosti merilnega mesta od vzdolžne osi difuzorja r s polmerom tekočega prečnega prereza difuzorja R.

Measurements of the velocity components with the LDA system were carried out for all the aforementioned operating conditions in a 15-mm-wide band directly at the diffuser wall in four equidistant transverse sections (A, B, C and D) inside the diffuser (Fig. 3a). Apart from that, the velocity components were also measured at the inlet- and outlet-diffuser transverse sections on four traverse lines (Fig. 3b). The Cartesian coordinate system shown in Fig. 3c was used throughout the experiment. The expression r/R on the diagrams denotes the ratio between the radial distance of the measuring point from the diffuser longitudinal axis, r, and the radius of the particular diffuser transverse section, R.

2 REZULTATI

2.1 Potek časovno povprečenih srednjih vrednosti obodnih komponent hitrosti (u_t)

Vrtenje difuzorja okoli njegove vzdolžne osi povzroči v toku zraka obodne komponente hitrosti, saj plasti zraka ob notranji steni difuzorja sledijo vrtenju stene. S tem se v ravnini x-y difuzorja pojavi vrtinec (sl. 4).

2 RESULTS

2.1 Distribution of time-averaged mean tangential velocity components (u_t)

Rotation of the diffuser around its longitudinal axis generates tangential velocity components because the layers of air at the inner diffuser wall follow the wall rotation. As a consequence a vortex appears in the x-y plane of the diffuser (Fig. 4).

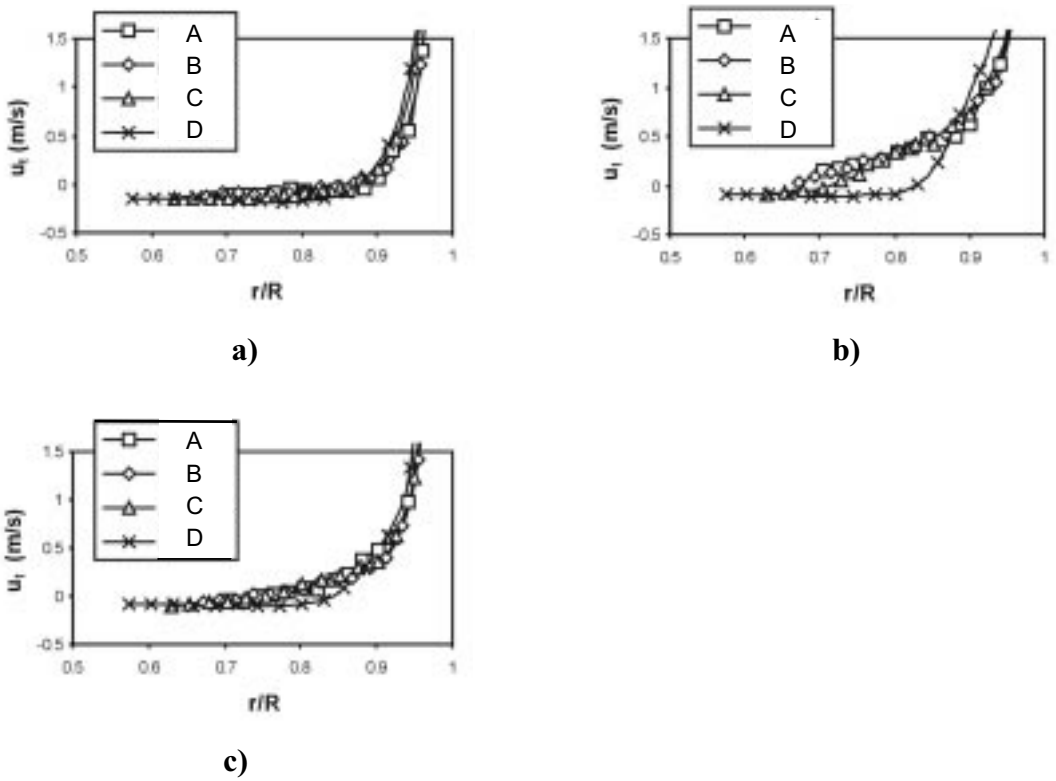

Sl. 5. *Časovno povprečene obodne komponente hitrosti na prečnih prerezih difuzorja A, B, C in D; a) –* f *= 30 Hz,* Re *= 1,17×10⁴; b) –* f *= 30 Hz,* Re *= 2,01×10⁴; c) –* f *= 52,8 Hz,* Re *= 2,01×10⁴*

Fig. 5. *Distribution of the time-averaged mean tangential velocity components on diffuser transverse sections A, B, C and D; a) –* f *= 30 Hz,* Re *= 1.17×10⁴; b) –* f *= 30 Hz,* Re *= 2.01×10⁴; c) –* f *= 52.8 Hz,* Re *= 2.01×10⁴*

S slike 4 je razvidno, da se v difuzorju vrti le del toka zraka v ozkem pasu ob vrteči se steni. Vrtilno območje je velikosti ~4 mm in obkroža nevrtilni del toka. Podoben pojav je bil opažen tudi v primeru vrtilne ravne cevi [5]. Oblika profilov obodnih komponent hitrosti se spreminja s spreminjanjem vrtinčnega razmerja $N = u_{t,stene}/\overline{u}_a$, ki predstavlja razmerje obodne hitrosti stene difuzorja in povprečne vzdolžne hitrosti zraka na izbranem prečnem prerezu difuzorja (sl. 5).

S slike 5 je razvidno, da se vpliv vrteče se stene na tok zraka v difuzorju poveča s povečevanjem prečnega premera difuzorja v smeri od vstopa proti izstopu difuzorja. Povečan vpliv vrteče se stene se kaže v širšem področju, kjer so obodne hitrosti zraka pozitivne oz. imajo isti predznak kot obodna hitrost stene difuzorja. Vrtinčno razmerje N je večje na prečnih prerezih, ki so bližje izstopu iz difuzorja (npr. prereza A in B), na teh prerezih pa je širše tudi območje pozitivnih obodnih hitrosti zraka.

Primerjava med slikama 5a in 5b pokaže, da je pri enakih vrtilnih frekvencah difuzorja in istih prečnih prerezih difuzorja vpliv vrteče se stene močnejši v primeru večjih vrednosti Reynoldsovega števila, torej pri manjšem razmerju N. Podoben pojav je opazen tudi v primeru, ko se pri enaki vrednosti Reynoldsovega števila zmanjša

It can be seen from Fig. 4 that only a small portion of the fluid inside the diffuser is rotating close to the diffuser wall. This region is about 4-mm wide and encircles the non-rotating core of the airflow. A similar phenomenon was also observed in the case of rotating straight pipes [5]. The shape of the tangential velocity profiles changes with the change of the swirl rate $N = u_{t,stene}/\overline{u}_a$, which represents the ratio between the diffuser-wall tangential velocity and averaged axial velocity of the air at a chosen diffuser transverse section (Fig. 5).

Fig. 5 shows that the influence of the rotating diffuser wall on the airflow in the diffuser generally increases together with the increasing diffuser transverse section in the direction from diffuser inlet to its outlet. The increased influence of the rotating wall reveals itself by means of a broader region, where the tangential velocity components of the airflow are positive (thus having the same sign as the tangential velocity of the diffuser wall). The swirl rate N is higher near the rotating diffuser outlet (e.g. at transverse sections A and B), therefore the region of positive tangential velocity components of the airflow is broader in the transverse sections at the diffuser outlet.

A comparison between Fig. 5a and Fig. 5b shows that at the same rotating frequency of the diffuser the influence of the rotating diffuser wall on the airflow is larger at higher Reynolds number values and therefore at a lower swirl rate, N, observed in a particular diffuser transverse section. A similar phenomenon can be observed when at

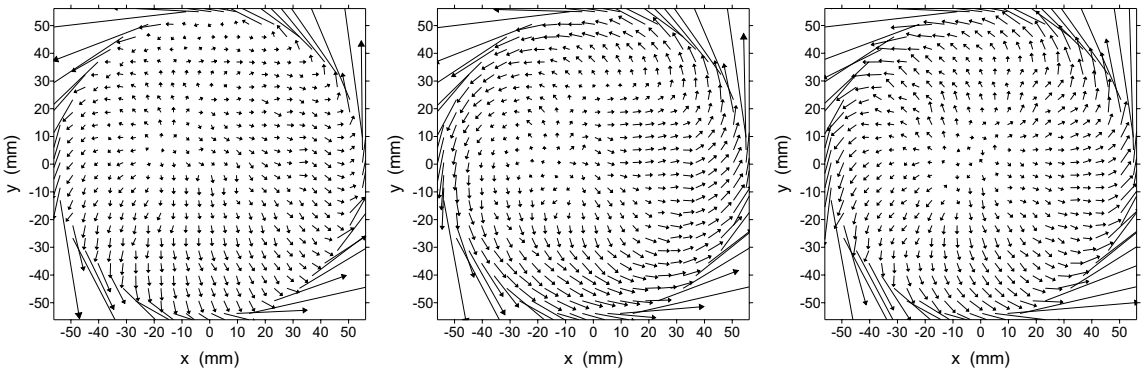

Sl. 6. *Diagrami hitrosti na izstopu iz difuzorja v ravnini x-y: a) – f = 30 Hz, Re = 1,17×10⁴; b) – f = 30 Hz, Re = 2,01×10⁴; c) – f = 52,8 Hz, Re = 2,01×10⁴)*

Fig. 6. *Velocity diagrams in x-y plane at the diffuser outlet: a) – f = 30 Hz, Re = 1.17×10⁴; b) – f = 30 Hz, Re = 2.01×10⁴; c) – f = 52.8 Hz, Re = 2.01×10⁴)*

vrtilna frekvenca difuzorja in s tem razmerje N (sl. 5b, 5c). To potrdijo tudi hitrostni diagrami v ravnini *x-y* na izstopu iz difuzorja (sl. 6).

2.2 Potek časovno povprečenih srednjih vrednosti radialnih komponent hitrosti (u_r)

V vrtečem se difuzorju se kot posledica radialnega tlačnega gradienta en. (1) pojavi radialna komponenta hitrosti zraka v smeri proti vrteči se steni difuzorja. Največje radialne komponente hitrosti se po pričakovanju pojavijo v območju največjih obodnih hitrosti, saj so le-te glavni vzrok za nastanek radialnih komponent (centrifugalna sila).

Na sliki 7 so prikazani diagrami radialnih komponent hitrosti v različnih delovnih razmerah difuzorja na njegovem izstopu.

Diagrama na sliki 7 kažeta, da se največje vrednosti radialne komponente hitrosti pojavijo tik ob steni difuzorja na oddaljenosti $r/R \approx 0{,}99$. Največje vrednosti obodne hitrosti se pojavijo sicer neposredno na vrteči se steni sami ($r/R = 1$), vendar zaradi stene tam radialne komponente ni. Poleg tega je razvidna odvisnost poteka radialnih komponent hitrosti od frekvence vrtenja difuzorja ter (vzdolžnega) Reynoldsovega števila, torej od razmerja N. Pri višji frekvenci vrtenja difuzorja in nespremenjeni vrednosti Reynoldsovega števila (višji N) se pojavijo večje vrednosti radialnih komponent hitrosti, kar lahko pričakujemo, saj so v tem primeru večje tudi obodne komponente hitrosti zraka. Po drugi strani pa se pri večjih vrednostih Reynoldsovega števila in nespremenjeni vrtilni frekvenci difuzorja (nižji N) pojavijo nižje vrednosti radialnih komponent hitrosti zraka; z naraščanjem radialne oddaljenosti od stene difuzorja pa vrednosti radialnih hitrosti pri manjših vrednostih N postopoma prerastejo tiste pri večjih vrednostih N.

the same value of the Reynolds number the values the rotating frequency and thus the swirl rate, N, is reduced (Figs. 5b and 5c). This is also confirmed by velocity diagrams in the *x-y* plane at the diffuser outlet (Fig. 6).

2.2 Distribution of time-averaged mean radial velocity components (u_r)

The radial velocity component in the airflow oriented towards the rotating diffuser wall appears in the rotating diffuser as a consequence of the radial pressure gradient (Eq.1). The peak radial velocities coincide with the region of the peak tangential velocities, as one would expect, since the tangential velocities are the main reason for the appearance of the radial velocities (centrifugal force).

Fig. 7 shows the diagrams of radial velocity components at the diffuser outlet at different operating conditions of the diffuser.

It can be clearly seen from the diagrams in Fig. 7 that the peak value of the radial velocity component occurs close to the wall in a rotating region of the airflow – at a relative distance of about $r/R \approx 0.99$. The highest values of the tangential velocity take place directly on the diffuser wall ($r/R = 1$), but there is no radial component because of the wall. Apart from that, the radial velocity distribution depends on the rotating frequency of the diffuser and on the (axial) Reynolds number of the airflow, i.e. on the swirl rate N. A higher rotating frequency leads to higher radial velocity values at fixed values of Re (higher N); this situation was anticipated because the peak tangential velocity values are also higher in this case. On the other hand, higher Re values at a fixed rotating frequency (lower N) produce lower peak radial velocity component values; the values of the radial velocity at lower N eventually exceed those at higher N when the radial distance from the diffuser wall is increased.

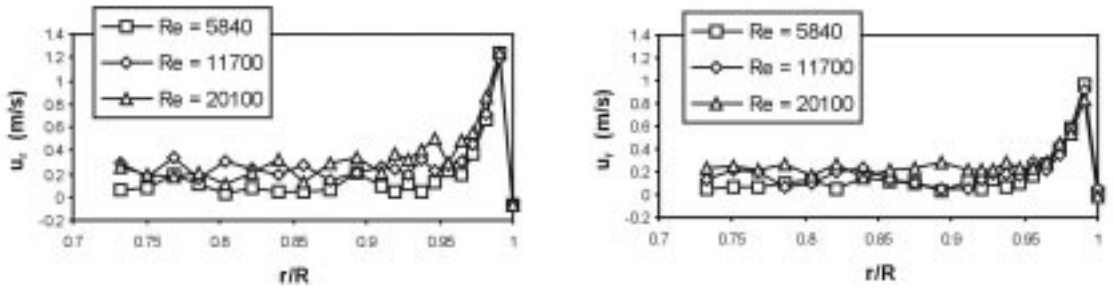

Sl. 7. *Potek časovno povprečenih radialnih komponent toka na izstopu iz difuzorja: a) – f = 52,8 Hz; b) – f = 30 Hz*
Fig. 7. *Distribution of the time-averaged mean radial velocity components at the diffuser outlet: a) – f = 52.8 Hz; b) – f = 30 Hz*

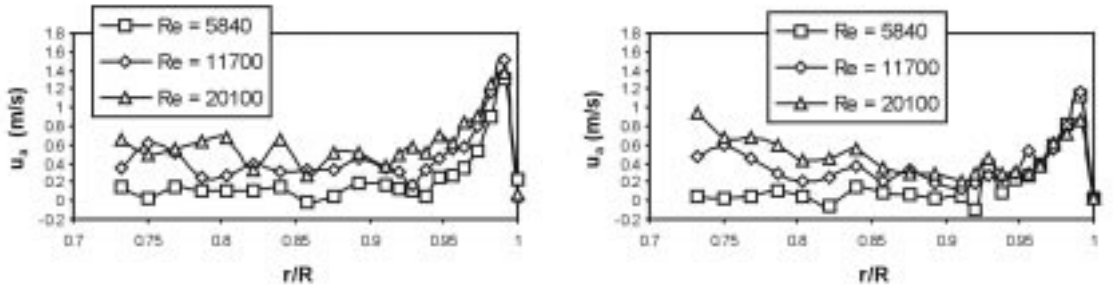

Sl. 8. *Potek časovno povprečenih vzdolžnih komponent toka na izstopu iz difuzorja: a) f = 52,8 Hz; b) f = 30 Hz*
Fig. 8. *Distribution of the time-averaged mean axial velocity components at the diffuser outlet: a) f = 52.8 Hz; b) f = 30 Hz*

2.3 Potek časovno povprečenih srednjih vrednosti vzdolžnih komponent hitrosti (u_a)

Na prečnih prerezih, ki so bliže izstopu iz difuzorja in kjer so obodne komponente hitrosti izrazitejše, se pojavi lokalni vrh vrednosti vzdolžnih hitrosti tik ob vrteči se steni difuzorja (sl. 8).

Povečanje vzdolžnih komponent tik ob steni ni bilo opaženo ne v primeru vrteče se ravne cevi [6], prav tako pa tudi ne v primeru vrtinčnega toka v mirujočem difuzorju [4]. Eden izmed vzrokov tega pojava leži v delovanju centrifugalne sile, ki potiska tok zraka proti steni difuzorja in s tem proti izstopu iz difuzorja (stena difuzorja se namreč razširja v smeri proti njegovemu izstopu). Drugi vzrok pa je čelna stena difuzorja oz. debelina stene difuzorja na njegovem izstopu; med vrtenjem difuzorja se zrak ob tej steni zaradi delovanja centrifugalne sile pomika v radialno-obodni smeri navzven v zunanji prostor [7], na njegovo mesto pa priteka nov zračni tok, ki ga čelna stena difuzorja "črpa" iz notranjosti difuzorja oziroma iz mejne plasti ob notranji steni difuzorja. Zaradi navedenih vzrokov ni med eksperimentom nikoli prišlo do odcepljanja plasti zraka tik ob notranji steni difuzorja (povratni tok), kljub temu, da je bil kot razširitve difuzorja večji od 14°.

2.3 Distribution of time-averaged mean axial velocity components (u_a)

There is a local peak of the axial velocities in the near-wall region in the transverse sections that are closer to the diffuser outlet and where the swirl is more intensive due to a higher wall tangential velocity (Fig. 8).

The increase in axial velocity component values near the diffuser wall has not been observed, neither in the case of the axially rotating straight pipes [6] nor in the case of the stationary diffuser with swirl flow [4]. One of the reasons for this phenomenon is in the action of the centrifugal force, which propels the airflow towards the diffuser wall and thus towards the diffuser outlet (since the diffuser cone diverges in the direction of its outlet). The second reason is the diffuser endplate – the thickness of the wall at the diffuser outlet. When the diffuser rotates, due to the centrifugal forces the air attached to this endplate is pushed out of the diffuser in the radially tangential direction [7]. Thus, the additional airflow is sucked in from the inner side of the diffuser cone (from the boundary layer at the inner diffuser wall) by the endplate. As consequence of the described phenomena, flow separation from the rotating diffuser wall (the so-called reverse flow) was never observed during the experiments, although the diffuser cone angle exceeded 14°.

Iz slike 8 je tudi razvidno, da je potek vzdolžnih komponent hitrosti zraka ob steni difuzorja podoben poteku radialnih komponent hitrosti v istem območju difuzorja (sl. 7).

2.4 Rezultati numeričnih modelov

Numerični izračun toka zraka v vrtečem se difuzorju je potekal z uporabo CFD programskega paketa CFX-TASCflow, verzija 2.10. Pri tem so bili uporabljeni trije turbulenčni modeli, ki so že vsebovani v omenjenem programskem paketu: model *k-ε*, model *k-ω SST* in model Reynoldsovih napetosti. Vstopni in robni pogoji so bili za vse tri modele podani z eksperimentalnimi meritvami, s katerimi so bile določene časovno povprečene hitrostne komponente toka zraka na vstopu v difuzor. Na sliki 9 je prikazano območje okrog difuzorja (okolica, robni pogoji), ki je bilo uporabljeno pri modeliranju.

Rezultati numeričnih modelov in primerjava z eksperimentalno dobljenimi vrednostmi so prikazani na sliki 10.

It is obvious from Fig. 8 that the axial velocity distribution in the near-wall region of the airflow in the rotating diffuser is analogous to the distribution of radial velocities in the same region of the diffuser (Fig. 7).

2.4 Results of the numerical models

Numerical calculation of the airflow inside the rotating diffuser was carried out using a CFD program package: CFX-TASCflow, version 2.10. Three different turbulent closure models were used, which were already included in the aforementioned program package: the *k-ε* model, the *k-ω SST* model and the Reynolds stresses model. The inlet and the boundary conditions for all three models were determined with experimental measurements, which were used for the calculation of the time-averaged velocity components of the airflow at the diffuser inlet. A region around the diffuser (surrounding, boundary conditions) used for modelling is shown in Fig. 9.

The results of the numerical models and the comparison with the experimentally acquired values are shown in Fig.10.

Sl. 9. *Shematski prikaz okolice difuzorja, ki je bila upoštevana pri numeričnem izračunu tokovnega polja v difuzorju (mere so v milimetrih)*

Fig. 9. *Schematic view of the diffuser surrounding used for the numerical calculation of the diffuser flow field (all dimensions in millimetres)*

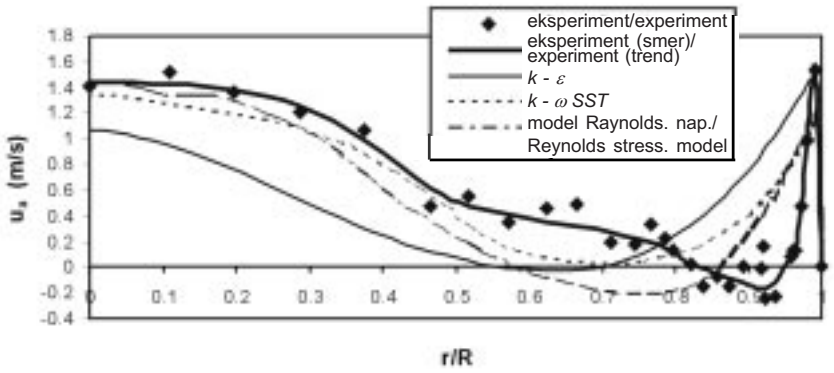

Sl. 10. *Primerjava vrednosti povprečenih aksialnih hitrosti na izstopu iz difuzorja - koordinatna os x (f = 30 Hz, Re = 1,17×10⁴)*

Fig. 10. *Comparison of values of averaged axial velocities at the diffuser outlet – coordinate axis x (f = 30 Hz, Re = 1.17×10⁴)*

Vsi turbulentni modeli napovejo povečanje vzdolžnih komponent hitrosti (sl. 10) tik ob steni vrtečega se difuzorja, kjer te vrednosti dosežejo velikost 1,1 m/s (model *k*-ω *SST*) do 1,4 m/s (model *k*-ε), torej so velikostnega razreda izmerjenih vrednosti. Vzdolžne hitrosti se pri preskusu zmanjšajo na vrednost ~ 0 m/s že na oddaljenosti $r/R = 0{,}95$, medtem ko je pri turbulentnih modelih to zmanjšanje bolj položno. Najhitreje se zmanjšajo vrednosti vzdolžne hitrosti pri rezultatih modela Reynoldsovih napetosti, najpočasneje pa pri modelu *k*-ε. Tudi majhno območje povratnega toka, ki se pojavi pri preskusu na oddaljenosti $r/R \approx 0{,}92$, napovedo turbulentni modeli pri nižjih vrednostih *r/R* (razen modela *k*-ω, ki povratnega toka na tem delu osi *x* ne napove).

Zaradi širšega pasu velikih vrednosti vzdolžnih komponent hitrosti zraka ob steni difuzorja model *k*-ε tudi ne napove dovolj velikih vzdolžnih hitrosti v bližini vzdolžne osi difuzorja. Tu sta eksperimentalnim vrednostim precej bliže ostala dva modela, še posebej model Reynoldsovih napetosti.

3 SKLEPI

V prispevku je bila izvedena analiza kinematike toka zraka v vrtečem se vzdolžnem difuzorju s kotom razširitve 18° z namenom ugotoviti vpliv vrteče se stene na tok v difuzorju. Analiza je bila opravljena z meritvami hitrostnega polja z metodo LDA ter z numeričnim modeliranjem toka v difuzorju.

Rezultati so potrdili pojav dveh tipov toka v vrtečem se difuzorju: vrteči se tok zraka ob steni in nevrteči tok v vzdolžni osi difuzorja; to pomeni, da vpliv vrtenja stene ne seže globoko v notranjost difuzorja. Profili obodne komponente hitrosti so zato vbočeni. V območju $r/R > 0{,}9$ se pojavi ekstrem vrednosti vseh treh komponent hitrosti, predvsem na tistih prečnih prerezih difuzorja, ki so bliže izstopu. Rezultati preskusa so poleg tega pokazali tudi odvisnost poteka komponent hitrosti zraka v vrtečem se difuzorju od vrtilne frekvence difuzorja in Reynoldsovega števila.

V splošnem so najbližje rezultatom preskusnih meritev rezultati modela Reynoldsovih napetosti, kar potrjujejo tudi rezultati modeliranja toka znotraj vrtečih se cevi [8]. To izhaja iz same narave tega turbulenčnega modela, saj upošteva precej manj poenostavitev kot dvoenačbni modeli. Posledica tega je daljši čas računanja oziroma večji računski napor, ki ga model Reynoldsovih napetosti zahteva.

All three turbulent closure models predict an increase in the axial velocity components (Fig. 10), directly at the rotating diffuser wall, where the axial velocities reach values from 1.1 m/s (model *k*-ω *SST*) up to 1.4 m/s (model *k*-ε) – the predicted values are therefore in the region of the measured values. The measured axial velocities during the experiment drop to ~ 0 m/s at a distance of $r/R = 0.95$, whereas the drop in the axial velocity values predicted by the turbulent closure models is not so steep. The fastest decrease in the axial velocity values is predicted by the Reynolds stresses model, and the slowest by the *k*-ε model. Apart from that, a small region of the reverse flow, which was observed at a distance $r/R \approx 0.92$ during the experiment, was predicted at lower values of *r/R* by the models (with the exception of the *k*-ω model, which does not predict the reverse flow on this part of the *x*-axis).

Because of the broader band of high values of the axial velocity components of the airflow near the diffuser wall the *k*-ε model fails to predict values of the axial velocities that are high enough at the diffuser longitudinal axis; the results of other two models in this region of the diffuser are thus closer to the experimental ones, especially in the case of the Reynolds stresses model.

3 CONCLUSIONS

An analysis of the flow kinematics in an axially rotating diffuser with an 18° cone angle was carried out in order to investigate the influence of the rotating diffuser wall on the airflow. This was achieved by the use of an LDA system and by numerical modeling of the airflow inside the diffuser.

The results confirm two general types of flow inside the rotating diffuser: one in the outer rotating region and the second within the inner non-rotating region. This means that the influence of the rotating wall on the airflow does not reach deep inside the diffuser. The tangential velocity profiles are therefore concave. There is a maximum of all three velocity components in the region $r/R > 0.9$ for the diffuser transverse sections that are close to the diffuser outlet. In addition, the results of the experiment showed the dependence of the distribution of airflow velocity components on the rotating frequency of the diffuser and on the Reynolds number.

The results of the Reynolds' stresses model are generally closest to the results of the experimental measurements, which is also confirmed by the results of the flow modelling inside the rotating straight pipes [8]. This comes from the nature of this turbulent closure model, since the model itself incorporates far fewer simplifications in comparison to the two-equation closure models. The consequence of this is the longer calculation time (greater calculation effort) required by the Reynolds stresses model.

4 LITERATURA
4 REFERENCES

[1] Kováts, A. (1964) Design and performance of centrifugal and axial flow pumps and compressors, *Pergamon Press Ltd*., Oxford.

[2] Gupta, A. K., D.G. Lilley, N. Syred (1984) Swirl flows, *Abacus Press*, Tunbridge Wells.

[3] Imao, S. M. Itoh, T. Harada T. (1996) Turbulent characteristics of the flow in an axially rotating pipe, *Int. J. Heat and Fluid Flow*, Vol. 17, No. 5, 444-451.

[4] Clausen, P. D., S.G. Koh, D.H. Wood (1993) Measurements of a swirling turbulent boundary layer developing in a conical diffuser, *Experimental Thermal and Fluid Science,* 6, 39-48.

[5] Cannon, J. N., W.M. Kays (1969) Heat transfer to a fluid flowing inside a pipe rotating about its longitudinal axis, *ASME Journal of Heat Transfer*, Vol. 91, No. 1, 135-139.

[6] Murakami, M., K. Kikuyama (1980) Turbulent flow in axially rotating pipes,*Journal of Fluids Engineering*, Vol. 102, 97-103.

[7] Schlichting, H., K. Gersten (2000) Boundary-layer theory, *Springer*, Berlin.

[8] Hirai, S., T. Takagi, M. Matsumoto (1988) Predictions of the laminarization phenomena in an axially rotating pipe flow, *Journal of Fluids Engineering*, Vol.110, 424-430.

Naslova avtorjev: mag. Tom Bajcar
prof.dr. Brane Širok
prof.dr. Ferdinand Trenc
Fakulteta za strojništvo
Univerza v Ljubljani
Aškerčeva 6
1000 Ljubljana
tom.bajcar@fs.uni-lj.si
brane.sirok@fs.uni-lj.si
ferdinand.trenc@fs.uni-lj.si

dr. Dragica Jošt
Turboinštitut
Rovšnikova 7
1000 Ljubljana
dragica.jost@turboinstitut.si

Authors' Addresses: Mag. Tom Bajcar
Prof. Dr. Brane Širok
Prof. Dr. Ferdinand Trenc
Faculty of Mechanical Eng.
University of Ljubljana
Aškerčeva 6
1000 Ljubljana, Slovenia
tom.bajcar@fs.uni-lj.si
brane.sirok@fs.uni-lj.si
ferdinand.trenc@fs.uni-lj.si

Dr. Dragica Jošt
Turboinštitut
Rovšnikova 7
1000 Ljubljana, Slovenia
dragica.jost@turboinstitut.si

Prejeto: 20.12.2002
Received:

Sprejeto: 31.1.2003
Accepted:

© Strojniški vestnik 48(2002)12,687-695
ISSN 0039-2480
UDK 532.57:519.61/.64
Izvirni znanstveni članek (1.01)

© Journal of Mechanical Engineering 48(2002)12,687-695
ISSN 0039-2480
UDC 532.57:519.61/.64
Original scientific paper (1.01)

Siskov model toka nenewtonskih tekočin z metodo končnih prostornin

The Sisko Model For Non-Newtonian Fluid Flow Using The Finite-Volume Method

Marjan Delić - Jure Marn - Zoran Žunič

Analizirali smo primernost metode končnih prostornin za izračun tokovnih razmer v nestisljivi viskozni nenewtonski tekočini ob uporabi Siskovega modela. Prav tako smo analizirali natančnost numeričnih rezultatov v odvisnosti od gostote mreže. Metodo smo testirali na primeru gnanega toka v kotanji in primeru toka v kanalu z nenadno zožitvijo. Numerično dobljene rezultate smo primerjali z vrednostmi iz literature. Za reološki model smo uporabili modelne parametre, dobljene na podlagi preskusa s cevnim viskozimetrom.

(Ključne besede: tekočine nenewtonske, modeli toka, metode končnih prostornin, modeli reološki)

We have analyzed the suitability of the finite-volume method for calculating incompressible, viscous, non-Newtonian fluid flow where the Sisko model was used. In addition, convergence criteria are presented and the convergence depending on the mesh size was analyzed. The method was tested for the driven-cavity case and flow in a channel with a sudden contraction. The numerical solution was compared with the results available in the open literature. For the rheological model, parameters obtained from an experiment with a capillary viscometer were used.

(Keywords: non-newtonian fluids, flow models, control-volume methods, rheological models)

0 UVOD

Nenewtonske tekočine so navzoče v vsakdanji inženirski praksi. Zaradi spremenljive viskoznosti je treba gibalne enačbe obravnavati brez običajnih poenostavitev. Viskoznost je lahko v splošnem odvisna od številnih parametrov, v tem prispevku pa obravnavamo posplošene newtonske tekočine, pri katerih je viskoznost odvisna od deformacijske hitrosti. Na področju posplošenih newtonskih tekočin obstaja več reoloških modelov z dvema, tremi ali štirimi parametri, npr. [5] do [7] in [9]. V pričujočem delu smo se osredotočili na Siskov triparametrični model.

Tokovne razmere v nestisljivi viskozni posplošeni newtonski tekočini smo obravnavali s sistemom parcialnih diferencialnih enačb osnovnih zakonov ohranitve, ki smo ga reševali z diskretno metodo končnih prostornin, opisano v [4] in povzeto po [1]. V skladu z opisanim načinom reševanja smo kontinuitetno in gibalno enačbo povezali z uporabo načela umetne stisljivosti. Konvektivne tokove smo računali po metodi karakteristik, difuzijske tokove in izvirne člene pa s končnimi razlikami (protivetrnimi in osrednjimi končnimi razlikami). Za napredovanje po

0 INTRODUCTION

Non-Newtonian fluids are very common in everyday engineering practice. Momentum equations can no longer be simplified with the usual simplifications due to variable viscosity. Viscosity is, in general, dependent on various parameters, whereas this paper deals with generalised Newtonian fluids, for which viscosity depends on the trace of the shear-rate tensor. There are several different rheological models, with two, three or four parameters among the generalised Newtonian fluids, see for example, [5] to [7] and [9]. In this study the main focus was on the Sisko three-parametric model.

The fluid conditions for an incompressible, generalised Newtonian fluid were treated as a system of partial differential equations of fundamental conservation laws, solved with a discrete, finite-volume method, as described in [4] and [1]. According to the described method the continuity and momentum equations were coupled with an artificial compressibility term. The convective fluxes were calculated using the method of characteristics, whereas the diffusive fluxes and source terms were computed using finite differences (upwind and central finite deferences). For time marching

času smo uporabili izrecno metodo Runge-Kutta četrtega reda. Natančnost in konvergenco metode smo preskusili na primeru gnanega toka v kotanji in primeru toka v kanalu z nenadno zožitvijo. Za reološki model smo uporabili modelne parametre, dobljene na podlagi preskusa s cevnim viskozimetrom ([8] in [3]).

the Runge-Kutta fourth-order explicit method was used. The accuracy and convergence of the method was tested with the driven-cavity test case and flow in a channel with a sudden contraction. The model parameters of the fluid were obtained from an experiment with a capillary viscosimeter ([8] and [3]).

1 DEFINICIJA PROBLEMA

Ravninski tok viskozne nestisljive tekočine lahko opišemo z gibalnima enačbama in kontinuitetno enačbo, ki jih ob zanemaritvi prostorninskih sil zapišemo v obliki:

$$\rho\frac{\partial v_i}{\partial t}+\rho\frac{\partial}{\partial x_j}(v_j v_i)=-\frac{\partial p}{\partial x_i}+\frac{\partial \tau_{ji}}{\partial x_j} \tag{1}$$

$$\frac{\partial v_i}{\partial x_i}=0 \tag{2}.$$

Reševanje enačb ohranitve gibalne količine, zapisanih za osnovne fizikalne spremenljivke za tok nestisljive tekočine, je težavno, ker tlak ni termodinamična veličina. To pomanjkljivost odpravimo z vključitvijo dodatnega člena, časovnega odvoda, v kontinuitetno enačbo. Problem nihanja numerične rešitve odpravimo z navidezno stisljivostjo:

1 PROBLEM DEFINITION

The planar flow of a viscous, incompressible fluid can be described with two momentum equations and one continuity equation, which with neglected volume forces take the following forms:

Solving the Navier-Stokes equations for incompressible fluid written with a primitive set of variables is difficult since the pressure is not a thermodynamic quantity. This drawback can be overcome with the introduction of an additional time derivative in the continuity equation. The problem of the oscillations of the numerical solution can be resolved with artificial compressibility:

$$\frac{1}{\beta}\frac{\partial p}{\partial t}+\frac{\partial(\rho v_i)}{\partial x_i}=0 \tag{3},$$

kjer je β umetna stisljivost.

Z vpeljavo brezrazsežnih spremenljivk, kjer sta L in v_∞, značilna dolžina in hitrost,

where the coefficient β is the artificial compressibility.

The introduction of nondimensional variables, where L and v_∞ are the characteristic length and the characteristic velocity, respectively:

$$x_i^- = \frac{1}{L}\,x_i \;,\quad v_i^- = \frac{1}{v_\infty}\,v_i \;,\quad p^- = \frac{1}{\rho_o v_\infty^2}\,p \;,\quad t^- = \frac{v_\infty}{L}\,t \;,\quad \beta^- = \frac{1}{v_\infty^2}\,\beta$$

prevedemo enačbi (1) in (2) v naslednjo obliko:

This results in the transformation of Equations (1) and (2) into:

$$\frac{1}{\beta^-}\frac{\partial p^-}{\partial t^-}+\frac{\partial v_i^-}{\partial x_i^-}=0.$$

$$\frac{\partial v_i^-}{\partial t^-}+\frac{\partial}{\partial x_j^-}(v_j^- v_i^-)=-\frac{\partial p^-}{\partial x_i^-}+\frac{\partial}{\partial x_j^-}\left((\mu_{NN}^-)(\frac{\partial v_i^-}{\partial x_j^-}+\frac{\partial v_j^-}{\partial x_i^-})\right)$$

V zgornjih enačbah se pojavljajo same brezrazsežne spremenljivke, zato bomo zaradi primernosti pisanje zvezdice (*) opustili.

Sistem enačb za ravninski tok nestisljive nenewtonske tekočine ob upoštevanju umetne stisljivosti lahko zapišemo v konzervativni obliki kot eno samo vektorsko enačbo ([1] in [10]):

These equations employ only nondimensional variables and we can, for convenience, skip the writing of (*).

The system of non-dimensional equations for the planar flow of an incompressible, non-Newtonian fluid with artificial compressibility can be written in conservative form as a single vector equation ([1] and [10]):

$$\frac{\partial Q}{\partial t}+\frac{\partial E}{\partial x}+\frac{\partial G}{\partial y}=\frac{\partial E_{vis}}{\partial x}+\frac{\partial G_{vis}}{\partial y} \tag{4},$$

kjer so:

where:

$$Q=\begin{Bmatrix} p/\beta \\ v_x \\ v_y \end{Bmatrix} \;,\quad E=\begin{Bmatrix} v_x \\ v_x^2+p \\ v_x v_y \end{Bmatrix} \;,\quad G=\begin{Bmatrix} v_y \\ v_x v_y \\ v_y^2+p \end{Bmatrix} \;,\quad E_{vis}=\begin{Bmatrix} 0 \\ \bar{\tau}_{xx} \\ \bar{\tau}_{xy} \end{Bmatrix} \;,\quad G_{vis}=\begin{Bmatrix} 0 \\ \bar{\tau}_{xy} \\ \bar{\tau}_{yy} \end{Bmatrix}$$

in

$$\bar{\bar{\tau}} = \mu_{NN} \begin{bmatrix} 2\frac{\partial v_x}{\partial x} & \frac{\partial v_x}{\partial y} + \frac{\partial v_y}{\partial x} \\ \frac{\partial v_x}{\partial y} + \frac{\partial v_y}{\partial x} & 2\frac{\partial v_y}{\partial y} \end{bmatrix}$$

Z vpeljavo lokalnih koordinat (ξ, η), katerih povezavo s kartezijevim koordinatnim sistemom podamo z:

$$\frac{\partial}{\partial x} = \frac{\partial \xi}{\partial x} \cdot \frac{\partial}{\partial \xi} + \frac{\partial \eta}{\partial x} \cdot \frac{\partial}{\partial \eta} \quad , \quad \frac{\partial}{\partial y} = \frac{\partial \xi}{\partial y} \cdot \frac{\partial}{\partial \xi} + \frac{\partial \eta}{\partial y} \cdot \frac{\partial}{\partial \eta}$$

prevedemo enačbo (4) v obliko

$$\frac{\partial \mathcal{Q}}{\partial t} + \frac{\partial \mathcal{E}}{\partial \xi} + \frac{\partial \mathcal{G}}{\partial \eta} = \frac{\partial \mathcal{E}_{vis}}{\partial \xi} + \frac{\partial \mathcal{G}_{vis}}{\partial \eta} \qquad (5),$$

kjer so:

$$\mathcal{Q} = JQ \; , \quad \mathcal{E} = J\left(\frac{\partial \xi}{\partial x}E + \frac{\partial \xi}{\partial y}G\right) \; , \quad \mathcal{G} = J\left(\frac{\partial \eta}{\partial x}E + \frac{\partial \eta}{\partial y}G\right), \mathcal{E}_{vis} = J\left(\frac{\partial \xi}{\partial x}E_{vis} + \frac{\partial \xi}{\partial y}G_{vis}\right)$$

$$\mathcal{G}_{vis} = J\left(\frac{\partial \eta}{\partial x}E_{vis} + \frac{\partial \eta}{\partial y}G_{vis}\right) \quad \text{in} \quad J = \frac{\partial x}{\partial \xi} \cdot \frac{\partial y}{\partial \eta} - \frac{\partial x}{\partial \eta} \cdot \frac{\partial y}{\partial \xi}$$

Pri reoloških modelih posplošenih newtonskih tekočin je $\underline{\tau}$ podan z izrazom $\underline{\tau} = -\mu\left(\dot{\gamma}\right)\underline{\dot{\gamma}}$, kjer lahko tenzor deformacijske hitrosti in deformacijsko hitrost zapišemo kot:

$$\underline{\dot{\gamma}} = \vec{\nabla}\vec{v} + \left(\vec{\nabla}\vec{v}\right)^T \quad , \quad \dot{\gamma} = \sqrt{\frac{1}{2}\left(\underline{\dot{\gamma}} : \underline{\dot{\gamma}}\right)}$$

kjer smo z operatorjem **:** označili sled tenzorja.

2 REOLOŠKI MODEL - SISKOV MODEL

V okviru sodelave s Premogovnikom Velenje smo opravili meritve viskoznosti na cevnem viskozimetru, prikazanem na sliki 1 [7]. Bistvena sestavna dela viskozimetra sta zalogovnik in kapilarna cev, skozi katero se pri različnih tlakih pretaka zmes, katere viskoznost določamo.

Meritve smo opravljali na treh različnih mešanicah elektrofiltrskega pepela (ostanek iz termoelektrarne Šoštanj) in vode.

and:

With the introduction of local coordinates (ξ, η) connected to the Cartesian coordinate system through the relation:

Equation (4) transforms into:

where:

Rheological models of generalised Newtonian fluids have $\underline{\tau}$ defined with the expression $\underline{\tau} = -\mu\left(\dot{\gamma}\right)\underline{\dot{\gamma}}$, where the shear-stress tensor and the shear rate are written as:

and the operator **:** means the trace of a tensor.

2 RHEOLOGICAL MODELS - SISKO MODEL

The setup of the viscosimeter is shown in Figure 1 [7], within the framework of a cooperation with Premogovnik Velenje. Measurements of viscosity using the capillary viscosimeter were performed. The essential parts of the viscosimeter are the container and the capillary pipe. The measured mixture flows through the pipe under various pressures.

The measurements were performed using three different mixtures of electro-filter ash (the product of the Šoštanj thermal powerplant) and water.

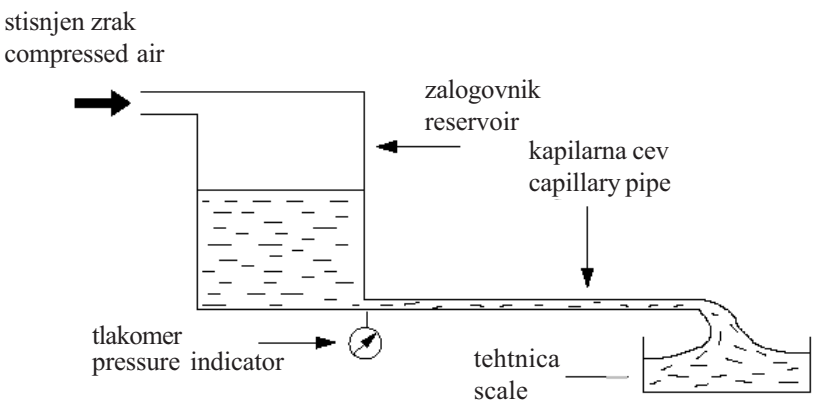

Sl. 1. *Vodoravni kapilarni viskozimeter*
Fig. 1. *Horizontal capilary viscosimeter*

Preglednica 1. *Masni deleži pepela in vode v zmeseh in gostota zmesi*
Table 1. *Mass fraction of ash and water in the mixtures and the density of the mixtures*

	$\dot{m}_{ash}/\dot{m}_{H_2O} \cdot 100$ [%]	ρ [kg/m^3]
A	50	1364
B	40	1469
C	37	1524

V preglednici 1 so podani masni deleži vode in pepela ter gostote izbranih zmesi.

Kakor smo že zapisali, smo izbrane zmesi modelirali s Siskovim zakonom tečenja kot reološkim modelom posplošenih newtonskih tekočin. Zapišemo ga v obliki:

Table 1 shows the mass fractions of the water and ash and the densities of the chosen mixtures.

The chosen mixtures were modelled using the Sisko model as a rheological model of generalized Newtonian fluids. It can be written in the following forms:

$$\underline{\tau} = -\mu(\dot{\gamma})\,\underline{\dot{\gamma}} = -\left(\mu_{\_} + m \cdot \dot{\gamma}^{n-1}\right)\underline{\dot{\gamma}} \tag{6}$$

oziroma

or

$$\mu\,(\dot{\gamma}) = \mu_{\_} + m\dot{\gamma}^{n-1} \tag{7}.$$

Triparametrski model je sestavljen iz klasičnega potenčnega zakona tečenja z asimptotično vrednostjo dinamične viskoznosti μ_∞. μ_∞, m in n so vrednosti, podane za vsako tekočino posebej, in se določijo na temelju meritev viskoznosti. Če je $\mu_\infty = 0$, $n = 1$ in $m = \mu$, preide model v Newtonov zakon tečenja.

Na temelju meritev so ob uporabi metode najmanjših kvadratov [8] izpeljani parametri Siskovega modela, in sicer:

The three-parameter model consists of the well-known power-law model with an added asymptotical coefficient of dynamic viscosity, μ_∞. The values μ_∞, m and n are specified for each fluid separately, and are obtained from experimental viscosity measurements. If one specifies $\mu_\infty = 0$, $n = 1$ and $m = \mu$ one gets an expression for a Newtonian fluid.

Based on the measurements performed, and with the use of the least-squares method [8], the following Sisko model parameters are obtained:

• za zmes A

• for mixture A

$$\mu\,(\dot{\gamma}) = 0.001339 + 0.000059\dot{\gamma}^{1.6771} \tag{8}$$

• za zmes B

• for mixture B

$$\mu\,(\dot{\gamma}) = 0.000628 + 0.000124\dot{\gamma}^{1.6171} \tag{9}$$

• za zmes C

• for mixture C

$$\mu\,(\dot{\gamma}) = 0.000008 + 0.006181\dot{\gamma}^{1.1719} \tag{10}.$$

3 REZULTATI

Model smo preskusili na primeru gnanega toka v kotanji. Gnana kotanja kot značilen dvorazsežni primer je pravokotnik s tremi mirujočimi stranicami in eno pomično stranico, ki se giblje z nespremenljivo hitrostjo. V našem primeru je to kvadrat z brezrazsežno dolžino stranice 1 in brezrazsežno hitrostjo pomika zgornje plošče 1. Geometrijska oblika kotanje je prikazana na sliki 2. Prekinjeni črti po sredini kotanje označujeta osrednji črti (navpično in vodoravno) po katerih smo primerjali hitrostne profile. Dodatna pričakovana težava tega primera je nezveznost v stičiščih mirujočih in gibajoče se stranice.

3 RESULTS

The model was tested with the driven-cavity flow. The driven cavity, as a typical two-dimensional example, is rectangular with three fixed walls and one moving wall that moves with constant velocity. In the selected case the cavity has a square form with a nondimensional side length of 1 and an nondimensional velocity of the top wall 1. The geometry is depicted in Figure 2. The dashed lines through the centre of the cavity show the locations (vertical and horizontal) where the velocity profiles were compared. An additional, but expected, difficulty with this case was the discontinuity in the top corners of the cavity, where the moving and fixed walls connect.

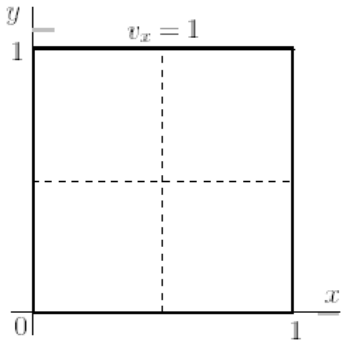

Sl. 2. *Geometrijska oblika in robni pogoji: gnana kotanja*
Fig. 2. *Geometry and boundary conditions: driven cavity*

V prvem delu rezultatov je prikazana konvergenca rezultatov v odvisnosti od gostote mreže. Rezultate smo primerjali z vrednostmi iz literature. Kot primerjalne vrednosti smo uporabili najnižje negativne vrednosti vodoravne in navpične komponente hitrosti na osrednjih črtah. Odstopanje od primerjalnih vrednosti smo definirali z izrazoma [4]:

$$\Delta v_x = \frac{\left|v_{x_{ref}} - v_x\right|}{\left|v_{x_{ref}}\right|} \cdot 100 \quad [\%] \quad , \quad \Delta v_y = \frac{\left|v_{y_{ref}} - v_y\right|}{\left|v_{y_{ref}}\right|} \cdot 100 \quad [\%]$$

Konvergenca rezultatov za različne gostote mreže je prikazana v preglednici 1. Rezultati so primerjani z referenčnimi vrednostmi za newtonsko tekočino za *Re = 400*.

In the first part of the results the convergence of the results due to mesh refinement is shown. The results were compared to the benchmark solution. The maximum negative values of the horizontal and vertical components of the velocity on the centre lines were used for comparison. Deviation from the benchmark solution was defined with the following expression [4]:

The convergence of the results for different mesh sizes is shown in Table 1. The results were compared to reference values for a Newtonian fluid with a Reynolds number value *Re=400*.

Preglednica 2. *Odstopanje rezultatov v odvisnosti od gostote mreže (Siskov model: $\mu_\infty = 0$, m = 0,0025, n = 1)*
Table 2. *Deviation of the results for different mesh sizes (Sisko model: $\mu_\infty = 0$, m = 0.0025, n = 1)*

	Δv_x %	Δv_y %
11×11	44.17	38.60
21×21	20.63	19.71
41×41	5.50	5.19
81×81	1.02	0.80
129×129	0.28	0.19

Pri redkejših enakomernih mrežah zaradi velikih gradientov ob trdnih stenah (predvsem zgornji) pride do večjih odstopanj od primerjalnih vrednosti. Z zgoščevanjem mreže se rezultati približujejo referenčnim vrednostim. Z najgostejšo mrežo (129×129) dobimo manj ko 0,3 % odstopanja od referenčnih vrednosti za izbrane parametre. Potek hitrostnih profilov v odvisnosti od gostote mreže je prikazan na sliki 3.

Na slikah 4, 5 in 6 so prikazani rezultati izračuna tokovnih razmer gnanega toka v kotanji z uporabo Siskovega modela.

Iz primerjave oblik profilov z rezultati iz literature za newtonske [2] tekočine je glede na gradiente hitrosti moč sklepati, da je zahtevnost izračuna za najredkejšo zmes (in s tem najmanj viskozno tekočino) primerljiva z izračunom newtonske tekočine za Reynoldsovo število *Re=1000*.

When using coarse equidistant meshes the differences from reference values are larger due to high velocity gradients near the walls (especially the top wall). With a refinement of the mesh the results approach reference values. With the finest mesh (129×129) a less-than-0.3% difference from the reference values for the chosen non-Newtonian model parameters was obtained. The velocity profiles for the different mesh densities are shown in Figure 3.

In Figures 4, 5 and 6 the results are shown for the calculation of the flow field in a driven cavity for model parameters of the Sisko model obtained from the experiment with a capilary viscosimeter.

A comparison of the calculated velocity profiles with the benchmark solution for Newtonian [2] fluids, taking into account velocity gradients, shows that the computation with the least dense mixture (meaning the least viscous fluid) corresponds to the computation of a Newtonian fluid with a Reynolds number value *Re=1000*.

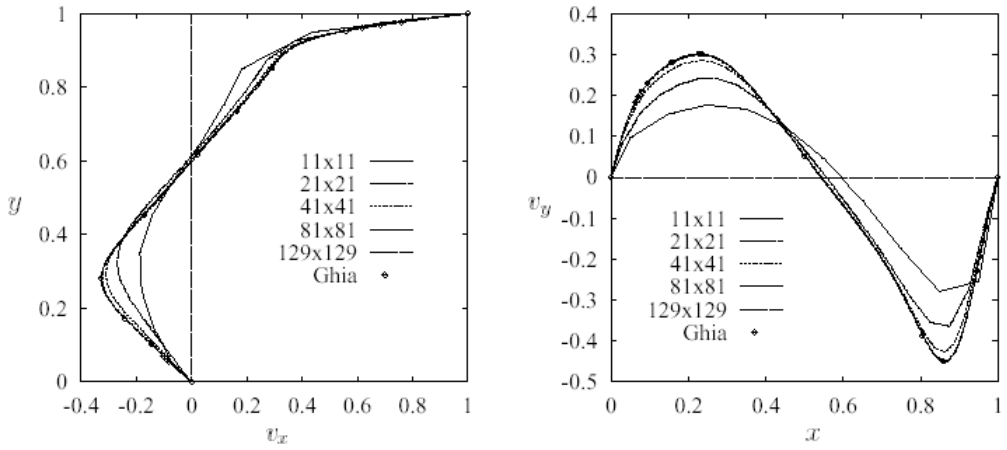

Sl. 3. *Profil vodoravne hitrosti v_x skozi navpično središčnico in navpične hitrosti v_y skozi vodoravno središčnico za različne gostote mreže (Sisko model: $\mu_\infty = 0$, m = 0,0025, n = 1)*

Fig. 3. *Horizontal velocity profile v_x through the vertical centreline and the vertical velocity profile v_y through the horizontal centreline for different mesh sizes (Sisko model: $\mu_\infty = 0$, m = 0.0025, n=1)*

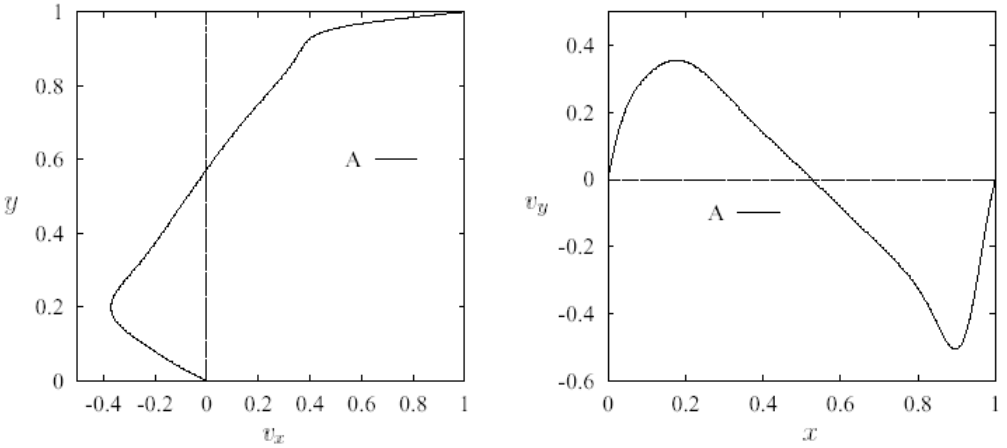

Sl. 4. *Profil vodoravne hitrosti v_x skozi navpično središčnico in navpične hitrosti v_y skozi vodoravno središčnico za zmes A (129×129 vozlišč)*

Fig. 4. *Horizontal velocity profile v_x through the vertical centreline and the vertical velocity profile v_y through the horizontal centreline for mixture A (129×129 nodes.)*

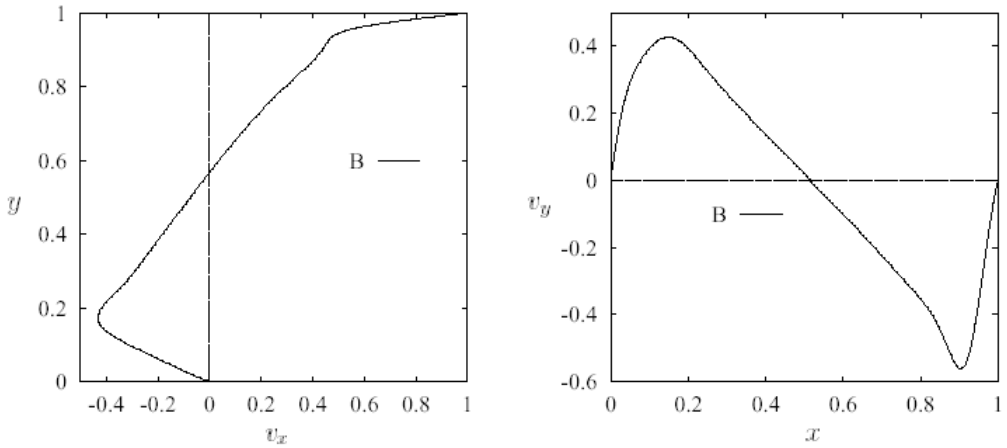

Sl. 5. *Profil vodoravne hitrosti v_x skozi navpično središčnico in navpične hitrosti v_y skozi vodoravno središčnico za zmes B (129×129 vozlišč)*

Fig. 5. *Horizontal velocity profile v_x through the vertical centreline and the vertical velocity profile v_y through the horizontal centreline for mixture B (129×129 nodes.)*

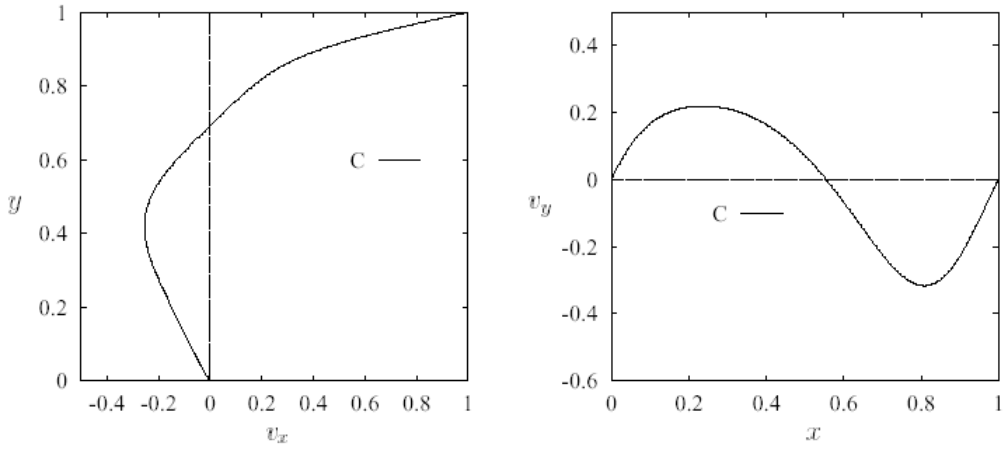

Sl. 6 *Profil vodoravne hitrosti v_x skozi navpično središčnico in navpične hitrosti v_y skozi vodoravno središčnico za zmes C (129×129 vozlišč)*

Fig. 6. *Horizontal velocity profile v_x through the vertical centreline and the vertical velocity profile v_y through the horizontal centreline for mixture C (129×129 nodes.)*

Model smo preskusili tudi na standardnem testnem primeru toka v kanalu z nenadno zožitvijo. Robni pogoji in geometrijska oblika so prikazani na sliki 7. Oba dela kanala merita 10 enot. Prvi del kanala je visok 4 enote, nato pa se kanal nenadno zoži na 1 enoto. Za izračun smo izdelali tri neenakomerne mreže, in sicer z 1500 (40×30 + 10×30), 6000 (80×60 + 20×60) in 13500 (120×90 + 30×90) končnimi prostorninami.

Za reološki model smo pri izračunih uporabili Siskov model za zmes A (enačba 8). Na stenah smo predpisali v_x, $v_y = 0$, na spodnji steni simetrijske robne pogoje ($\partial v_x/\partial y = v_y = 0$), na iztoku prosti iztok ($\partial v_x/\partial x = v_y = 0$) in na vtoku parabolični profil s povprečno hitrostjo v_{av} = 0,0393. (Ob uporabi newtonske dinamične viskoznosti μ = 0,01339 bi primer ustrezal *Re=400,* računano na izstopni prerez iz kanala).

Na sliki 8 je prikazana primerjava hitrostnih profilov na polovici dolžine kanala za vse tri gostote mreže. Po pričakovanju se profili hitrosti slabše ujemajo na mestu zožitve, kjer rezultati, dobljeni z najredkejšo mrežo, še dokaj odstopajo; rezultati, dobljeni z gostejšima mrežama, pa se že dokaj dobro ujemajo. Z zgoščevanjem mreže na področju razvijanja hitrostne mejne plasti rastejo gradienti hitrosti ob trdnih stenah in zaradi tega se hitrosti zmanjšujejo proti srednjici kanala.

The model was also tested on a standard test case of flow in a channel with a sudden contraction. The boundary conditions and geometry are shown in Figure 7. The inlet and outlet channels have a length of 10 units. The inlet channel has a height of 4 units and contracts to an outlet height of 1 unit. Three, non-equidistant meshes were generated: 1500 (40×30 + 10×30), 6000 (80×60 + 20×60) and 13500 (120×90 + 30×90) finite volumes.

We used the Sisko rheological model with parameters for mixture A (Equation 8). We prescribed v_x, v_y = 0, on the walls, the symmetry boundary condition ($\partial v_x/\partial y = v_y = 0$) on the bottom edge, the developed profile ($\partial v_x/\partial x = v_y = 0$) at the outlet and the parabolic velocity profile with mean value v_{av} = 0.0393 at the inlet. (Using the Newtonian dynamic viscosity μ = 0.01339 and the outlet channel height, the equivalent Reynolds number would be *Re=400*).

In Figure 8 is the comparison of the velocity profiles on the contraction cross-section for three mesh densities. As expected, the profiles disagree in this area, especially for the coarsest mesh, whereas the two finest meshes show reasonably good agreement. With finer meshes in the area of the development of the boundary layer the velocity gradients near the wall increase and the velocity near the centreline of the channel decreases.

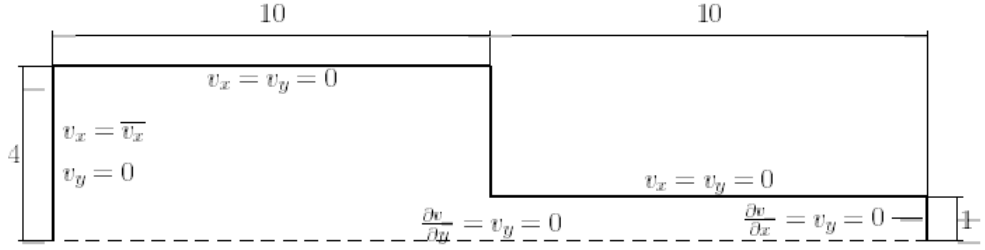

Sl. 7. *Geometrijska oblika in robni pogoji: nenadna zožitev (4:1)*

Fig. 7. *Geometry and boundary conditions: sudden contraction (4:1)*

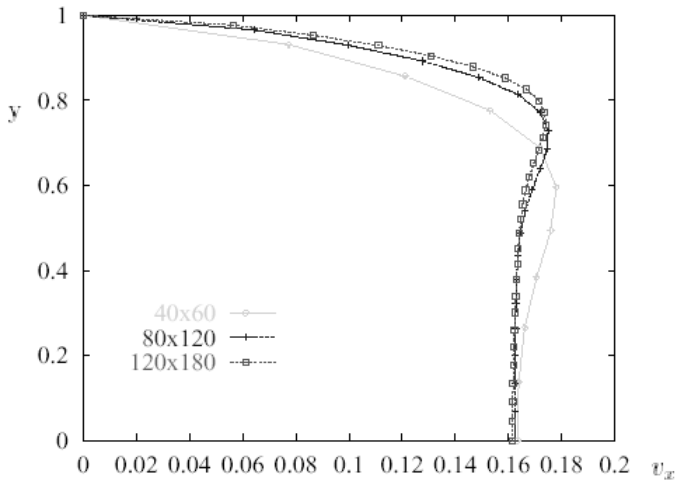

Sl. 8. *Primerjava profilov hitrosti na 1/2 dolžine kanala*
Fig. 8. *Comparison of velocity profiles on 1/2 the channel length*

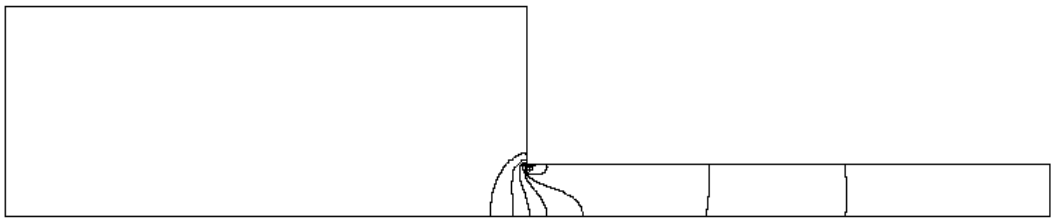

Sl. 9. *Tlačno polje v kanalu*
Fig. 9. *Pressure field in the channel*

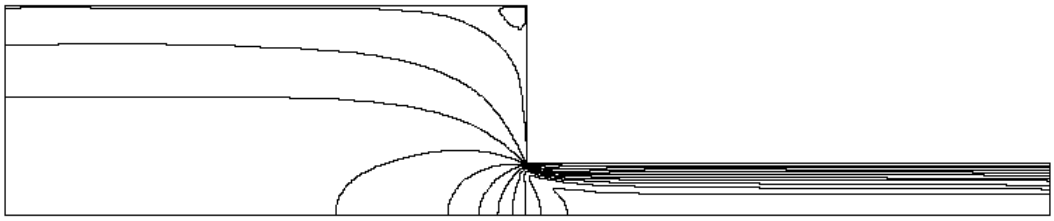

Sl. 10. *Izolinije hitrosti v smeri koordinatne osi x (v_x)*
Fig. 10. *Constant x component velocity contours (v_x)*

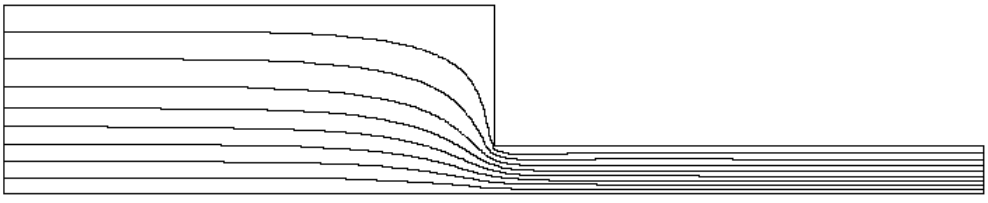

Sl. 11. *Tokovnice (zožitev 4:1)*
Fig. 11. *Streamlines (contraction 4:1)*

Na sliki 9 je prikazano tlačno polje v kanalu, izračunano z najgostejšo mrežo.

Na sliki 10 so prikazane izolinije hitrosti v smeri koordinatne osi *x* (najgostejša mreža).

Na sliki 11 so prikazane tokovnice v kanalu (najgostejša mreža).

4 SKLEP

Metodo končnih prostornin smo uporabili za računanje tokovnih razmer v laminarni viskozni

Figure 9 shows the pressure field in the channel computed using the finest mesh.

Figure 10 shows the constant *x* component velocity contours (the finest mesh).

Figure 11 shows the streamlines in the channel (the finest mesh).

4 CONCLUSIONS

The finite-volume method was used to compute the flow conditions for a laminar, viscous,

nestisljivi nenewtonski tekočini, pri čemer smo kot reološki model uporabili Siskov model. Formulacija je testirana na primeru gnanega toka v kotanji. Prikazan je vpliv natančnosti rezultatov v odvisnosti od gostote mreže. Prikazani rezultati za primer gnanega toka v kotanji, dobljeni z najgostejšo mrežo (129×129 vozlišč) se zelo dobro ujemajo s primerjalnimi vrednostmi v literaturi. Modelni parametri Siskovega modela so določeni na temelju preskusa s cevnim viskozimetrom za tri različne gostote zmesi pepela in vode.

incompressible non-Newtonian fluid. The Sisko rheological model was used for capturing non-linear fluid properties. The proposed formulation was tested on driven-cavity flow. The influence of the mesh density on the accuracy of the numerical results was shown. The results obtained on the finest mesh (129×129 nodes) agree well with the values published in the literature. The computational examples conclude with three computations based on the model parameters of the Sisko model, obtained from an experiment with a capillary viscosimeter for three different mixtures of ash and water.

5 LITERATURA
5 REFERENCES

[1] Drikakis, D., P.A. Govatsos, D.E. Papantonis (1994) A characteristic-based method for incompressible flows, *Int. J. for Numerical Methods in Fluids 19*, 667-685.
[2] Ghia, U., K.N. Ghia, C.T. Shin (1982) High Re solutions for incompressible flow using the Navier-Stokes equations and a multigrid method, *Journal of computational physics 48*, 387-411.
[3] Kanduti, D., J. Marn (2002) Eksperimentalna določitev toka zmesi pepela in vode, *Zbornik Kuhljevih dnevov 2002*, 129-136.
[4] Marn, J., M. Delić, Z. Žunič (2001) Non-Newtonian fluid flow analysis with finite difference and finite volume numerical models, *Applied Rheology 11*, 325-335.
[5] Škerget, L. (1994) Mehanika tekočin, *Tehniška fakulteta v Mariboru in Fakulteta za strojništvo v Ljubljani.*
[6] Tanner, R.I. (1985) Engineering rheology, *Oxford University Press*, New York.
[7] Ternik, P. (2002) Modeliranje toka nenewtonskih disperznih sistemov, magistrsko delo, *Univerza v Mariboru*, 2002a.
[8] Ternik, P. (2002) Neobjavljene analize eksperimentov v viskozimetru na vzorcih Premogovnika Velenje, *Univerza v Mariboru*, 2002b.
[9] Turian, R.M., T.W. Ma, F.L.G. Hsu, M.D.J. Sung (1998) Flow of concentrated non-Newtonian slurries: 1. friction losses in laminar, turbulent and transition flow through straight pipe, *Int. J. Multiphase Flow 24*, No. 2, 225-242.
[10] Žunič, Z. (1997) Numerična obravnava problema aerodinamike vozil, Magistrsko delo, *Univerza v Mariboru*.

Naslov avtorjev: mag. Marjan Delić
prof.dr. Jure Marn
mag. Zoran Žunič
Fakulteta za strojništvo
Univerza v Mariboru
Smetanova 17
2000 Maribor
marjan.delic@uni-mb.si
jure.marn@uni-mb.si
zoran.zunic@uni-mb.si

Author's Address: Mag. Marjan Delić
Prof.Dr. Jure Marn
Mag. Zoran Žunič
Faculty of Mechanical Eng.
University of Maribor
Smetanova 17
2000 Maribor
marjan.delic@uni-mb.si
jure.marn@uni-mb.si
zoran.zunic@uni-mb.si

Prejeto: 20.12.2002
Received:

Sprejeto: 31.1.2003
Accepted:

© Strojniški vestnik 48(2002)12,696-706
ISSN 0039-2480
UDK 532.5:536.22
Izvirni znanstveni članek (1.01)

© Journal of Mechanical Engineering 48(2002)12,696-706
ISSN 0039-2480
UDC 532.5:536.22
Original scientific paper (1.01)

Vpliv Prandtlovega števila na turbulentni prenos toplote ob ravni steni

The Influence of Prandtl Number on Near-Wall Turbulent Heat Transfer

Robert Bergant - Iztok Tiselj

Za opis turbulentnega prenosa toplote iz stene na tekočino je pri nizkih vrednosti Reynoldsovih in Prandtlovih številih mogoče uporabiti neposredno numerično simulacijo (NNS-DNS), ki opiše vse krajevne in časovne skale pojava. Vpliv Reynoldsovega števila na turbulentni prenos toplote (hitrosti, temperature, fluktuacije itn.) je razmeroma majhen, medtem ko je vpliv Prandtlovega števila veliko večji. Pri naših simulacijah toka v kanalu smo pri Reynoldsovem številu Re ≈ 5000 analizirali tri različna Prandtlova števila, in sicer Pr = 0,025, Pr = 1 in Pr = 5,4.

Ločljivost NNS turbulentnega prenosa gibalne količine je premo sorazmerna z $Re^{3/4}$ v vseh smereh koordinatnega sistema. Pri upoštevanju prenosa toplote, za tekočine s Prandtlovim številom, večjim od ena, velja, da je ločljivost premo sorazmerna z $Re^{3/4}Pr^{1/2}$. Pri Re = 5260 in Pr = 5,4 smo opravili tri numerične simulacije pri različnih ločljivostih. Vse tri simulacije so NNS za hitrostno polje, samo simulacija z največjo ločljivostjo je tudi NNS za temperaturno polje. Rezultati so pokazali, da je mogoče temperaturno polje zelo natančno napovedati tudi z nekoliko slabšo ločljivostjo od teoretično zahtevane.

(Ključne besede: tok ob steni, tok turbulentni, prenos toplote, števila Prandtl, simuliranje numerično)

For describing the heat transfer from a wall to a fluid at low Reynolds and Prandtl numbers we can use a direct mumerical simulation (DNS), which describes all the length and time scales of the phenomenon. The Reynolds number has a weak influence on the turbulent heat transfer (velocities, temperatures, RMS-fluctuations…), whereas the increasing Prandtl number has a stronger influence. In our flow simulations in the channel, three different Prandtl numbers, i.e. Pr = 0.025, Pr = 1 and Pr = 5.4, at a Reynolds number Re ≈ 5000 were analyzed.

The resolution of the DNS for turbulent momentum transfer is proportional to $Re^{3/4}$ in all directions. When considering heat transfer in fluids for a Prandtl number higher than one, the resolution is proportional to $Re^{3/4}Pr^{1/2}$. Three different numerical simulations at different resolutions were performed at Re = 5260 and Pr = 5.4. All three simulations are a DNS for the velocity field, whereas only the simulation at the highest resolution is also a DNS for the thermal field. The results showed that the thermal field could be accurately described with a lower resolution than theoretically required.

(Keywords: near-wall flow, turbulent flow, heat transfer, Prandtl numbers, direct numerical simulation)

0 UVOD

V zadnjih 15 letih se je neposredna numerična simulacija (NNS) uveljavila kot pomembno orodje pri razumevanju mehanizma prenosa toplote v turbulentni mejni plasti. NNS pomeni natančno reševanje Navier-Stokesovih enačb brez dodatnih turbulentnih modelov. Prve NNS hitrostnega polja pri nižjih vrednostih Reynoldsovih številih sta opravila Kim in Moin [5], ki sta raziskovala hitrostno polje ter opazovala turbulentne strukture v kanalu (Re = 5700). Pozneje sta Kim in Moin [6] k enačbam hitrostnega polja dodala še energijsko enačbo za prenos toplote. Tako sta med dvema stenama preučevala tudi

0 INTRODUCTION

Over the past 15 years direct numerical simulation (DNS) has become an important research tool in understanding near-wall turbulent heat transfer. A DNS means a precise solving of the Navier-Stokes equations without any extra turbulent models. The first DNS of a velocity field at a low Reynolds number was performed by Kim and Moin [5], who investigated the velocity field and observed turbulent structures in the channel (Re = 5700). Later, they [6] also added an energy equation to the equations of velocity field for the heat-transfer calculations. When considering heat transfer, the

temperaturno polje ter opazovala koherentne strukture, ki so se pojavljale v bližini sten. Uporabila sta nekoliko nenavaden postopek, saj sta predpostavila enakomerno gretje tekočine po celotni prostornini, steni pa sta predstavljali toplotni ponor. Tudi Kasagi [2] je raziskoval temperaturno polje, vendar je za geometrijsko obliko vzel kanal, ki je bil gret z zgornjo in spodnjo steno. Vse te simulacije so potekale pri nizkih vrednostih Reynoldsovih in Prandtlovih števil. Pozneje so raziskovalci (Kawamura [4], Na in Hanraty [7]) mejo Prandtlovega števila dvignili do deset. Kawamura [4] je raziskoval vpliv Reynoldsovega (do Re = 14000) in Prandtlovega števila (do Pr = 5). V območju tik ob steni je ugotovil majhen vpliv Reynoldsovega števila in veliko večji vpliv Prandtlovega števila na statistiko turbulentnega prenosa toplote (hitrostni profili, fluktuacije hitrosti, turbulentni toplotni tokovi).

Prispevek je vsebinsko razdeljen na dva dela. V prvem delu je posebna pozornost namenjena vplivu Prandtlovega števila na prenos toplote. NNS so bile izvedene pri Reynoldsovem številu Re = 4580 in Re = 5260 ter treh različnih Prandtlovih številih: Pr = 0,025, Pr = 1 in Pr = 5,4 (glej preglednico 1).

Drugi del je namenjen preučevanju ločljivosti pri Re = 5260 in Pr = 5,4. Analizirane so bile računske mreže s tremi različnimi ločljivostmi. Teoretično naj bi bila ločljivost NNS pri Prandtlovih številih, večjih od ena, sorazmerna kvadratnemu korenu Prandtlovega števila v vseh smereh koordinatnega sistema v primerjavi z ločljivostjo za Pr = 1 [8]. Zahtevo sta v svojih NNS upoštevala Kawamura [3] in Tiselj [9]. Pri Pr = 5,4 to pomeni, da moramo število točk računske mreže, ki je zadostno za opis hitrostnega polja pri Re= 5260, povečati približno za faktor $\sqrt{5,4}$ v vsaki smeri. Za prvo simulacijo je bila tako vzeta dovolj gosta mreža, ki zmore opisati najmanjše skale hitrostnega in temperaturnega polja (NNS).

Da je zahtevana gostitev mreže pri Pr > 1 nekoliko preostra, sta nakazala že Na in Hanratty [7], ki sta pri Pr = 10 uporabila večjo ločljivost le v smeri pravokotno na steno. Tako je v drugi simulaciji v tem prispevku izboljšana ločljivost v smeri pravokotno na steno, tretja simulacija pa je opravljena z najmanjšo ločljivostjo, ki je zadostna le za NNS hitrostnega polja. Zadnji dve simulaciji tako izpolnjujeta pogoj za NNS hitrostnega polja, na pa tudi za NNS temperaturnega polja.

1 ENAČBE IN NUMERIČNI POSTOPEK

Pri numeričnih simulacijah turbulentnega prenosa toplote sta bili uporabljeni dve različni geometrijski obliki neskončnega kanala. Zaprt kanal (sl. 1-levo), omejen s spodnjo in zgornjo steno, grejemo z nespremenljivim toplotnim tokom, vmes pa zaradi razlike tlakov teče tok tekočine. Pri odprtem kanalu (sl. 1-desno) grejemo spodnjo steno, nad katero teče tok tekočine s prosto površino. Uporabili smo brezrazsežne

temperature field between two walls and the coherent structures near the walls were studied. But this was an unusual approach, because uniform volumetric heat generation was assumed, where the walls represented a heat sink. Kasagi et al [2] also investigated the thermal field, but in this case the channel was heated by the top and bottom walls. All these simulations were performed for low Reynolds and Prandtl numbers. Later, Kawamura et al [3], and Na and Hanratty [7] raised the limit of the Prandtl number to ten, while Kawamura et al [4] studied the influence of Reynolds numbers (up to Re = 14000) and Prandtl numbers (up to Pr = 5). They found a weak influence of the Reynolds number and a stronger influence of the Prandtl number near the wall for turbulent heat transfer (velocity profiles, velocity fluctuations, turbulent heat fluxes).

The content of this article is divided into two parts. In the first part we investigate the influence of the Prandtl number on the heat transfer. DNSs were performed at Reynolds numbers Re = 4580 and Re = 5260, and at three different Prandtl numbers: Pr = 0.025, Pr = 1 and Pr = 5.4 (see Table 1).

The resolution requirements at Re = 5260 and Pr = 5.4 are studied in the second part of the paper, where three different resolutions were analyzed. Theoretically, the resolution for Prandtl numbers higher than one should be proportional to the square root of the Prandtl number in all three directions. This requirement was taken into account in the simulations of Kawamura et al [3] and Tiselj et al [9]. Therefore, at Pr = 5.4 the grid should be improved by approximately a factor of $\sqrt{5.4}$ in all directions. In the first simulation sufficient grid was taken so as to be capable of describing the smallest scales of the velocity and thermal fields (DNS).

The grid-refinement study of Na and Hanratty at the Prandtl number Pr = 10 shows that a finer grid is not required in the streamwise and spanwise directions, but it is necessary in the wall-normal direction. This finding was considered in the second simulation, where a finer grid was applied only in the wall-normal direction, whereas the third simulation was performed with the lowest resolution, which was only sufficient for the DNS of the velocity field. Therefore, the last two simulations are sufficient for the DNS of the velocity field and insufficient for the DNS of the thermal field.

1 EQUATIONS AND NUMERICAL PROCEDURE

Two different geometries for the numerical simulations of turbulent heat transfer in the infinite channel and the flume were used. Channel (Fig.1 - left) is bounded by top and bottom walls, which are heated with a constant heat source, whereas the pressure gradient drives the fluid flows between them. In the flume (Fig. 1 - right), the fluid flows above the heated bottom wall, whereas the top surface is free.

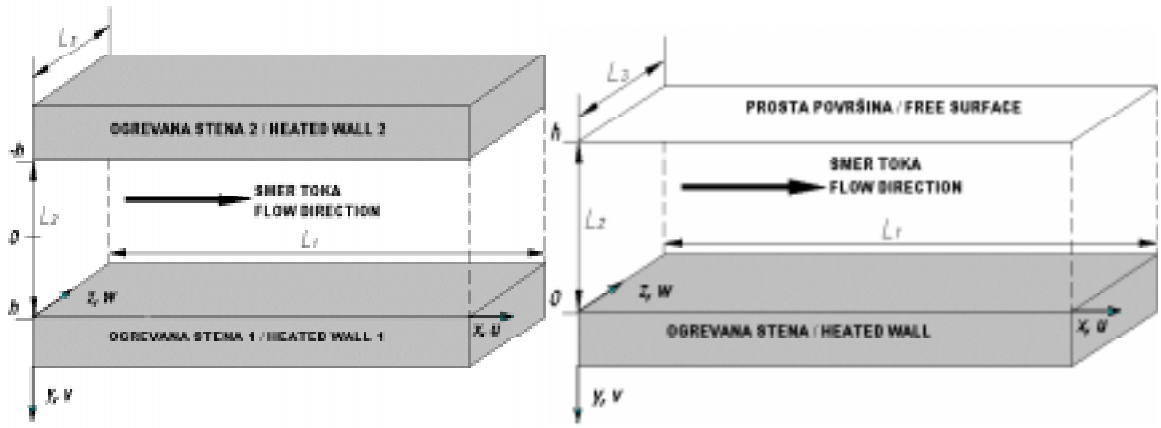

Sl. 1. *Geometrija toka tekočine: levo) zaprt kanal, desno) odprt kanal*
Fig. 1. *Flow geometry: left) channel, right) flume*

Navier-Stokesove enačbe, normalizirane s polovično višino kanala h v zaprtem kanalu oziroma z višino h v odprtem kanalu, disipativno hitrostjo $u_\tau = \sqrt{\tau_w / \rho}$ in disipacijsko temperaturo $T_\tau = q_w / \left(u_\tau \rho_f c_{pf}\right)$. Pri tem je τ_w strižna napetost na steni in je enaka $\tau_w = -\mu (du/dy)_w$. Takšen postopek lahko najdemo tudi v objavah Kasagija [2] ali Kawamure [3]:

The dimensionless Navier-Stokes equations, normalized by the flume height h (or the channel half height h), the friction velocity $u_\tau = \sqrt{\tau_w / \rho}$, and the friction temperature $T_\tau = q_w / \left(u_\tau \rho_f c_{pf}\right)$, were used. τ_w stands for the wall shear stress, defined as $\tau_w = -\mu (du/dy)_w$. Such scaling can be found in the papers of Kasagi et al [2] or Kawamura et al [3]:

$$\nabla \cdot \vec{u}^{+} = 0 \tag{1}$$

$$\frac{\partial \vec{u}^{+}}{\partial t} = -\nabla \cdot \left(\vec{u}^{+}\vec{u}^{+}\right) + \frac{1}{\mathrm{Re}_\tau} \nabla^2 \vec{u}^{+} - \nabla p + \vec{l}_x \tag{2}$$

$$\frac{\partial \theta^{+}}{\partial t} = -\nabla \cdot \left(\vec{u}^{+}\theta^{+}\right) + \frac{1}{\mathrm{Re}_\tau \,\mathrm{Pr}} \nabla^2 \theta^{+} + \frac{u_x^{+}}{u_B^{+}} \tag{3}.$$

Člena $\vec{l}_x$ (enotski vektor v smeri vzdolž toka) in u_x^{+} / u_B^{+} se v en. (2) in (3) pojavita zaradi numerične sheme, ki zahteva periodične robne pogoje v vzdolžni (x) in prečni smeri (z). Re_τ je Reynoldsovo število disipacije in je določeno kot:

The terms $\vec{l}_x$ (unit vector in the streamwise direction) and u_x^{+} / u_B^{+} appear in equations (2) and (3) due to the numerical scheme, which requires periodic boundary conditions in the streamwise and spanwise directions. Re_τ is the friction Reynolds number and is defined as:

$$\mathrm{Re}_\tau = \frac{u_\tau h}{\nu} \tag{4},$$

kjer je h polovica višine kanala. Ne smemo ga mešati z običajnim Reynoldsovim številom, ki je v kanalu definirano kot $\mathrm{Re} = u_B \cdot 2h / \nu$. Iz Reynoldsovega števila disipacije dobimo običajno Reynoldsovo število, če Re_τ pomnožimo z dvakratno vrednostjo povprečne hitrosti u_B v kanalu. Reynoldsovo število $\mathrm{Re} = 4580$ ustreza $\mathrm{Re}_\tau = 150$.

Na osnovi Reynoldsovega števila disipacije priredimo brezrazsežne stenske enote, ki so označene z zgornjim indeksom $^{+}$. Višina kanala je po definiciji enaka dvakratniku Reynoldsovega števila disipacije. Smisel stenskih enot je v tem, da lahko v območju ob steni med seboj primerjamo turbulentne tokove z različnimi Reynoldsovimi števili. Brezrazsežna temperaturna razlika je določena kot:

where h is the channel half height. It should not be confused with the usual Reynolds number in the channel, which is defined as $\mathrm{Re} = u_B \cdot 2h / \nu$. The usual Reynolds number in the channel can be obtained from the friction Reynolds number multiplied by the double bulk velocity u_B. The Reynolds number $\mathrm{Re} = 4580$ corresponds to $\mathrm{Re}_\tau = 150$.

The dimensionless wall units, denoted by the superscript $^{+}$, are based on the friction Reynolds number. By definition, the height of the channel is equal to two times the friction Reynolds number. The meaning of the wall units is in the comparison of the turbulent flows near the wall at different Reynolds numbers. The dimensionless wall-temperature difference is defined as:

$$\theta^{+}(x,y,z,t) = \left(\frac{\langle T_w \rangle - T(x,y,z,t)}{T_\tau} \right) \tag{5}.$$

Na prosti površini tekočine sta robna pogoja za komponenti hitrosti, ki sta vzporedni s steno, enaka $du/dz = 0$ in $dw/dz = 0$, hitrost, pravokotno na steno, pa je enaka $v_{prostapovršina}$=0. Takšen robni pogoj ni fizikalen, ker ne dopušča površinskih valov. Vendar so preskusi Hetsronija (1997, 1999) [12] pokazali, da so površinski valovi pri majhnih Reynoldsovih številih skoraj neznatni in ne vplivajo na obnašanje tekočine tik ob steni. Na stiku stene in tekočine so vse tri komponente hitrosti enake nič. Poleg robnega pogoja hitrosti moramo upoštevati še temperaturni robni pogoj. Prosto površino obravnavamo kot adiabatno: $d\theta^+/dy = 0$, na stiku stene in tekočine pa sta mogoča dva različna temperaturna robna pogoja. Prvi, ki ga v tem prispevku ne obravnavamo, je robni pogoj nespremenljive temperature [11], drugi pa robni pogoj nespremenljivega toplotnega toka, za katerega velja:

The boundary conditions for the velocity components on the top, free surface, parallel to the wall, are $du/dz = 0$ and $dw/dz = 0$, whereas the wall-normal velocity is $v_{free\ surface}$=0. The velocity boundary condition at the free surface is not physical since it does not allow surface waves. However, the experiments of Hetsroni et. al. (1997, 1999) [12] show that this is an acceptable approximation at low Reynolds numbers, where the surface waves are negligible and do not affect the near-wall behavior. The velocity components at the interface of the wall and the fluid are set to zero. Besides the velocity boundary conditions, the thermal boundary conditions have to be considered. The free surface is treated as an adiabatic surface, $d\theta^+/dy = 0$, whereas two different thermal boundary conditions can be applied at the wall-fluid interface. The first, which is not presented in this paper, is the isothermal boundary condition [11], and the second isoflux boundary condition is described as:

$$\frac{d\theta^+}{dy^+} = 0 \qquad (6).$$

Pri tem je brezrazsežna temperatura θ na stiku stene in tekočine povprečena po času in koordinatah vzdolž in prečno na tok enaka nič:

The dimensionless temperature θ at the heated wall, averaged by time and the coordinates in the streamwise and spanwise directions is zero:

$$\left\langle \theta^+\left(y = 1\right)\right\rangle = 0 \qquad (7).$$

Na vstopu v kanal moramo zagotoviti polno razvit turbulentni tok, ki ga dosežemo s periodičnimi robnimi pogoji v smeri vzdolž (x) in prečno (z) na smer toka. To pomeni, da stanje, ki ga dobimo na izhodu iz kanala, preslikamo na vstop, stanje na levi strani pa na desno stran. Pri tem je treba poskrbeti, da sta dolžina in širina kanala dovolj veliki za mešanje tekočine [11].

Kakor je razvidno iz enačb (1) do (3), je temperatura pasivni skalar, ki ne vpliva na turbulenco. To pomeni, da je vzgon zanemarjen in da lastnosti tekočine (viskoznost, toplotna prevodnost itn.) niso odvisne od temperature. Dobljeni rezultati so točni le za sisteme, pri katerih ni velikih temperaturnih razlik, medtem ko je pri večjih temperaturnih razlikah potrebna večja previdnost. Takšen približek so že uporabili Kasagi [2], Kawamura [3] in Tiselj [11].

Za reševanje enačb je bila uporabljena spektralna shema, ki uporablja Fourierjeve vrste v smereh x in z ter polinome Čebiševa v smeri y. Kontinuitetno, gibalno in energijsko enačbo rešujemo z računalniškim programom, ki temelji na delu Gavrilakisa [1].

Vse numerične simulacije so bile izvedene pri Re_τ = 150 in Re_τ = 170,8 ter Pr = 0,025, 1 in 5,4. Geometrijska oblika toka tekočine je bila v primeru Re_τ = 150, pri katerem je bil uporabljen zaprt kanal, enaka 2356 x 942 x 300 stenskih enot v smereh x, z in y. V primeru Re_τ = 170,8 je bil uporabljen odprti kanal, pri katerem je bila geometrijska oblika enaka

Fully-developed turbulent flow must be ensured in the channel entrance. This is achieved with periodic boundary conditions in the streamwise (x) and spanwise (y) directions. It means that the fields at the channel exit are mapped to the channel entrance, and the situation on the left-hand side to the right-hand side, respectively. The length and the width of the channel should ensure sufficient mixing of the fluid [11].

As can be seen from Eqs. (1) to (3) the temperature is assumed to be a passive scalar. This assumption introduces two approximations: neglected buoyancy and neglected temperature dependence of the fluid properties (viscosity, heat conductivity, etc.). The results are thus very accurate, but only for the systems where the temperature differences are not too large; and some caution is required for the systems where the temperature differences are not negligible. Such an approximation was used by Kasagi et al [2], Kawamura et al [3], and Tiselj et al [11].

The equations are solved with a pseudo-spectral scheme using a Fourier series in the x and z directions, and Chebyshev polynomials in the wall-normal y direction. The numerical procedure and the code of Gavrilakis et al[1] are used to solve the continuity, momentum and energy equations.

All the numerical simulations were performed for Re_τ = 150 and Re_τ = 170.8 at Pr = 0.025, 1 and 5.4. At Re_τ = 150, where a channel was used, the computational domain was 2356 x 942 x 300 wall units in the x, z and y directions, respectively. At Re_τ = 170.8, where a flume was used, the computational

2146 x 537 x 171 stenskih enot v smereh *x*, *z* in *y*. Rezultate so začeli povprečiti potem, ko je bil dosežen polno razvit turbulentni tok, kar pomeni, da se tok statistično gledano ni več spreminjal.

Simulacije lahko glede na vrednosti Prandtlovih števil razdelimo na tri glavne skupine (preglednica 1). V prvem delu so prikazane NNS za Pr = 0,025, kjer je bila uporabljena ločljivost, zadostna za hitrostno in temperaturno polje. Ko je Prandtlovo število manjše od 1, so najmanjše krajevne skale temperaturnega polja večje od najmanjših krajevnih skal temperaturnega polja. Drugi del vsebuje NNS za Pr = 1, kjer je bila izbrana ločljivost zadostna za hitrostno in temperaturno polje. Tretji del vsebuje tri različne NNS za Pr = 5,4. Ločljivost prve študije NNS je bila zadostna za hitrostno in temperaturno polje, druga študija je imela približno 2-krat manjšo ločljivost v vzdolžni (*x*) in prečni smeri (*z*), tretja študija pa je imela v primerjavi s prvo približno 2-krat manjšo ločljivost v vseh treh smereh. Zadnjih dveh numeričnih simulacij pravzaprav ne smemo več imenovati NNS, ker ne popišeta najmanjših skal temperaturnega polja, ki se pojavijo pri visokih valovnih številih. Takšne simulacije sva poimenovala ″navidez″ NNS.

domain was 2146 x 537 x 171 wall units in the *x*, *z* and *y* directions, respectively. The results were averaged after the fully-developed turbulent flow was achieved, which means that the flow did not change from the statistical point of view.

The simulations can be divided into three main parts, according to the Prandtl numbers (see table 1). In first part the DNS at Pr = 0.025 is shown, where the applied resolution was sufficient for the velocity and thermal fields. If the Prandtl number is less than 1, the smallest length scales of the temperature field are larger than the smallest length scales of the velocity field. The second part involves a DNS at Pr = 1, where the chosen resolution was sufficient for the velocity and thermal fields. The third part involves three different DNSs at Pr = 5.4. The first DNS resolution was sufficient for the velocity and thermal fields, the second resolution had an approximately two-times smaller resolution in the streamwise (x) and spanwise (z) directions, and the third resolution had a two-times smaller resolution in all three directions. Strictly speaking, the last two numerical simulations cannot be called DNS due to the smallest scales of the thermal field at high wave-number modes. Such simulations were named “quasi” DNSs.

Preglednica 1. *Izračuni pri različnih Pr in mrežah*
Table 1. *Computational conditions at different Pr and grids*

geometrija geometry	Re_τ	Pr	mreža grid	Δt^+	Δx^+	Δz^+	Δy^+	čas povprečenja averaging time
zaprt kanal channel	150	0,025	128x128x97	0,09	18,41	7,36	0,08-4,9	4500
odprt kanal flume	170,8	1	128x72x65	0,0512	16,77	7,46	0,10-4,19	3074
	170,8	5,4	256x128x129	0,0256	8,38	4,19	0,05-2,10	2560
	170,8	5,4	128x72x129	0,0427	16,77	7,46	0,05-2,10	2562
	170,8	5,4	128x72x65	0,0683	16,77	7.46	0,10-4,19	4099

2 REZULTATI

2.1 Vpliv Prandtlovega števila

Prvi sklop rezultatov so NNS, kjer smo analizirali vpliv naraščanja Prandtlovega števila na temperaturne profile, fluktuacije temperatur in turbulentne toplotne tokove pri treh različnih Prandtlovih številih: Pr = 0,025, Pr = 1 in Pr = 5,4.

Na sliki 2a so prikazani povprečni brezrazsežni temperaturni profili za tri različne vrednosti Prandtlovih števil. Brezdimenzijsko temperaturo θ dobimo s povprečenjem po ravninah, vzporednih z greto steno in po času (~ 10000 časovnih korakov). Poudariti je treba, da je θ negativna brezrazsežna temperaturna razlika, kar pomeni, da se največje brezrazsežne temperaturne razlike med tekočino in greto steno pojavijo v sredini zaprtega kanala oziroma na prosti površini odprtega kanala. Večje ko je Prandtlovo število, večja je brezrazsežna temperaturna razlika med steno in površino tekočine. Slika 2b

2 RESULTS

2.1 Prandtl number influence

The first part of the results presents the influence of the Prandtl number on the temperature profiles, temperature fluctuations and turbulent heat fluxes at Pr = 0.025, Pr = 1 and Pr = 5.4.

Fig. 2a shows the average dimensionless temperature profiles at three different Prandtl numbers. The dimensionless temperature θ is averaged in the planes parallel to the heated wall and in time (~ 10000 time steps). It should be emphasized that the temperature θ is a negative dimensionless difference. This means that the maximum temperature differences appear in the middle of the channel or on the top free surface in the flume. A higher Prandtl number means a higher dimensionless temperature difference between the wall and the middle of the fluid in the channel or on the top surface in the flume, respectively. Fig. 2b shows the temperature

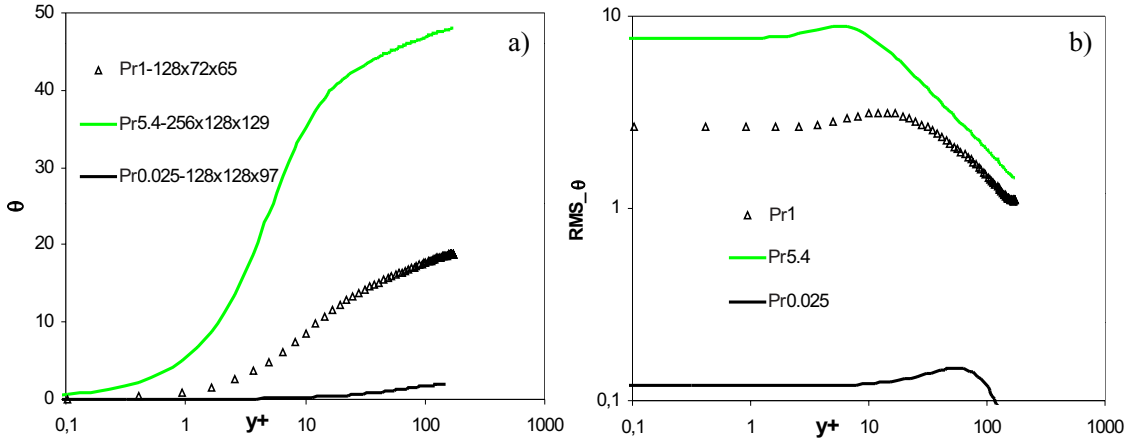

Sl. 2. *a) Povprečni brezrazsežni temperaturni profili, b) fluktuacije temperatur*
Fig. 2. *a) Dimensionless profiles of mean temperature, b) temperature fluctuations*

prikazuje fluktuacije temperatur. Fluktuacije temperatur *RMS_θ* dobimo tako, da trenutne temperature odštejemo od povprečnih, nato pa kvadrate razlik povprečimo po ravninah, vzporednih s steno, in času. Večje ko je Prandtlovo število, večje so fluktuacije. Pri preučevanem robnem pogoju temperature (robni pogoj nespremenljivega toplotnega toka) so fluktuacije opazne že ob steni in ostanejo konstantne v območju laminarne podplasti. Največjo vrednost dosežejo v vmesni plasti, med laminarno in turbulentno podplastjo, nato pa se zmanjšujejo do sredine zaprtega kanala oziroma do proste površine odprtega kanala.

Slika 3a prikazuje turbulentni vzdolžni toplotni tok $\theta' u'$ v odvisnosti od razdalje od stene za različna Prandtlova števila: Pr = 0,025, Pr = 1 in Pr = 5,4. Izračunamo ga tako, da zmnožek fluktuacij temperature θ in fluktuacij komponente hitrosti u v smeri vzdolž kanala (x) povprečimo po ravninah, vzporednih s steno, in po času. Vidimo, da večje Prandtlovo število pomeni večjo največjo vrednost toplotnega toka in manjšo razdaljo do stene. Zelo podobne ugotovitve sledijo za turbulentni toplotni tok v smeri pravokotno na steno $\theta' v'$ (sl. 3b).

fluctuations. The temperature fluctuations *RMS_θ* are obtained as the root mean square difference of the instantaneous and averaged temperatures averaged in planes parallel with the heated wall and in time. The temperature fluctuations already appear near the wall and remain constant through the viscous sublayer for the applied thermal boundary condition (isoflux boundary condition). In the buffer sublayer, between the turbulent and viscous sublayers, the maximum is reached; afterwards the *RMS*_θ is decreasing towards the middle of the channel or the top free surface of the flume.

Fig. 3a shows the profiles of the turbulent axial heat fluxes $\theta' u'$ versus the dimensionless distance from the wall at different Prandtl numbers: Pr = 0.025, Pr = 1 and Pr = 5.4. It is calculated as a product of the temperature fluctuations and the streamwise (x) velocity fluctuations averaged by planes parallel with the wall and by time. It is seen that the higher Prandtl number means a higher maximum value of heat flux and a smaller distance to the wall. Very similar conclusions were found for the turbulent wall-normal heat flux $\theta' v'$ (Fig. 3b).

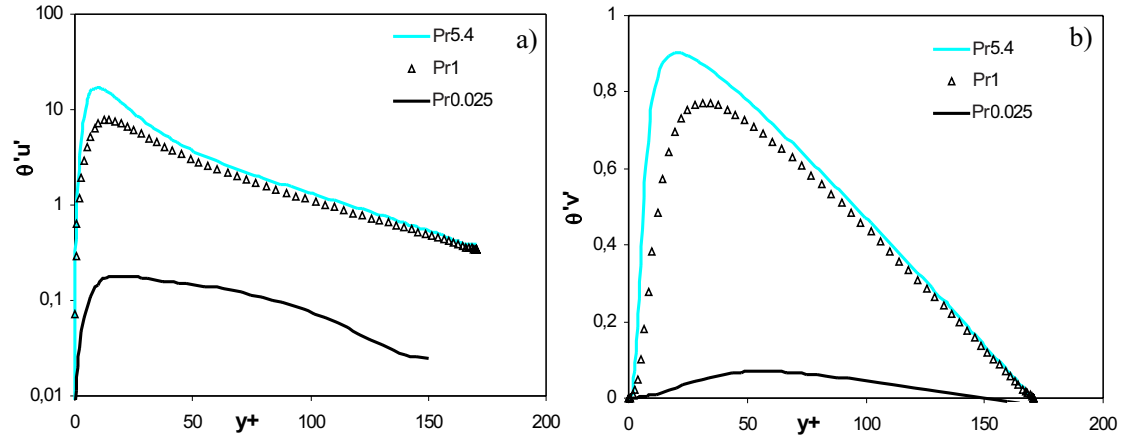

Sl. 3. *Turbulentni toplotni tok: a) vzdolžno, b) v smeri pravokotno na steno*
Fig. 3. *Profiles of turbulent heat flux: a) axial, b) wall normal*

2.2 Vpliv ločljivosti pri Pr = 5,4

Drugi sklop rezultatov predstavljajo numerične simulacije pri Prandtlovem številu Pr = 5,4 in treh različnih računskih mrežah: 256x128x129, 128x72x129 in 128x72x65. Zaradi Prandtlovega števila, večjega od ena, samo ločljivost prve mreže ustreza teoretičnim zahtevam NNS za hitrostno in temperaturno polje, preostali dve mreži zadostujeta le za hitrostni polji.

Rezultati na sliki 4a kažejo, da različno število mrežnih točk ne vpliva na povprečne temperaturne profile. Razlike, ki se pojavijo, so kvečjemu istega reda velikosti kot negotovosti zaradi statistične obravnave rezultatov (~0,5%). Podobno lahko povzamemo za temperaturne fluktuacije na sliki 4b. V tem primeru je statistična napaka manjša od 2%.

Pri turbulentnih toplotnih tokovih (sl. 5) so razlike nekoliko večje kakor v prejšnjih primerih, vendar so ocenjene napake še vedno znotraj statistične negotovosti, razen odstopanja vzdolžnega turbulentnega toplotnega toka pri $y^+ > 100$ na najbolj grobi mreži (sl. 5a).

2.2 Resolution at Pr = 5.4

The second part of the results presents numerical simulations at the Prandtl number Pr = 5.4, and three different computational grids: 256x128x129, 128x72x129 in 128x72x65. Because the Prandtl number is bigger than one, only the resolution of the first grid corresponds to the theoretical requirements of the DNS for the velocity and thermal field, while the other grids are sufficient only for the DNS of the velocity fields.

The results in Fig. 4 show that the number of grid points does not influence the mean temperature profiles. All the differences that appear are of the same order of magnitude as the uncertainties. A similar conclusion can be made for the temperature fluctuations (Fig. 4b), where the statistical uncertainties are less than 2%.

The differences are slightly larger in the turbulent heat fluxes (Fig. 5), but the estimated errors are still within the statistical uncertainties, except the turbulent axial heat flux deviations of the smaller grid at $y^+ > 100$ (Fig. 5a).

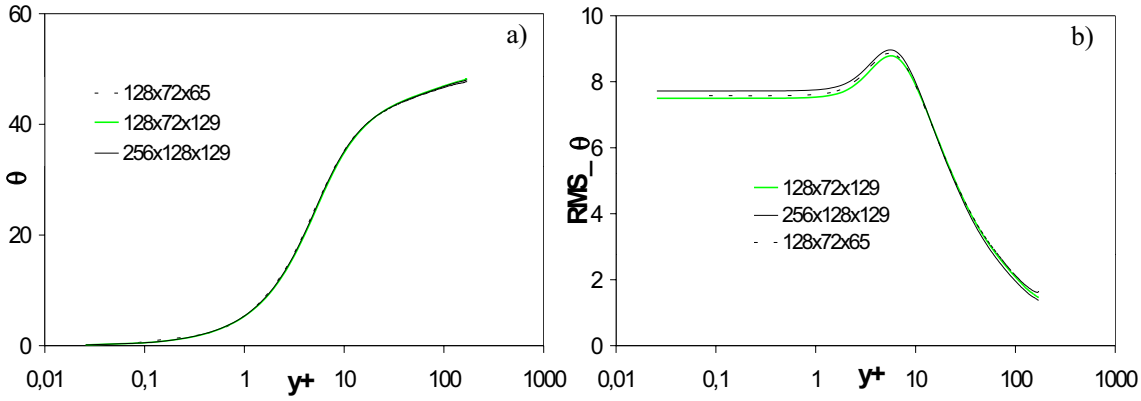

Sl. 4. *a) Povprečni brezrazsežni temperaturni profili, b) fluktuacije temperatur pri Pr = 5,4 in treh različnih ločljivostih*

Fig. 4. *a) Dimensionless profiles of mean temperatures, b) temperature fluctuations at Pr = 5.4 and three different resolutions*

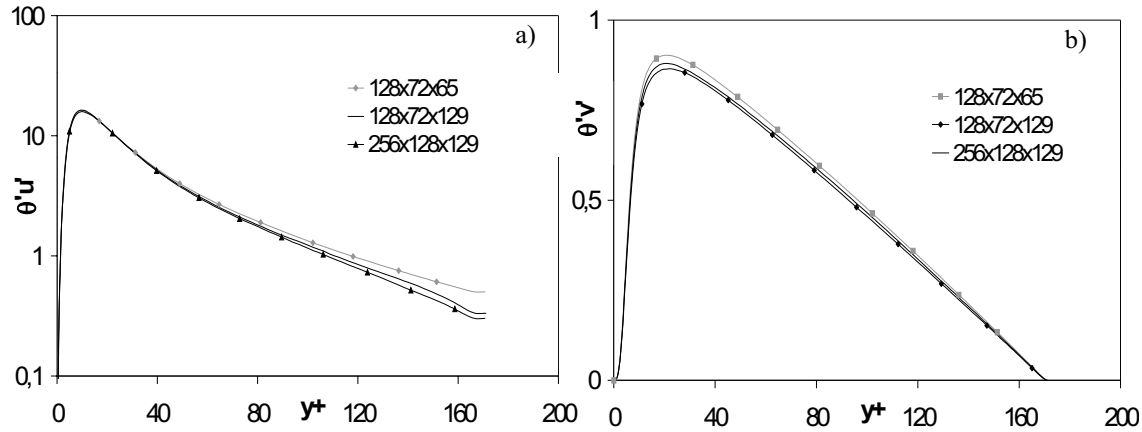

Sl. 5. *Turbulentni toplotni tok: a) vzdolžno, b) v smeri pravokotno na steno*

Fig. 5. *Turbulent heat fluxes: a) axial, b) wall normal*

Pri preučevanju ločljivosti računske mreže se uporabljajo spektri, ki prikazujejo, kako so v toku zastopane različne krajevne skale. Spekter fluktuacij temperature (komponente hitrosti) izračunamo z avtokorelacijsko funkcijo temperature (komponente hitrosti). Tako npr. avtokorelacijsko funkcijo temperature vzdolž kanala (x) pri izbrani razdalji od stene y_0 dobimo kot:

$$R(x_1) = \sum_{j=\frac{-N_2}{2}}^{\frac{N_2}{2}} \sum_{i=\frac{-N_1}{2}}^{\frac{N_1}{2}} \theta(x_i, y_0, z_j) \cdot \theta(x_i + x_1, y_0, z_j) \quad (8).$$

Če avtokorelacijske funkcije preslikamo po Fourier-ju in rezultat ustrezno normiramo [6], dobimo spekter temperature pri izbrani oddaljenosti od stene y_0 v smeri vzdolž toka x. Na podoben način pridemo do spektrov v prečni smeri z.

Turbulentno gibanje sestavljajo vrtinci različnih izmer. Geometrijska oblika sistema povzroča največje vrtince, najmanjši pa so določeni z viskoznimi silami. Za najmanjše vrtince je značilna velik raztros kinetične energije turbulentnega gibanja v toploto. Viskozna strižna napetost opravi deformacijsko delo, ki poveča notranjo energijo tekočine na račun kinetične energije turbulence. Povedano drugače, večji vrtinci, ki jih v diagramih spektrov opisujejo nižje vrednosti valovnih števil, difundirajo v manjše vrtince, ki jih opisujejo višje vrednosti valovnih števil. Energija manjših vrtincev je manjša od energije večjih vrtincev, zato se spektri z večanjem valovnih števil zmanjšujejo. Primerjave spektrov fluktuacij hitrosti (na slikah so spektri za najbolj pomembno komponento hitrosti u_x) in temperatur kažejo pričakovane rezultate: hitrostni spektri se hitreje zmanjšujejo proti nič kakor temperaturni spektri pri Pr > 1. Približno enako stopnjo zmanjševanja dobimo za Pr = 1. Večja vrednost Prandtlovega števila pomeni počasnejši razpad nižjih valovnih števil v višja, kar zahteva večjo ločljivost za opis vseh najmanjših temperaturnih skal.

To potrjuje slika 6, ki prikazuje spektre fluktuacij temperatur in hitrosti vzdolžno in prečno na smer toka pri razdalji y^+=3,7 od stene. Manjše razlike so vidne v spektrih fluktuacij hitrosti (6a, 6b), medtem ko so te razlike večje v spektrih fluktuacij temperatur (6c, 6d). Največje razlike med numeričnimi simulacijami različnih ločljivosti so v območju visokih valovnih števil, kjer obe manjši ločljivosti (128x72x65 in 128x72x129) kažeta večjo moč kakor NNS največje ločljivosti (256x128x129), kar kaže na nekoliko prepočasno dušenje turbulentnih fluktuacij. Kljub temu v obravnavanih spektrih ni zaslediti kopičenja pri visokih vrednostih valovnih številih. Kopičenje (spekter pri visokih valovnih številih začne naraščati) se pojavi takrat, ko najmanjše skale niso dovolj natančno modelirane in viskozni (temperaturni) disipaciji na viskozni (konduktivni) skali ne uspe spremeniti vse turbulentne kinetične energije v

In a study of the resolution requirements the spectra are usually used to show how different length scales are represented. The spectrum of the temperature (velocity component) fluctuations is derived from an auto-correlation function of the temperature (velocity component). For example, the auto-correlation function of the temperature in the streamwise direction at a given distance from the wall y_0 is:

If a Fourier transformation over the auto-correlation function is made, and the result is appropriately normalized [6], the temperature spectrum at a given distance from the wall y_0 in the streamwise direction x is obtained. Spectra in the spanwise direction z are obtained in a similar way.

Turbulent motion consists of vortices of different dimensions. The largest vortices are defined by the flow geometry, whereas the smallest one is defined by the viscous forces. A high dissipation of the turbulent kinetic energy into the heat is typical for the smallest vortices. Viscous shear stress makes deformation work, which transforms the turbulent kinetic energy into the internal energy of the fluid. In other words, larger vortices represented by lower wave-number modes diffuse into smaller vortices represented by higher wave-number modes in the spectrum diagrams. The energy of the smaller vortices is smaller than the energy of the larger vortices, therefore the spectra decrease with increasing wave-number modes. The comparisons of the velocity (the most important velocity spectra for the velocity component u_x are shown in the figures) and the temperature spectra show the expected results: the velocity spectra decay faster to zero than the temperature spectra at Pr > 1. Approximately the same decay rate is obtained for Pr = 1. A higher Prandtl number means slower decays of low wave-number modes into the high wave-number modes, and thus requires a more detailed resolution to capture all the significant thermal scales.

This is confirmed in Fig. 6, which shows the streamwise and spanwise spectra of the temperature and the velocity fluctuations at y^+=3.7 from the wall. Minor differences are seen in the velocity-fluctuation spectra (Figs. 6a and 6b), whereas these differences are larger in the temperature-fluctuation spectra (Figs. 6c and 6d). The main differences between the numerical simulations at different resolutions are observed at higher wave-number modes, where both lower resolutions (128x72x65 in 128x72x129) show stronger modes than the well-resolved DNS at the higher resolution. This indicates too-slow damping of the turbulent fluctuations. However, there are no "pile-up" phenomena seen at high wave-number modes. The pile-up phenomenon (the spectrum starts to grow at high wave-number modes) appears when the smallest scales are not properly modeled and viscous (temperature) dissipation and viscous (conductive) scale cannot

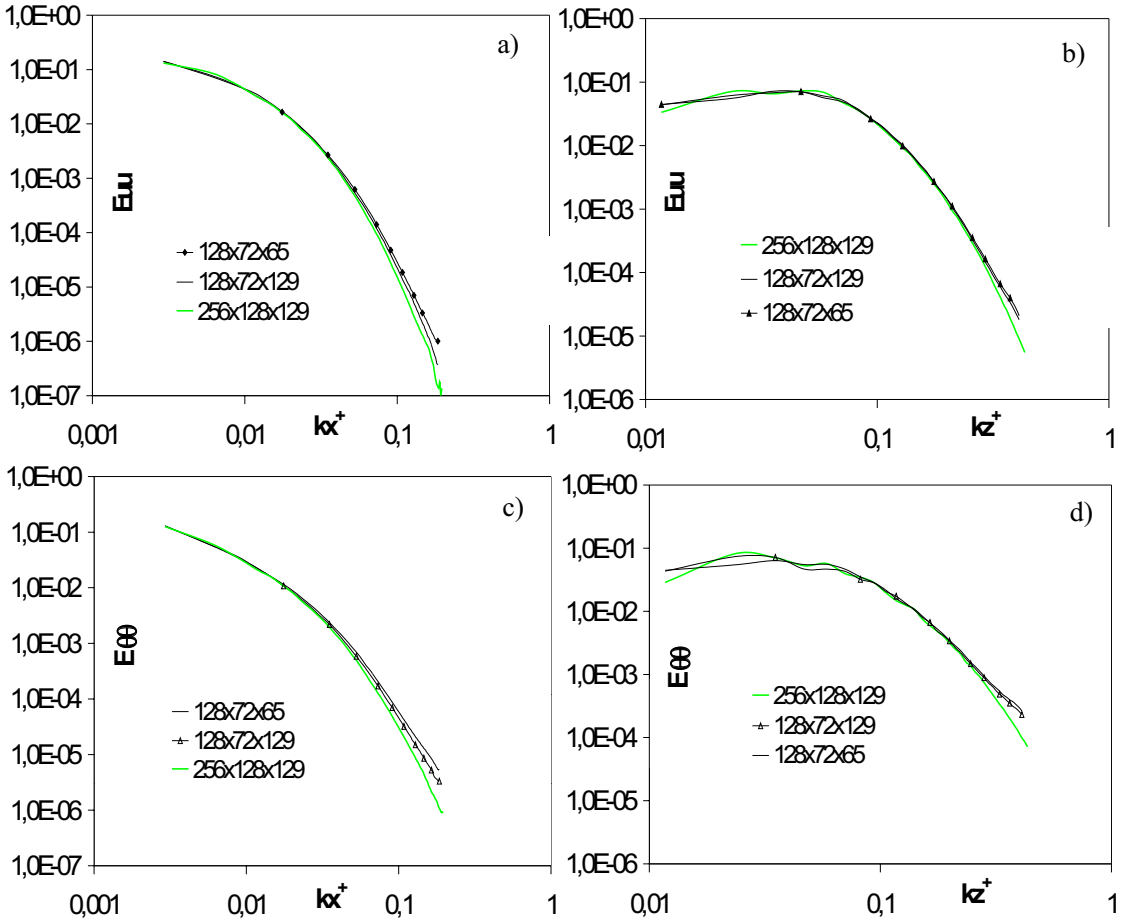

Sl. 6. *Spektri vzdolž (a, c) in prečno na kanal (b, d) $y^+ = 3.7$ od grete stene: a, b) temperatura, c, d) hitrost vzdolž toka*

Fig. 6. *Spectra in streamwise (a, c) and spanwise (b, d) directions at $y^+ = 3.7$ from the heated wall: a, b) temperature, c, d) streamwise velocity*

notranjo energijo. To pomeni, da moramo povečati ločljivost računske mreže, če hočemo zajeti najmanjše (Kolmogorovove) skale.

3 SKLEP

V prvem delu je bila opisana neposredna numerična simulacija (NNS) polno razvitega turbulentnega toka pri Reynoldsovem številu Re = 4580 (Re_τ = 150) in Prandtlovem številu Pr = 0,025 ter Re = 5260 (Re_τ = 170,8) in Prandtlovih številih Pr = 1 in Pr =5,4. Rezultati kažejo, da Prandtlovo število močno vpliva na statistiko turbulentnega polja. Rezultati opravljenih NNS lahko rabijo pri razvoju turbulentih modelov za tokove v bolj zapletenih geometrijskih oblikah in pri višjih vrednostih Reynoldsovih števil.

V drugem delu smo preučevali numerične simulacije treh različnih ločljivosti pri Re_τ = 170,8 in Pr = 5,4. Ločljivost naj bi bila teoretično sorazmerna kvadratnemu korenu Prandtlovega števila [8], vendar rezultati kažejo, da je vsaj pri Pr = 5,4 ta zahteva nekoliko preostra. Naši rezultati (profili povprečnih

change all the turbulent kinetic energy into internal energy. It means that the resolution should be increased in order to capture the smallest (Kolmogorov) scales.

3 CONCLUSION

In the first part of the paper the DNS of the fully-developed turbulent flow at Reynolds number Re = 4580 (Re_τ = 150) and Prandtl number Pr = 0.025, and at Re = 5260 (Re_τ = 170.8) and Prandtl numbers Pr = 1, 5.4, were performed. The results show that the Prandtl number has a strong influence on the turbulent statistics. The obtained results can be used for developing turbulent models for flows in a more complex geometry and at higher Reynolds numbers.

In the second part the numerical simulations of three different resolutions at Re_τ = 170.8 and Pr = 5.4 were performed. Theoretically, the resolution for the DNS should be proportional to the square root of the Prandtl number [8]; however, results show that this requirement is too stringent in the case of Pr = 5.4. Our results at Pr = 5.4 (mean temperature profiles,

hitrosti, fluktuacije, toplotni pretoki) pri najslabši ločljivosti kažejo, da je ločljivost, ki zadošča za simulacijo NNS hitrostnega polja dovolj velika tudi za simulacijo temperaturnega polja pri Pr = 5,4. Majhne razlike so vidne v spektrih fluktuacij temperatur v območju višjih valovnih števil, kjer obe računski mreži z nižjima ločljivostma kažeta počasnejšo spremembo turbulentne kinetične energije v notranjo kot NNS največje ločljivosti.

fluctuations, heat fluxes) for the lowest resolution show that the resolution, which is sufficient for the DNS of the velocity field, is also sufficient for the simulation of the thermal field at Pr = 5.4. Small differences in the temperature spectra are seen at high wave-number modes, where both low resolutions show a slower conversion of the turbulent kinetic energy into internal energy compared with the DNS of the highest resolution.

4 SPREMENLJIVKE
4 NOMENCLATURE

spekter	E	spectrum
polovična višina kanala	h	channel half height
enotski vektor v smeri x (1,0,0)	$\vec{\mathrm{I}}_x$	unit vector in x direction (1,0,0)
valovno število	k	wave number
vzdolžna in prečna dolžina kanala	L_1, L_3	streamwise and spanwise length of box
tlak	p	pressure
Prandtlovo število	Pr	Prandtl number
toplotni tok iz stene na tekočino	q_w	wall-to-fluid heat flux
Reynoldsovo število	Re	Reynolds number
Reynoldsovo število raztrosa	Re_τ	friction Reynolds number
avtokorelacijska funkcija	R	auto-correlation function
čas	t	time
temperatura	T	temperature
smer vzdolž, prečno, pravokotno na kanal	x, y, z	streamwise, spanwise, wall normal distance
komponente hitrosti v smereh x, y in z	u, v, w	velocity components in x, y and z directions
raztrosna hitrost	u_τ	dissipative velocity
toplotna difuzivnost	α	thermal diffusivity
brezrazsežna temperaturna razlika	θ	dimensionless temperature difference
toplotna prevodnost	λ	thermal conductivity
kinematična viskoznost	γ	kinematic viscosity
gostota	ρ	density
tekočina	$()_\mathrm{f}$	fluid
stena	$()_\mathrm{w}$	wall
disipacija	$()_\tau$	dissipation
normalizirano z u_τ, T_τ, v	$()^+$	normalized by u_τ, T_τ, v

5 LITERATURA
5 REFERENCES

[1] Gavrilakis, S., H.M. Tsai, P.R. Voke, D.C. Leslie (1986) Direct and large eddy simulation of turbulence, *Notes on Numerical Fluid Mechanics* Vol. 15, ed. U. Schumann, R. Friedrich, Vieweg, Braunschweig, D.B.R., 105.

[2] Kasagi, N., Y. Tomita, A. Kuroda (1992) Direct numerical simulation of passive scalar field in a turbulent channel flow, *Jornal of Heat Transfer -Transactions of ASME*, Vol. 114, 598-606.

[3] Kawamura, H., K. Ohsaka, H. Abe, K. Yamamoto (1998) DNS of turbulent heat transfer in channel flow with low to medium-high Prandtl number fluid, *International Journal of Heat and Fluid Flow*, Vol. 19, 482-491.

[4] Kawamura, H., H. Abe, Y. Matsuo (1999) DNS of turbulent heat transfer in channel flow with respect to Reynolds and Prandtl number effects, *International Journal of Heat and Fluid Flow,* Vol. 20, 196-207.

[5] Kim, J., P. Moin, R.D. Moser (1987) Turbulence statistics in fully developed channel flow at low Reynolds number, *J. Fluid Mech*., Vol. 130, 133-166.

[6] Kim, J., P. Moin (1989) Transport of passive scalars in a turbulent channel flow, Turbulent shear flows VI, *Springer-Verlag*, Berlin.

[7] Na, Y., T.J. Hanratty (2000) Limiting behavior of turbulent scalar transport close to a wall, *International Journal of Heat and Mass Transfer*, Vol. 43, 1749-1758.
[8] Tennekes, H., J.L. Lumley (1972) A first course in turbulence, *MIT Press*, Cambridge, MA.
[9] Tiselj, I., E. Pogrebnyak, C. Li, A. Mosyak, G. Hetsroni (2001) Effect of wall boundary condition on scalar transfer in a fully developed turbulent flume, *Physics of Fluids,* 13 (4), 1028-1039.
[10] Kader, B.A. (1981) Temperature and concentration profiles in fully turbulent boundary layers, *Int. J. Heat Mass Transf.,* 24, 1541.
[11] Tiselj, I., R. Bergant, B. Mavko, I. Bajsic, G. Hetsroni (2001) DNS of turbulent heat transfer in channel flow with heat conduction in the solid wall, *J. Heat Transf.*, 123, 849-857.

Naslov avtorjev: Robert Bergant
Doc.dr. Iztok Tiselj
Institut "Jožef Stefan"
Odsek za reaktorsko tehniko
Jamova 39
1000 Ljubljana, Slovenija
robert.bergant@ijs.si
iztok.tiselj@ijs.si

Authors' Address: Robert Bergant
Doc.Dr. Iztok Tiselj
"Jožef Stefan" Institute
Reactor Engineering Division
Jamova 39
1000 Ljubljana, Slovenia
robert.bergant@ijs.si
iztok.tiselj@ijs.si

Prejeto: 20.12.2002
Received:

Sprejeto: 31.1.2003
Accepted:

© Strojniški vestnik 48(2002)12,707-718
ISSN 0039-2480
UDK 621.924.9:531.76
Izvirni znanstveni članek (1.01)

© Journal of Mechanical Engineering 48(2002)12,707-718
ISSN 0039-2480
UDC 621.924.9:531.76
Original scientific paper (1.01)

Mehanski in elektronski merilnik hitrosti delcev v stroju za peskanje

A Mechanical and Electronic Measurement System for Particle Velocity Measurements in a Shotblasting Machine

Aleš Hribernik - Gorazd Bombek - Ivan Markočič

Osnovni problem merjenja hitrosti zrnc peska v peskalnem stroju je zelo velika abrazivnost peska in velika koncentracija prašnih delcev v zaprti testni napravi. Uporaba brezstičnih optičnih merilnih metod je zato pogosto nemogoča. Stične merilne metode so omejene na uporabo merilnikov, ki so zaščiteni z robustnimi oklepi. Kot alternativo robustnemu mehanskemu merilniku hitrosti zrnc peska smo razvili elektronski merilni sistem, ki ga odlikujeta dobra vodljivost vzdolž obeh prečnih osi curka peska in preprosta zgradba merilnega zaznavala, ki z uporabo cenenih elementov dovoljuje pogosto zamenjavo in ne potrebuje robustnega oklepa. V prispevku so predstavljeni razvoj, delovanje in uporaba mehanskega in elektronskega merilnega sistema. Prikazani so rezultati meritev in podana je primerjava obeh metod z razpravo in sklepi.

(Ključne besede: stroji za peskanje, meritve hitrosti, hitrosti delcev, merilniki mehanski, merilniki elektronski)

Two of the main problems for particle velocity measurement in a shotblasting machine are very abrasive shotblasting particles and a high concentration of dust within the closed testing chamber. The application of noncontacting optical methods is usually impossible; and robust shields protecting the sensors from abrasion have to be used for contacting velocity measurements. An electronic measurement system has been developed as an alternative to the robust, mechanical measurement device. This alternative electronic system has a simple construction and uses low-cost elements that can be replaced very quickly and, therefore, no robust shields are necessary. This enables very good mobility and positioning of the sensor along both axes in a cross-section plane of a particle stream. The development, operation and application of this mechanical and electronic particle velocity measurement system are described in this paper. Experimental results are presented, discussed and both methods are compared.

(Keywords: shotblasting machines, velocity measurements, particle velocity, mechanical measurnig devices, electronic measuring systems)

0 UVOD

Učinkovitost peskalnih naprav merimo s količino materiala, ki ga s postopkom odstranimo z nadzorne površine na enoto porabljene energije. Učinek peskanja je neposredno odvisen od hitrosti zrnc peska ob udarcu v nadzorno površino, saj odnašanje materiala zagotovi le dovolj velika kinetična energija zrnc. Zaradi tega je poznavanje hitrosti zrnc peska ob trku s peskano površino izrednega pomena za pravilno izbiro parametrov peskanja in za dosego kar največje učinkovitosti peskanja.

Pri merjenju hitrosti peska v peskalnem stroju smo se podali na razmeroma neraziskano področje. V literaturi ni zaslediti podobnih primerov, obstajajo pa določene podobnosti z načinom merjenja hitrosti izstrelkov v balistiki [1]. Ker so

0 INTRODUCTION

The efficiency of a shotblasting machine is measured by the quantity of material removed from a surface by a certain amount of energy. The effect of shotblasting depends on the velocity of the particles hitting the surface, since only those particles with enough kinetic energy can remove the material. A knowledge of particle velocity is, therefore, essential when selecting the optimum operation parameters of a shotblasting machine, thus ensuring the highest possible shotblasting efficiency.

Particle velocity measurements in shotblasting machines have been insufficiently investigated so far. No similar examples can be found in the literature; however, some similarities exist with velocity measurements in ballistics [1]. The application of noncontacting optical methods, commonly used for particle velocity measurements in sprays [2], has been impossible due to the

bile koncentracije prahu v preskuševalni napravi izredno velike, je bila uporaba brezstičnih optičnih metod [2] nemogoča. Zato smo razvili dve stični metodi: mehanski merilnik hitrosti z vrtečima obročema in elektronski merilni sistem z mikrofonskimi zaznavali, ki ju v nadaljevanju predstavljamo.

1 MEHANSKI MERILNIK HITOSTI Z VRTEČIMA SE PLOŠČAMA

Mehanski merilnik je prikazan na sliki 1. Sestavljata ga dve plošči na skupni gredi, ki jo poganja elektromotor. Pred ploščama je postavljena stena, ob katero udarja pesek iz peskalnega stroja. Na steni je izvrtina s premerom 10 mm, skozi katero pesek neovirano nadaljuje pot do prednje plošče, ki se vrti z izbrano vrtilno frekvenco. Tudi na prednji plošči je izvrtina s premerom 10 mm, ki se stožčasto (pod kotom 45°) širi od prednje proti zadnji strani. V trenutku, ko se izvrtini prekrijeta, lahko pesek nadaljuje pot proti zadnji plošči in udari ob papirnato tarčo, nalepljeno nanj. Kot φ razberemo s tarče in je kot med projekcijo izvrtine na prvi plošči in zadetki na tarči (slika 1). Hitrost zrnc peska pa nato izračunamo z izrazom:

$$w = \frac{l}{t} = \frac{\omega}{\varphi} \cdot \frac{180}{\pi} \cdot l \qquad (1),$$

pri čemer je: l – razdalja med ploščama, ω - kotna hitrost plošč.

2 ELEKTRONSKI MERILNIK HITROSTI DELCEV Z MIKROFONSKIMI ZAZNAVALI

Elektronski merilnik (sl. 2a) sestavlja nosilo, na katerem sta dve mikrofonski zaznavali. Nosilo je prek prečne konzole pritrjeno na koordinatni podajalni sistem, ki omogoča navpično in vodoravno postavitev zaznaval ter izbiro strmine nosila mikrofonskih zaznaval. Mikrofonsko zaznavalo sestavlja jeklen okrov z

high concentration of dust within the closed testing chamber. Two particle velocity measurement systems have, therefore, been developed: a mechanical measuring device using the principle of rotating discs, and an electronic system applying microphone sensors. This paper presents both systems.

1 MECHANICAL MEASURING DEVICE USING THE ROTATING DISCS PRINCIPLE

The measuring device is shown in Fig. 1. The discs on the common shaft are driven by an electric motor. The particles from the shotblasting turbine hit the screen that protects both discs. A 10-mm bore is made on the screen. The particles can continue their way unhindered through this bore to the front disc, which rotates at a known rotation speed. A 10-mm bore is made on the front disc, which is conically opened to the rear disc side. When both bores coincide the particles continue their way to the rear disc and hit the paper target that is fixed on it. The angle φ between the hits on the target and the projection of the front disc bore is then measured and used to calculate the velocity of the particles with the following equation:

where: l is the distance between the discs, and ω is the angular velocity of the discs.

2 AN ELECTRONIC PARTICLE VELOCITY MEASUREMENT SYSTEM WITH MICROPHONE SENSORS

Two specially designed microphone sensors are used, which are mounted on a longitudinal carrier (Fig 2a). The sensor's carrier is attached by a transverse cantilever to the coordinate tender system, which enables horizontal and vertical positioning of the sensors, and selection of the sensor carrier's inclination. A capacitor-type microphone encapsulated in a metal hous-

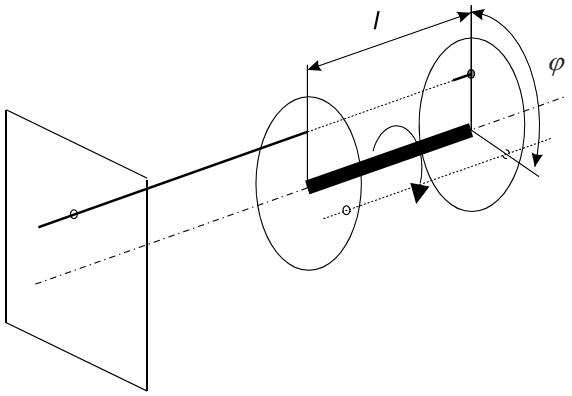

Sl. 1. *Mehanski merilnik hitrosti zrnc peska*
Fig. 1. *Mechanical device for particle velocity measurements*

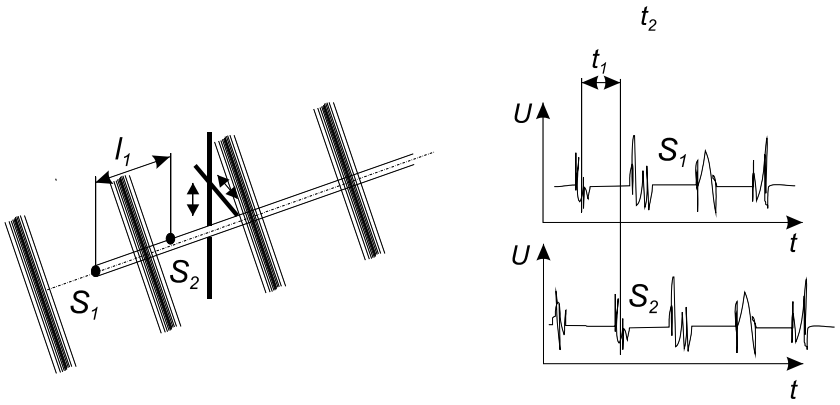

a) nosilo mikrofonskih zaznaval
a) carrier of mircrophone sensors

b) električni signal
b) electric signals

Sl. 2. *Elektronski merilnik hitrosti zrnc*
Fig. 2. *Electronic particle velocity measurement system*

membrano, pod katero je nameščen kondenzatorski mikrofon. Zaznavalo S1 je zatisnjeno neposredno v jekleno cev nosila, zaznavalo S2 pa je bočno pritrjeno na nosilo. Udarec na površino jeklene membrane povzroči nihanje membrane in se prenese na mikrofon, kar povzroči naglo spremembo signala. Pri uporabi elektronskega merilnika izkoriščamo pulzno delovanje peskalne turbine. V nasprotju z običajno centrifugalno radialno črpalko, ki jo tekočina polni po celotnem notranjem obodu, poteka polnjenje kanalov med lopaticami peskalne turbine le na določenem delu notranjega oboda. Zato izmetavajo lopatice pesek le v izbranem delu zunanjega oboda, neposredno v peskalno napravo. Pri tem je tok peska v neki opazovani točki izrazito ponavljajoč, prihaja v obliki zgoščenih paketov zrnc peska s frekvenco, ki je enaka zmnožku vrtilne frekvence rotorja turbine in števila lopatic turbine. Tak je tudi signal, ki ga zaznata mikrofonski zaznavali (sl. 2b). Zaradi vzdolžnega odmika med zaznavali sta signala časovno premaknjena. Pri tem je čas zakasnitve sorazmeren razmerju hitrosti zrnc in razdalje med zaznavali. Torej je mogoče hitrost zrnc peska preprosto izračunati z izrazom:

ing and placed under the metal membrane forms the microphone sensor. The sensor S1 is impressed directly into the front opening of the sensor's carrier, while the S2 sensor is mounted on the upper side of the carrier. The vibration of the membrane resulting from the impact of particles is transmitted to the microphone which signals any sudden changes (a sudden change of microphone's electric signal occurs). The electric measuring system makes use of a pulsatile shotblasting turbine operation. Only partial admission is used by the shotblasting turbine, in contrast to the radial pump where admission takes place over the whole inner circumference. The turbine blades eject the particles at the selected position on the outer circumference, directly into the shotblasting machine. The particle flow is, therefore, pulsatile: it rises in waves of high and low particle concentrations with a frequency that is equal to the product of the rotor's rotational speed and the number of blades. The signals from both sensors, S1 and S2 (Fig. 2b), which are phased over a particular time interval are similar to the particle flow. This time interval (time delay) is inversely proportional to the longitudinal distance between the sensors, and it is proportioned according to the velocity of the particles. The particle velocity can, therefore, be calculated as:

$$w = \frac{l_1}{t_1} \qquad (2).$$

2.1 Zgradba mikrofonskega zaznavala

Mikrofonsko zaznavalo (sl. 3) sestavlja teflonska puša, v katero je privita jeklena membrana. Tik pod membrano je nameščen kondenzatorski mikrofon, ki se tesno prilega teflonski puši. Med membrano in teflonsko pušo je vstavljena ploščica iz mehke silikonske gume. Teflonska puša je zatisnjena v jekleno pušo, ki je okrov zaznavala in prek katere je zaznavalo pritrjeno na nosilo.

Razvoj mikrofonskega zaznavala je potekal v več korakih. Osnovno vodilo razvoja je bilo

2.1 Microphone sensor

A microphone sensor is shown in Fig. 3. It is made of a plastic tube, into the top of which a metal membrane is screwed. A capacitor-type microphone fastened in the plastic tube is placed under the membrane. A washer made of soft silicone rubber is placed between the plastic tube and the metal membrane. This plastic tube is impressed into the metal housing, which is then fixed to the sensor's carrier (Fig. 2a).

The development of this microphone sensor was performed over a number of successive steps. The basic

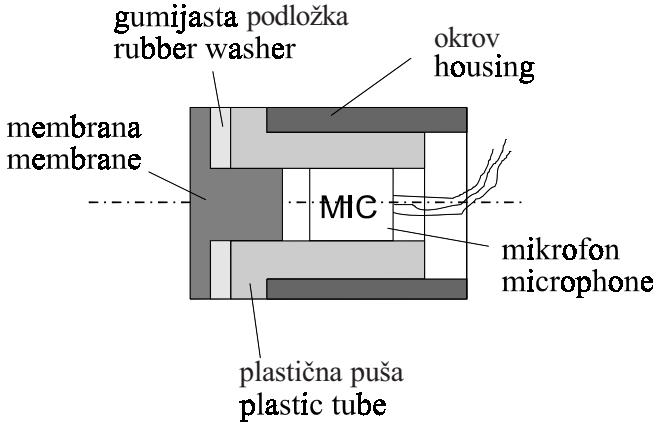

Sl. 3. *Mikrofonsko zaznavalo*
Fig. 3. *Microphone sensor*

doseči čim močnejši signal na enoto obremenitve membrane ob hkratnem dobrem dušenju lastnih nihanj in nihanj, ki so posledica udarcev v bok nosila in pomenijo motnjo. Preskusili smo tri tipe zaznaval A, B in C. Zaznavalo tipa A je sestavljeno iz jeklene puše, v katero je zatisnjen mikrofon, vstavljen v teflonski obroč. Membrana nad mikrofonom debeline 4 mm je pritrjena na jekleno pušo. Na sliki 4 je prikazan odziv zaznavala na udarec, ki ga povzroči trk jeklene kroglice mase 1,5 g s hitrostjo 0,3 m/s (učinek trka ustreza trku povprečno velikega zrnca peska s hitrostjo 60 m/s). Ugotovimo lahko, da je sprememba signala

task was to increase the sensitivity of the microphone sensor (as high an output signal as possible per unit of membrane load), and to reduce the oscillations caused by the resonance in the system's natural frequency domain or induced by the side impact of the particles. Three different types of sensor – Types A, B and C – were tested. The type-A sensor was made up of a metal housing covered with a metal membrane. The microphone was placed into this housing and fixed by a plastic ring. The membrane was 4-mm thick. The impulse response for the type-A sensor is shown in Fig. 4. The impulse input force was applied to the middle of the membrane by the impact ball. The ball's mass was 1.5 g, and the speed

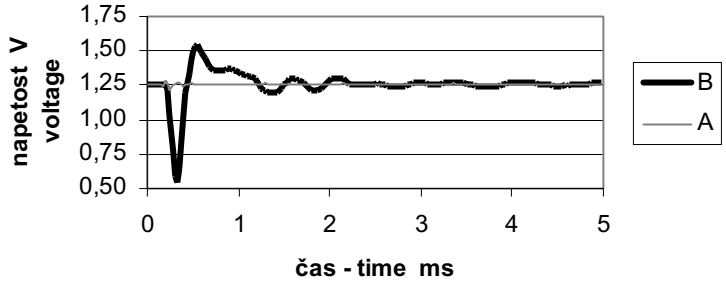

Sl. 4. *Odziv zaznavala na udarec (A – membrana zatisnjena v jekleno pušo, B – membrana zatisnjena v silikonsko pušo)*
Fig. 4. *Impulse response of sensor (A – membrane impressed directly into the metal housing, B – membrane impressed into the plastic tube)*

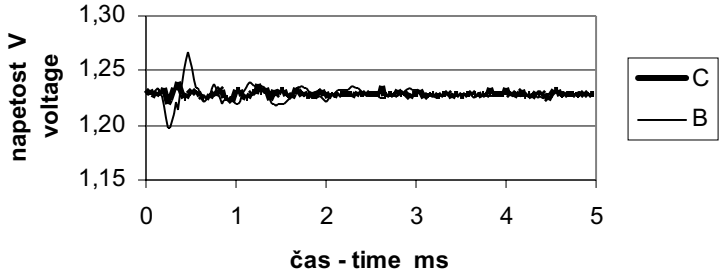

Sl. 5. *Odziv zaznavala na bočni udarec (B - membrana zatisnjena v silikonsko pušo brez podloge; C - membrana zatisnjena v silikonsko pušo s podlogo)*
Fig. 5. *Sensor response on the side impact (B – membrane impressed into the plastic tube without rubber washer, C - membrane impressed into the plastic tube with rubber washer)*

majhna, reda velikosti 50 mV, kar je le 4% srednje vrednosti signala in ne zadošča za izvedbo meritev. V primeru zaznavala tipa B je amplituda odziva neprimerno večja. Največja sprememba signala doseže kar 60 % srednje vrednosti signala. Tako veliko amplitudo odziva smo dosegli s spremenjenim vpetjem membrane. Da bi kar se da zmanjšali togost vpetja, smo membrano zatisnili v silikonsko pušo, ki je bila vstavljena v jeklen okrov zaznavala, kakor to prikazuje slika 3. Slaba stran tega vpetja pa so razmeroma velike motnje, ki jih povzročajo udarci ob bok zaznavala (sl. 5). Te nam je uspelo zmanjšati tako, da smo med jekleno membrano in teflonsko pušo vstavili mehko silikonsko gumo (senzor tipa C - sl. 3), s katero nam je uspelo povečati dušenje sistema in zmanjšati motnje (sl. 5). S tem smo sicer zmanjšali amplitudo odziva sistema (sl. 6), ki pa je še vedno dovolj velika (20 do 30 % srednje vrednosti signala), da lahko zaznavalo uporabimo za meritve hitrosti. Jeklena membrana ima dvojno nalogo. Ena je, da zaščiti mikrofon pred neposrednim vplivom peska, druga pa je, da ob udarcu peska odda zvok, ki ga zazna mikrofon. Pri tem je zvočni tlak neposredno odvisen od debeline membrane. Ker pa je membrana med delovanjem izpostavljena intenzivni abraziji (hitrost odnašanja materiala 1,5 mm/uro), je treba najti kompromis med amplitudo odziva in dobo trajanja zaznavala. Preskusili smo tri membrane debelin 2 mm, 3,5 mm in 5 mm. Vpliv debeline membrane na odziv sistema prikazuje slika 6. S povečevanjem debeline amplituda odziva slabi in znaša pri debelini 5 mm le še 10 % povprečne vrednosti signala. Zato smo se odločili za membrano debeline 3,5 mm. Ta zagotavlja vsaj 90 minutno dobo trajanja zaznavala in ima tudi pri začetni debelini amplitudo odziva enako 20 % povprečne vrednosti signala.

of the ball was 0.3 m/s (the effect of the ball's impact is similar to the impact of an average shotblasting particle with a velocity of 60 m/s). The change of the signal was low, as shown in Fig. 4. It did not exceed 50 mV, which is less than 4% of the mean magnitude of the signal. This is far too small for the application of a type-A sensor for particle velocity measurements. The change of the signal was much higher for the type-B sensor (Fig. 4). The maximal signal change was 60 % of the mean signal magnitude. This was achieved by modifying the membrane fixture. In order to reduce the stiffness of the membrane's fixture, the membrane was screwed into the plastic tube, which was then fixed into the metal housing (see Fig. 3). The weakness of this type of sensor is its high sensitivity to side impacts (undesired disturbances, Fig. 5). This problem was solved by the application of a soft silicone-rubber washer placed between the metal membrane and the plastic tube (Fig. 3). The damping of the membrane's vibrations was increased and the sensitivity to side impacts was reduced by the application of a soft rubber washer. Unfortunately, this modification reduced the overall sensor sensitivity as well (Fig. 6). However, the signal alteration remained high enough (20–30 % of the mean signal magnitude) to carry out the particle velocity measurement. The metal membrane placed in front of the microphone performs a dual role. First, to protect the microphone from the direct impact of abrasive particles. Second, as a source of sound that is sensed by the microphone. The intensity of the sound pressure depends on the membrane thickness. Since the amount of material removed from the membrane surface during measuring is very high (approximately 1.5 mm/hour), a compromise had to be found between the signal intensity and the sensor lifetime. Three membranes with thickness of 2 mm, 3.5 mm and 5 mm were, therefore, tested. The influence of the membrane thickness on the sensor-impulse response is shown in Fig. 6. The intensity of the signal change was reduced by increasing the membrane thickness. A signal from the 5-mm membrane was too low and, since the lifetime of a 2-mm-membrane sensor would be less than 45 minutes, a 3.5-mm membrane was chosen. The lifetime of this membrane is at least 90 minutes, and the change of the signal with each impulse impact is 20 % of the mean signal magnitude of the initial membrane thickness.

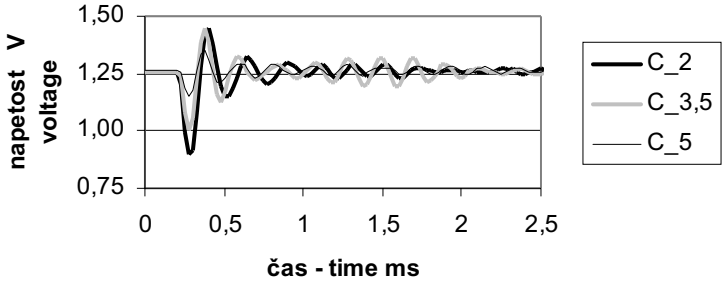

Sl. 6. *Vpliv debeline membrane na odziv zaznavala tipa C*
Fig. 6. *The influence of the membrane thickness on the response of type C sensor*

2.2 Sistem za zbiranje in analizo podatkov

Uporaba mikrofonskih zaznaval zahteva ustrezno opremo tako za zbiranje podatkov kakor tudi za njihovo obdelavo. Uporabili smo računalniško podprt sistem, ki ga sestavlja prenosni osebni računalnik (Celeron 1000 MHz, 256 MB RAM) z večnamensko kartico DaqCARD 6062 (format PCMCIA). Fizično smo električne povezave izvedli tako, da smo uporabili sistem za pripravo signalov SCXI. Večfunkcijska kartica, sistem za pripravo signalov in programska oprema so izdelek podjetja National Instruments.

Analogne vhodne signale smo pripeljali v modul SCXI-1140. Signale smo vezali diferencialno. Za napajanje mikrofonov smo uporabili modul SCXI-1124. Povezavo smo izvedli tako, da smo izenačili potenciale vseh negativnih potencialov, analogne zemlje in potenciala okrova. Poleg tega smo na maso vezali tudi kovinsko ogrodje in tako dobili Faradejevo kletko ter tako zmanjšali motnje, ki so posledica elektrostatičnega delovanja zrnc peska, ki udarjajo ob stene preskusne komore.

Za zbiranje podatkov in njihovo obdelavo smo uporabili program LabVIEW. Ta program omogoča nadzor nad delovanjem večnamenske kartice (zajemanje električnih signalov in napajanje mikrofonov), pa tudi shranjevanjem in obdelavo podatkov.

3 MERITVE IN REZULTATI

Meritve smo izvajali v sredini curka peska na oddaljenosti 650 mm od vrha lopatic rotorja turbine. Os merilnika smo postavili vzporedno s smerjo zrnc peska. Zato smo za vsako posamezno turbino pred začetkom meritev posneli t.i. sliko curka. V ta namen smo v testno komoro na oddaljenosti 1100 mm od turbine postavili zaslon, na katerem je bila pritrjena tarča. Pred zaslon smo postavili odklonsko mrežico. Med peskanjem zaslona so na tarči ostala mesta v senci odklonske mrežice nepoškodovana. Na podlagi navpičnega odmika med točko na odklonski mrežici in njej pripadajočo senco ter razdaljo med točko in zaslonom smo nato ugotavljali kot poti zrnc proti vzdolžni smeri. Analizirali smo delovanje štirih različnih turbin. Za vsako smo izvedli večje število meritev z mehanskim in elektronskim merilnikom hitrosti v eni sami točki curka. Pri tem smo meritve ponavljali v isti točki vsaj trikrat, točko meritve pa smo izbrali tako, da so bile razmere (smer curka, oddaljenost merilnika od turbine itn.) za vse turbine približno enake. V nadaljevanju bomo predstavili rezultate, izmerjene s prototipno izvedbo turbine z osmimi naprej ukrivljenimi lopaticami (G 300U) pri vrtilni frekvenci rotorja 50 Hz.

2.2 Data acquisition and data-analysis system

Data acquisition and a data-analysis system are required for the particle velocity measurements using microphone sensors (electronic system). A computer-aided measuring system was used, which incorporates a personal computer (Celeron 1000 MHz, 256 MB RAM) and a multifunction card (DaqCARD 6062, format PMCIA). The electric signals were conditioned by an SCXI data-conditioning system. The multifunction card, data-acquisition system and application software are all products from National Instruments.

The differential analog input signals were fed to the SCXI - 1140 module. The microphones were supplied with a constant DC voltage source from the SCXI – 1124 module. The sensor wiring was made by a common negative potential, which was connected to the analog ground with the SCXI chassis and the sensor's carrier construction. A Faraday cage was formed in this way, and the disturbances caused by the large amount of electrostatic noise (resulting from particles hitting the walls of the testing chamber) were reduced.

LabVIEW software was used to build the computer applications for the data acquisition and the data analyses. These applications are used to control the operation of the multifunction card (data acquisition, DC voltage output for microphones) and for data logging and post-processing of the data.

3 MEASUREMENTS AND RESULTS

The measurements were carried out in the centre of the particles' stream, 650 mm from the tip of the shotblasting turbine's blade. The longitudinal sensor axis was set parallel to the particle trajectories. A so-called stream image was, therefore, determined first showing the particle trajectories. A paper target was fixed on the vertical screen 1100 mm away from the turbine. An inclination mesh was placed in front of the screen and the turbine was allowed to run for a short period. The target in the shadow of the inclination mesh remained undamaged. The flow angle of particles within the stream intersected using the inclination mesh was determined based on the differences between the coordinates of the particular point on the mesh and the coordinates of its matching point on the target. The operation of four different turbines was analysed. Several measurements were performed using both methods, all in just one central point of the particle stream. The flow conditions were similar for all turbines. Each measurement was repeated at least three times. The results for the prototype G300U turbine with eight forward curved blades measured at 3000 revolutions per minute (50 Hz) are presented in more in detail.

3.1 Rezultati meritev hitrosti z mehanskim merilnikom

Merilnik smo postavili nad ravnino osi turbine, v višino, pri kateri je bila smer zrnc $+6{,}25^0$ nasproti vodoravnici. Sredina zaslonke se je ujemala s sredino curka. Izvedli smo tri zaporedne meritve. Vsaka meritev je bila sestavljena iz dveh faz. V prvi fazi smo obstreljevali tarčo med mirovanjem plošč. Tako smo določili projekcijo izvrtine prednje plošče na tarči, prilepljeni na zadnji obroč. Nato smo z elektromotorjem plošči zavrteli in pri ustaljenih vrtljajih obstreljevali tarčo v kratkem presledku. Rezultate meritve, t.j. položaj zadetkov na tarči, smo določili z odbiranjem, pri čemer je bila delitev lestvice na tarči 1°. Rezultat so zbrani v preglednici 1.

Kakor je razvidno iz preglednice 1, je ujemanje izmerjenih srednjih hitrosti zrnc zelo dobro; odstopki ne presežejo 1,3 m/s. Vendar je merilna negotovost precej večja. Vzrok za to je precej širok pas zadetkov tarče v območju $\pm 10^0$. Tak raztros je delno posledica širine odprtine na prednjem obroču (∅=10 mm), ki tudi pri mirovanju plošč povzroči raztros v območju $\pm 5^0$. Dodaten prispevek k raztrosu pa prinese neenakost hitrosti posameznih zrnc peska. Delno je ta neenakost opazna že v samem toku zrnc pred merilnikom, dodatno pa k njej prispevajo medsebojni trki zrnc, ki jih povzročajo od merilnika odbita zrnca na vstopu skozi zaslonko in pri prehodu skozi odprtino prednje plošče.

3.1 Results of the mechanical measuring device

The measuring axis of the mechanical measuring device was placed above the zero plane defined by the turbine axis, and the particle velocity was inclined by 6.25 degrees from the horizontal at this particular position. The orifice (front bore) was in line with the centre of the particle stream. Three successive measurements were carried out. Each measurement was performed in two stages. In the first stage the disks and the target were at a standstill, and they were briefly exposed to the particles. The projection of the front disk bore on the target was determined in this way. In the second stage the discs were driven by an electric motor. The target was briefly exposed to the particles again at a constant rotational speed. The result of the measurement, i.e. the angle between the hits into the target when held still and the hits into the rotating target, was read from the scale that was printed on the table with a 1 degree increment. The results are shown in Table 1.

The measured particle velocities agree well, and as can be seen from Table 1 the deviation from the average value is less than 1.3 m/s. However, the measurement uncertainty is much higher due to the large scatter of the hits on the target. The scatter of the hits was ± 10 degrees. One of the reasons for this scatter is the wide bore (∅=10 mm) on the front disc, which resulted in ± 5 degrees scatter of hits onto the target held still (first step of the velocity measurement). The unequal speed of the particles within the stream expanded the scatter even more when the disc and target were rotated. The particles already had a different velocity ahead of the measuring plane. These speed differences within the measuring device increase due to the collisions between the particles when passing the orifice in the screen and in the front disc.

Preglednica 1. *Rezultati meritve hitrosti zrnc peska z mehanskim merilnikom za turbino G300U*
Table 1. *Results of the particle velocity measurement of the G300U shotblasting turbine using a mechanical measuring device*

Meritev Measurement	Vrtilna hitrost Rotational speed min^{-1}	Kot Angle φ^0	Hitrost zrnc Particle velocity m/s	Standardna merilna negotovost Standard measurement uncertainty m/s
1	7650	155	73,4	±3,1
2	7780	153	75,7	±3,2
3	7720	155	74,1	±3,1
Povprečna vrednost Average value			**74,4**	**±3,1**

3.2 Rezultati meritev hitrosti z elektronskim merilnikom

Ker imajo mikrofoni frekvenčni odziv prilagojen zvoku, ki ga lahko zaznava človeško uho (do 17 kHz), smo se odločili za približno 2-krat višjo frekvenco zajemanja - 40000 Hz. Signal, zajet s to frekvenco, lahko kasneje analiziramo in prepoznamo frekvence do 20000 Hz (po Nyquistovem teoremu) [3]. Odločili smo se, da bomo zajeli 200000 merilnih točk na kanal, kar ustreza času 5 sekund. Meritev smo izvedli tako, da smo ob zagonu turbine

3.2 Results of the electronic measurement system

The frequency response of the applied standard microphones is adjusted to the audible sound of the human ear (up to 17 kHz). Therefore, the signals were acquired using a 40-kHz acquisition frequency. According to the Nyquist theorem [3], the discrete signal acquired using this frequency can be post-analysed and frequencies up to 20 kHz can be recognised. The amount of acquired data was 200,000 per channel. This corresponds to a period of 5 seconds. A screen placed in front of the

elektronski merilnik zastrli z zastorom, postavljenim 300 mm pred prvo mikrofonsko zaznavalo. Ko so se razmere v turbini ustalile, smo zaslon umaknili in zajeli signale.

Slika 7 prikazuje zajeta neobdelana signala. Zaradi velike gostote zapisa je slika nepregledna, vidi pa se trenutek, ko je pesek začel udarjati po mikrofonih.

Da bi lahko zajeta signala uporabili za določitev hitrosti zrnc peska, smo v programskem okolju LabVIEW izdelali poseben algoritem. Pri tem smo uporabili standardna programska orodja, ki jih programsko okolje ponuja. Z algoritmom obdelamo signal v dveh korakih. V prvem koraku s frekvenčno analizo z uporabo hitre Fourierjevo preslikavo (HFP - FFT) [4] določimo diskretni frekvenčni spekter diskretnega (digitaliziranega) signala. Frekvenčni spekter pokaže, katere frekvence in s kakšno amplitudo se pojavljajo v signalu. Frekvenčni spekter signala prvega zaznavala je prikazan na sliki 8. Opazimo, da obstajata dve frekvenčni območji večje intenzivnosti. Frekvenčno območje 3500 Hz do 7000 Hz je posledica lastnih nihanj sistema. Bolj zanimivo je območje med 0 in 1000 Hz, ki je prikazano na sliki 9. Ugotovimo, da se prva izrazita amplituda

sensors was used to cover the sensors when the turbine was started up and until steady-state operation was achieved. At that moment the screen was removed.

The raw, acquired signals are shown in Fig. 7. The diagram lacks clarity because of the high density of the recorded data, although the moment when the first particles hit the membrane of the sensor is clearly recognisable.

In order to use the signals for particle velocity determination a special algorithm was made in the LabVIEW programming language. Standard LabVIEW program routines were used. The signals were processed in two steps using the algorithm. In the first the discrete Fourier frequency spectrum from the digitised input signal was determined by the application of the fast Fourier transform algorithm [4]. The frequency spectrum shows significant frequency components. The frequency spectrum of the signal from the first sensor (S1) is shown in Fig. 8. There are two frequency domains of higher intensity. The frequency domain between 3500 and 7000 Hz corresponds to the natural frequencies of the coordinate tender system and sensors. More important is the domain between 0 and 1000 Hz, shown in Fig. 9. The first significant frequency is 50 Hz, and this corresponds to the rota-

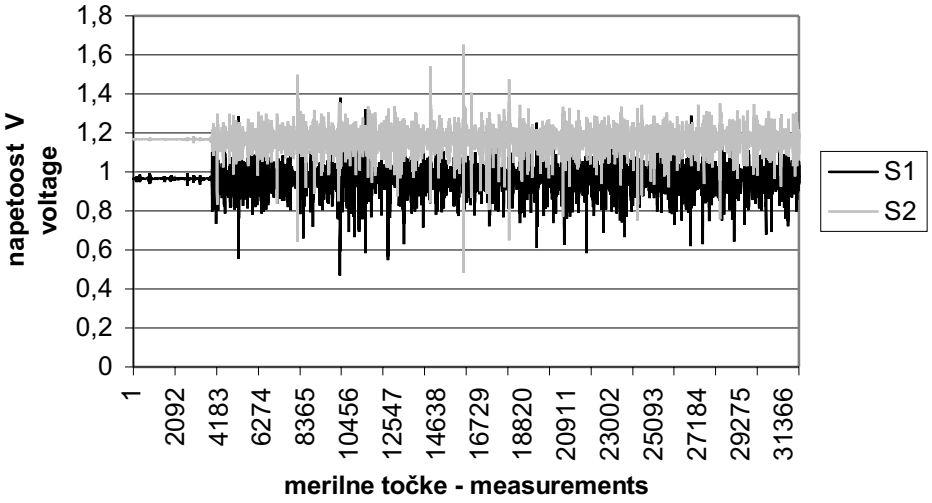

Sl. 7. *Signala z zaznaval S1 in S2 posneta s frekvenco 40.000 Hz*
Fig. 7. *Signals from sensors S1 and S2 recorded by 40,000 Hz*

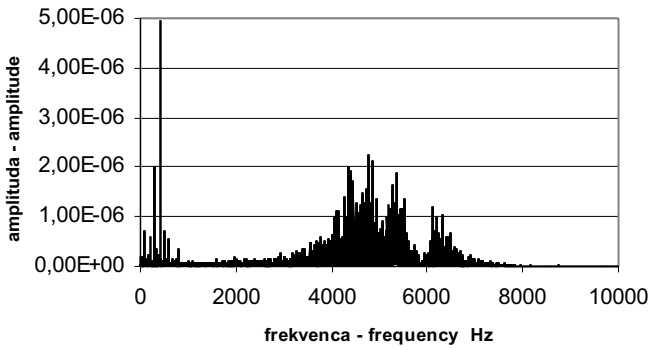

Sl. 8. *Frekvenčni spekter signala z zaznavala S1*
Fig. 8. *Frequency spectre of a signal from sensor S1*

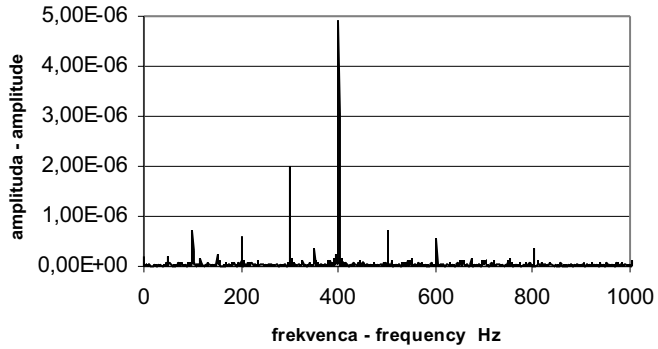

Sl. 9. *Frekvenčni spekter v območju 0-1000Hz – signal z zaznavala S1*
Fig. 9. *Frequency spectre of 0-1000 Hz domain - signal from sensor S1*

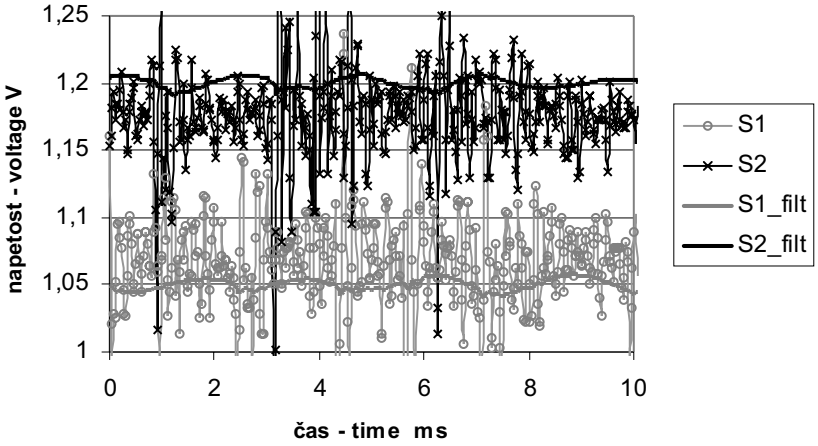

Sl. 10. *Primerjava osnovnih in filtriranih signalov z zaznaval S1 in S2*
Fig. 10. *Comparison of non-filtered and filtered signals from sensors S1 and S2*

pojavi pri 50 Hz, kar ustreza vrtilni frekvenci turbine. Z enako ali višjo amplitudo se nato pojavijo tudi vse njene višje harmonske. Najizrazitejša amplituda se pojavi pri 400 Hz in ustreza frekvenci vzpodbude, ki je zmnožek vrtilne frekvence turbine in števila lopatic (50 Hz, 8 lopatic). Veliko število izrazitih nižjih in višjih harmonskih napoveduje, da je delovanje prototipne turbine še precej neubrano.

Frekvenčni analizi sledi naslednji korak, to je filtriranje signala. Namen filtriranja je, da iz osnovnega signala izluščimo tisti del, ki je posledica vzbujanja sistema z osnovno frekvenco 400 Hz, s katero lopatice turbine izmetavajo pesek. Uporabili smo ozkopasovni filter z območjem 350 do 450 Hz. Zaradi nadaljnje obdelave mora biti filtriran signal čim bolj gladek prehod v območje zavrnitve pa čim bolj strm. To smo dosegli z uporabo digitalnega Čebišovovega filtra II [5]. Ta ima ravno karakteristiko v frekvenčnem območju prepuščanja signala in izredno strm, odsekan prehod v območje zavrnitve. Na sliki 10 sta prikazana osnovna in filtrirana signala z zaznaval S1 in S2. V obeh primerih je rezultat filtriranja razmeroma gladka krivulja z dovolj izrazitimi ekstremi, ki nam jih je uspelo lokalizirati z uporabo algoritma za iskanje dolov in vrhov diskretnega signala. Ker lokalni doli filtriranega signala ustrezajo naglim spremembam osnovnega

tional frequency of the turbine. All higher harmonics are presented with the same or higher intensity. The most significant frequency is 400 Hz, and this corresponds to the excitation frequency that is the product of the number of turbine blades and turbine rotational frequency (8 blades, 50 Hz). The very large number of distinctive higher and lower harmonics show evidence of a poorly tuned turbine.

The next step was signal filtering. The intention was to isolate that part of the signal which corresponds to the excitation frequency (400 Hz), at which the blades eject the particles, from the raw signal. A bandpass filter was used with a bandpass between 350 Hz and 450 Hz. The Chebyshev II design digital filter was applied [5]. These filters are maximally flat in the passband and give a sharp transition between the passband and the stop band. The filtered signal is, therefore, smooth, which is necessary for subsequent signal processing. The filtered and non-filtered signals from sensors S1 an S2 are presented in Fig. 10. The filtered curves are smooth with distinctive extremes. The extremes are localised by the algorithm for the determination of the maximum and minimum values of the discrete signal. The local minimum of the filtered signal corresponds to the rapid change of the non-filtered signal (caused by the impact of the particles on the membrane) as can be seen in Fig. 10. The time delay between the impacts on the first and

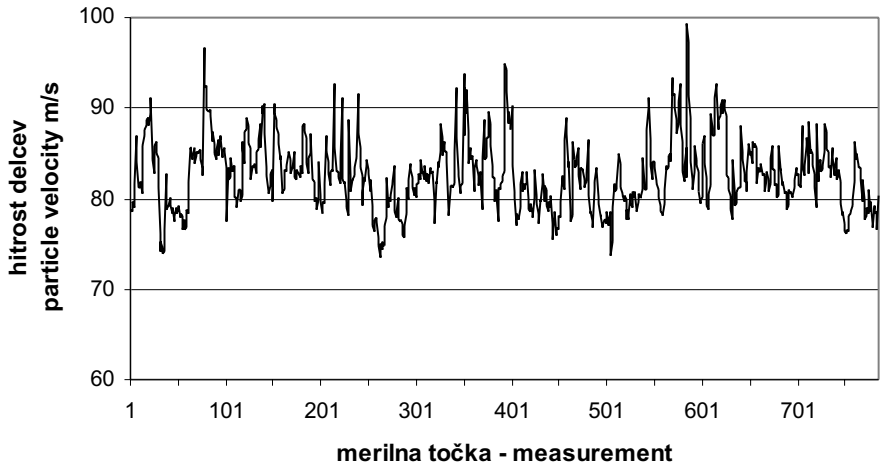

Sl. 11. *Diagram izračunanih hitrosti v merilnih točkah 1 do 800*
Fig. 11. *Diagram of calculated particle velocities of measurements 1 to 800*

signala (padec napetosti – slika 10), ki jih povzročajo udarci peska ob membrano zaznavala, smo časovni premik med udarci v prvo in drugo zaznavalo določili na podlagi časovnih razlik med lokalnimi doli obeh filtriranih signalov. Časovni premik smo nato uporabili v izrazu (2) in izračunali hitrost potovanja zrnc peska med zaznavali 1 in 2. Končni rezultat obdelave obeh signalov v območju dolžine 2 s prikazuje slika 11. Razvidno je, da je raztros hitrosti precej velik. Povprečna vrednost izračunane hitrosti je 82,6 m/s, standardna deviacija pa znaša 3,87 m/s. Zaradi velikega števila meritev je standardna merilna negotovost majhna in je 0,15 m/s. V primerjavi z izmerjeno hitrostjo z mehanskim merilnikom je hitrost večja za 11% (8,2 m/s). Enako velike razlike so se pokazale tudi pri meritvah drugih turbin, ki se od obravnavane razlikujejo po obliki in številu lopatic. Zato lahko sklepamo, da na nastanek teh razlik ne vpliva netočnost merilne metode, pač pa so posledica različne zasnove obeh merilnikov. Mehanski merilnik izmeri srednjo hitrost zrnc, medtem ko v primeru mikrofonskega merilnika izmerimo hitrost najhitrejših delcev, ki prvi udarijo ob membrano in povzročijo njeno nihanje in s tem naglo spremembo signala. Poskusili smo najti tudi pojasnilo za velik raztros izmerjenih hitrosti. Nanj gotovo vpliva različna zrnavost peska (∅ = 0,05 do 1 mm), kar povzroča različno intenzivne udarce ob membrano zaznavala s tem pa bolj in manj izrazite spremembe osnovnega signala in premik lokalnih dolov v filtriranem signalu. Dodatno prinese k večjemu raztrosu tudi neubrano delovanje turbine, ki je posledica nenatančnosti pri izdelavi (litju) ležišč lopatic v rotorju, montaže lopatic in predvsem različne obrabe lopatic. Da bi določili stopnjo neubranosti, smo analizirali filtriran signal s prvega zaznavala. Ugotavljali smo dolžino premika med zaporednimi udarci ob membrano. Vsaki od osmih lopatic smo poiskali zakasnitev glede na prejšnjo lopatico. To smo naredili tako, da smo matriko, ki je vsebovala

second sensor can, therefore, be determined from the local phase between both filtered signals. This time interval is then used in equation (2), and the particle velocity between the sensors S1 and S2 is calculated. The final result of processing a 2-seconds period of the raw signals is shown in Fig. 11. Velocity scatter is relatively high. The average particle velocity is 82.6 m/s and the RMS (Root Mean Square) is 3.87 m/s. The standard measurement uncertainty is 0.15 m/s. This value is low due to the large number of measurements. The average measured velocity is 8.2 m/s, i.e. 11 % higher than the particle velocity measured by the mechanical device. It is interesting that similar differences were observed for other turbines as well, although they have different designs and a different number and curvature of blades. It may be assumed, therefore, that this difference is not the result of a measurement error, but is conditioned by the different measurement approaches applied in both velocity measurement methods. The average particle velocity is measured by a mechanical device, whilst the maximum particle speed is measured by an electronic system that reacts to the first hit of the membranes caused by the fastest particles. An explanation for the high velocity scatter was also found. The composition of shotblasting particles is not uniform. The particle diameter may vary from 0.05 mm to 1 mm. This causes a very high variation in the particle's impact force intensity and, therefore, causes less distinctive magnitude changes in the measured signal and some phase shift of the filtered signal. The next reason for the large scatter of the measured velocities is a poorly tuned, prototype turbine. This is primarily due to different degrees of turbine-blade wear and non-optimised matching of the cast blades with the grooves of the cast rotor ring. An attempt was made, therefore, to establish the degree of non-tunableness in the shotblasting turbine's operation. The filtered signal from the first sensor was analysed. The time delays between the successive membrane hits were determined first. The results were then split into eight rows, each of them corresponds

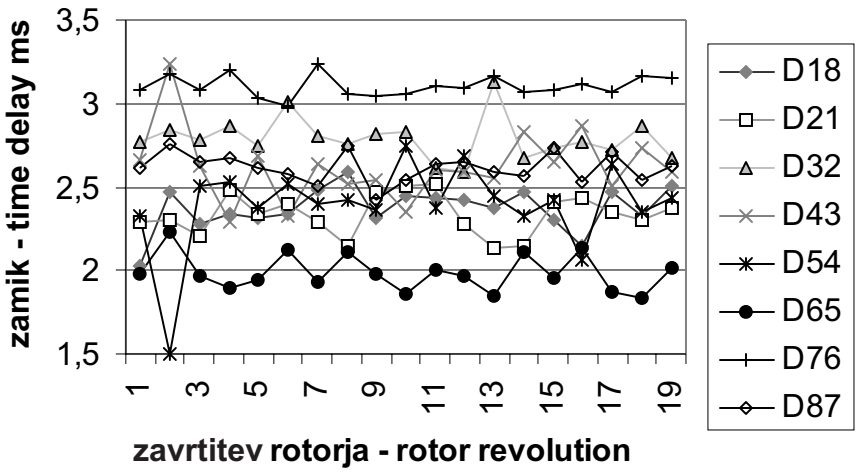

Fig. 12. *Time delays between the particle ejection from individual blades*

zakasnitve med udarci v prvi mikrofon, razdelili na 8 stolpcev. Rezultat prikazuje slika 12. Opazimo, da je povprečna dolžina premika 2,53 ms, kar dobro ustreza frekvenci vzbujanja 400 Hz. Močno izstopata krivulji Δ65 in Δ76. To pomeni da, izmetavanje peska z lopatice 6 prehiteva, zaradi česar se skrajša korak med udarci z lopatic 5 in 6 ter podaljša korak med udarci z lopatic 6 in 7. Podobno, vendar precej manj, odstopata tudi krivulji Δ12 in Δ32, kar kaže na prehitevanje izmetavanja peska z lopatice 2. Ugotovitve, ki smo jih dobili z analizo signala, so se potrdile pri pregledu rotorja. Izkazalo se je, da je obraba dveh simetrično postavljenih lopatic precej večja od obrabe preostalih lopatic. Povečana obraba je bila posledica različnih materialov, iz katerih so bile preskusno izdelane lopatice v prototipni turbini.

4 SKLEPI

V prispevku sta prikazana dva merilnika, ki omogočata merjenje hitrosti delcev v stroju za peskanje. Merilnik z rotirajočima ploščama je robusten in omogoča merjenje hitrosti delcev le v majhnem številu točk. Njegova največja prednost je, da potrebuje malo dodatne opreme (usmernik, merilnik frekvence), pomanjkljivost pa, da zaradi svojih izmer in teže ni primeren za merjenje hitrostnega profila. Elektronski merilnik je primernejši za merjenje hitrosti v večjem številu točk. Njegova prednost so predvsem manjše izmere in teža zaznavalskega dela, kar omogoča premikanje po merilni ravnini pa tudi po kotu. Dodatna prednost elektronskega merilnika je, da lahko analiziramo delovanje turbine in v določeni meri sklepamo tudi o obrabi lopatic in drugih nepravilnostih. Povzamemo torej lahko, da je elektronsko zaznavalo perspektivnejše, verjetno pa se bo zaradi primerjave rezultatov še nekaj časa uporabljalo hkrati z mehanskim merilnikom.

Obstaja kar nekaj možnosti za izboljšave, predvsem pri elektronskem merilniku. Z optimiranjem

to one of eight turbine blades and represents the time delay between the particles' ejection of the observed blade and its forerunner blade. The results are shown in Figure 12. The average delay is 2.53 ms and corresponds well to the excitation frequency of 400 Hz. Curves Δ65 and Δ76 deviate the most from the average level. Blade 6 ejects the particles too soon, and the delay between the ejection of blades 5 and 6 is reduced. On the other hand, the delay between the ejection of blades 6 and 7 is increased. The similar, but less distinctive, deviation can be observed for curves Δ21 and Δ32, and shows evidence of blade 2 malfunctioning. These findings were confirmed by an inspection of the rotor. It was found that two of the symmetrically mounted blades were worn out much more than the other six blades, which are made from a different, more abrasion-resistant, alloy.

4 CONCLUSIONS

This paper presents two different methods for particle velocity measurement in a shotblasting machine. The mechanical device with two rotating disks is robust and can only be applied for velocity measurements in a few locations within a testing chamber. Its advantage over the electronic system is that almost no extra equipment is necessary except a rotational speed controller and an electronic tachometer. Its main disadvantage is the lack of mobility. It cannot, therefore, be used for the velocity profile measurements of a particle stream. Measurements using the electronic system can be performed in almost any location within a testing chamber. Its sensors are small and light and can be easily positioned in a measuring plane and inclined at a specified angle. Its additional advantage over the mechanical measuring device is that it can be used to analyse the operation of the turbine and make conclusions about turbine-blade wear and other similar malfunctions.

There are still some possible modifications for the electronic system. The construction of the micro-

konstrukcije mikrofonskega zaznavala (debelina jeklene membrane, vpetje membrane, dušenje motenj) lahko povečamo občutljivost elektronskega merilnika in se v idealnem primeru izognemo uporabi filtrov, kar bi zelo poenostavilo algoritem za štetje udarcev in izračun hitrosti, s tem pa tudi povečalo točnost rezultatov.

phone sensor can be optimised (membrane thickness, membrane support, disturbances damping) for higher sensitivity of the sensor. In an ideal case, signal filtering would be unnecessary. This would simplify the algorithm for the signal analysing and particle velocity calculation, and the accuracy of the algorithm would also increase.

5 LITERATURA
5 REFERENCES

[1] Marinković, J. (1950) Unutrašnja balistika, *Izdavačko poduzeće Narodne republike Srbije*, Beograd.
[2] Jamakawa, M., S. Isshiki, J. Lee, K. Nishida (2001) 3-D PIV analysis of structural behavior of D.I: gasoline spray, *SAE Paper* 2001-01-3669.
[3] Merjenje zvoka in oktavna analiza, National Instruments, *NI DAN 1999*, Ljubljana.
[4] Cooley, J.W., J.W. Tukey (1965) An algorithm for the machine calculation of complex Fourier series, *Mathematics of Computation*, vol. 19, 297-301.
[5] LabVIEW Measurements manual, *National Instruments*, 2000.

Naslova avtorjev: dr. Aleš Hribernik
mag. Gorazd Bombek
Univerza v Mariboru
Fakulteta za strojništvo
Smetanova 17
2000 Maribor
ales.hribernik@uni-mb.si
gorazd.bombek@uni-mb.si

Ivan Markočič
Gostol-TST
Tolmin

Author's Addresses: Dr. Aleš Hribernik
Mag. Gorazd Bombek
Faculty of Mechanical Eng.
University of Maribor
Smetanova 17
2000 Maribor, Slovenia
ales.hribernik@uni-mb.si
gorazd.bombek@uni-mb.si

Ivan Markočič
Gostol-TST
Tolmin

Prejeto: 20.12.2002
Received:

Sprejeto: 31.1.2003
Accepted:

Strokovna literatura
Professional Literature

Ocene knjig

Klaus-Jürgen Matthes/Erhardt Richter: Schweisstechnik

Zal.: Fachbuchverlag Leipzig, Carl Hanser Verlag, München, Wien.
Obseg: format 17 × 24 cm, 471 strani, 508 slik, 130 preglednic, 164 lit.pod.

V predloženi knjigi sta urednika v dvanajstih poglavjih podala izčrpen pregled današnjega stanja v varilni tehniki kovinskih materialov. Posamezna poglavja je obdelalo pet različnih avtorjev, ki pa pri delu niso bili najbolje usklajeni. To se kaže tako pri različnih ravneh strokovnih razlag kakor tudi pri neuravnoteženem obsegu, ki ga obsegajo nekatera poglavja. Kratek pregled vsebine posameznih poglavij.

1. Osnove z razmejitvijo izdelovalnih tehnik po standardih DIN 8580 in načelno shemo razmejitve varilnih postopkov po standardu DIN 1910.

2. Varivost z osnovnimi kriteriji, ki odločajo o primernosti osnovnega in dodajnega materiala ter vrste zvarnih spojev na izbiro varilnega postopka in varilnih parametrov.

3. Obločni postopki varjenja so podani izredno temeljito in obenem pregledno. Ob opisu fizikalnih osnov obločnega varjenja, pregledu osnovnih vrst izvorov varilnega toka in ob predstavitvi najpogostejših načinov obločnega varjenja je zbrana še obilica tehnoloških napotkov.

4. Plamenska tehnika je predstavljena s podrobno razlago značilnosti kisik-acetilenskega plamena, opisom osnovne, dodatne in pomožne opreme, ki jo uporabljajo pri tej tehniki varjenja in z obilico koristnih tehnoloških napotkov, ki jih zlepa ne najdemo v novejših učbenikih podobne vsebine.

5. Postopki uporovnega varjenja so glede na pomen in obseg uporabe teh postopkov v današnji industrijski praksi ter v primerjavi z obsegom predstavljenih vsebin prejšnjih poglavij, predstavljeni izredno skopo.

6. Indukcijsko varjenje je predstavljeno na vsega treh straneh, podobno skopo kakor pred tem postopki uporovnega varjenja.

7. Varjenje z velikimi gostotami energije, predstavljata varjenje z elektronskim snopom in lasersko varjenje. Za oba varilna postopka so podane fizikalne osnovne tehnične značilnosti in prikazani so posnetki neposredne uporabe naprav in izvedenih zvarov.

8. Postopki varjenja s kinetično energijo so zastopani z opisom različnih načinov varjenja: s trenjem, ultrazvočno varjenje, varjenje v hladnem s stiskanjem in eksplozijsko varjenje.

9. Varjenje s stiskanjem prek togega telesa, ki je ali ni dodatno ogrevano. Gre za opis različnih načinov mikro varjenja, ki jih uporabljajo predvsem v elektroindustriji.

10. Alumoterično varjenje je avtor razmejil na talilno varjenje in varjenje s stiskanjem, oboje pa podkrepil s skromno razlago in preprostimi skicami mogočih izvedb.

11. Difuzijsko varjenje je predstavljeno s preprosto skico, ponazorjenim varilnim krogom, tremi različnimi izvedbami spojev in z razlago osnovnih značilnosti tega postopka varjenja.

12. Navarjanje je predstavljeno s podrobno razlago tehnoloških posebnosti, ki so odvisne od namena, obsega in števila izvedb, vrste osnovnega in dodajnega materiala ter izbranega varilnega postopka.

V trinajstem poglavju je podan pregled uporabljene literature, ločeno za posamezne tehnike varjenja, na koncu je še stvarno kazalo, ki je označeno kot štirinajsto poglavje.

Knjigo bodo s pridom uporabljali tehnologi in konstrukterji v industrijski praksi ter študentje univerzitetnega in visokega strokovnega študija, če jim le nemščina ni povsem tuj jezik.

I. Polajnar

Osebne vesti
Personal Events

Doktorati, magisteriji, diplome

DOKTORATI

Na Fakulteti za strojništvo Univerze v Ljubljani so z uspehom zagovarjali svoje doktorske disertacije, in sicer:

dne 16. decembra 2002: **mag. Franc Cimerman**, z naslovom: "Odzivnost dotikalnih temperaturnih zaznaval";

dne 17. decembra 2002: **mag. Jure Knez,** z naslovom: "Zanesljivost delovanja strojev na osnovi meritev vibracij";

dne 20. decembra 2002: **mag. Primož Rus,** z naslovom: "Paralelno reševanje fizikalno sklopljenih sistemov" in **mag. Ted Prodan**, z naslovom: "Vpliv hidrostatičnega tlaka in temperature na strižni modul časovno odvisnih materialov".

Na Fakulteti za strojništvo Univerze v Mariboru je z uspehom zagovarjal svojo doktorsko disertacijo, in sicer:

dne 16. decembra 2002: **mag. Gorazd Lojen**, z naslovom: "Sinteza tiksotropnih mešanic".

S tem so navedeni kandidati dosegli akademsko stopnjo doktorja tehničnih znanosti.

MAGISTERIJI

Na Fakulteti za strojništvo Univerze v Ljubljani so z uspehom zagovarjali svoja magistrska dela, in sicer:

dne 3. decembra 2002: **Matej Supej**, z naslovom: "Povezava prostega volumna z mehanskimi lastnostmi viskoelastičnih materialov";

dne 23. decembra 2002: **Damjan Klobčar**, z naslovom: "Matematično modeliranje navarjanja" in **Robert Ivančič**, z naslovom: "Reparaturno varjenje orodij".

Na Fakulteti za strojništvo Univerze v Mariboru je *dne 6. decembra 2002* **Simon Kovačič** z uspehom zagovarjal svoje magistrsko delo z naslovom: "Model razširitve CNC krmilnika za posebne postopke frezanja zahtevnih oblik".

S tem so navedeni kandidati dosegli akademsko stopnjo magistra tehničnih znanosti.

DIPLOMIRALI SO

Na Fakulteti za strojništvo Univerze v Ljubljani so pridobili naziv univerzitetni diplomirani inženir strojništva:

dne 19. decembra 2002: Boštjan JARC, Aljoša ROŽMAN, Jože JENKOLE, Dalibor PERUŠKO.

Na Fakulteti za strojništvo Univerze v Mariboru so pridobili naziv univerzitetni diplomirani inženir strojništva:

dne 19. decembra 2002: Tomaž ČERNEC, Bojan GOJKOŠEK, Davorin RIŽNAR.

*

Na Fakulteti za strojništvo Univerze v Ljubljani so pridobili naziv diplomirani inženir strojništva:

dne 12. decembra 2002: Rober AVSENIK, Peter BOSCAROL, Simon KRANJC, Damjan MIHALIČ, Robert ŠPERNJAK, Ivan UMEK;

dne 13. decembra 2002: Andrej BENSA, Tomaž KALAN, Borut KUTNJAK, Viktor ROJŠEK, Anže ROVANŠEK, Miha TRČEK;

dne 16. decembra 2002: Sebastjan BOGATAJ, Domen KLEMENC, Tadej NADRIH, Anton PERC.

Na Fakulteti za strojništvo Univerze v Mariboru so pridobili naziv diplomirani inženir strojništva:

dne 19. decembra 2002: Boštjan CAFUTA, Leon GAJSER, Matej KUHAR, Milan KUŠER, Janko PLAJNŠEK, Marjan REJC, Simon VRŠIČ.

© Strojniški vestnik 48(2002)12,721
Mesečnik
ISSN 0039-2480

© Journal of Mechanical Engineering 48(2002)12,721
Published monthly
ISSN 0039-2480

Recenzenti letnika 2002

Reviewers of 2002 Volume

Tuji recenzenti / International reviewers:
prof. dr. Francesco d'Auria, University of Pisa
prof. dr. Ivan Catton, University of California
prof. dr. Adolf Frank, TU Graz
prof. dr. Bernard Franković, University of Rijeka
prof. dr. Glenn R. Heppler, University of Waterloo
prof. dr. Roman Klasinc, TU Graz
prof. dr. Heinz-Bernd Matthias, TU Wien
doc. dr. Klaus J. Michaelis, TU München
prof. dr. Herbert Schulz, TU Darmstadt
prof. dr. Božo Vranješ, FSB Zagreb
prof. dr. Paul White, University of Southampton
prof. dr. Luiz C. Wrobel, Brunel University
prof. dr. Felix Ziegler, TU Berlin

Domači recenzenti / National reviewers:
prof. dr. Andro Alujevič
prof. dr. Ivan Anžel
prof. dr. Jože Balič
doc. dr. Anton Bergant
prof. dr. Ivan Bratko
prof. dr. Franci Čuš
prof. dr. Matija Fajdiga
doc. dr. Karl Gotlih
dr. Jože Jurkovič
doc. dr. Zoran Kariž
doc. dr. Breda Kegl
prof. dr. Janez Kopač
dr. Mitja Kožuh
prof. dr. Jurij Krope
prof. dr. Milan Marčič
prof. dr. Jure Marn
prof. dr. Dragica Noe
prof. dr. Peter Novak
prof. dr. Andrej Polajnar
prof. dr. Ivan Prebil
doc. dr. Andrej Predin
prof. dr. Rudolf Pušenjak
dr. Zlatko Rek
prof. dr. Marko Starbek
mag. Jože Stropnik
prof. dr. Leopold Škerget
prof. dr. Matija Tuma
prof. dr. Iztok Žun

© Strojniški vestnik 48(2002)12, 722-724
Mesečnik
ISSN 0039-2480

© Journal of Mechanical Engineering 48(2002)12, 722-724
Published monthly
ISSN 0039-2480

Vsebina 2002
Contents 2002

Uvodnik

Razprave

Editorial

Papers

Navodila avtorjem
Instructions for Authors

Članki morajo vsebovati:
- naslov, povzetek, besedilo članka in podnaslove slik v slovenskem in angleškem jeziku,
- dvojezične preglednice in slike (diagrami, risbe ali fotografije),
- seznam literature in
- podatke o avtorjih.

Strojniški vestnik izhaja od leta 1992 v dveh jezikih, tj. v slovenščini in angleščini, zato je obvezen prevod v angleščino. Obe besedili morata biti strokovno in jezikovno med seboj usklajeni. Članki naj bodo kratki in naj obsegajo približno 8 tipkanih strani. Izjemoma so strokovni članki, na željo avtorja, lahko tudi samo v slovenščini, vsebovati pa morajo angleški povzetek.

Vsebina članka

Članek naj bo napisan v naslednji obliki:
- Naslov, ki primerno opisuje vsebino članka.
- Povzetek, ki naj bo skrajšana oblika članka in naj ne presega 250 besed. Povzetek mora vsebovati osnove, jedro in cilje raziskave, uporabljeno metodologijo dela,povzetek rezulatov in osnovne sklepe.
- Uvod, v katerem naj bo pregled novejšega stanja in zadostne informacije za razumevanje ter pregled rezultatov dela, predstavljenih v članku.
- Teorija.
- Eksperimentalni del, ki naj vsebuje podatke o postavitvi preskusa in metode, uporabljene pri pridobitvi rezultatov.
- Rezultati, ki naj bodo jasno prikazani, po potrebi v obliki slik in preglednic.
- Razprava, v kateri naj bodo prikazane povezave in posplošitve, uporabljene za pridobitev rezultatov. Prikazana naj bo tudi pomembnost rezultatov in primerjava s poprej objavljenimi deli. (Zaradi narave posameznih raziskav so lahko rezultati in razprava, za jasnost in preprostejše bralčevo razumevanje, združeni v eno poglavje.)
- Sklepi, v katerih naj bo prikazan en ali več sklepov, ki izhajajo iz rezultatov in razprave.
- Literatura, ki mora biti v besedilu oštevilčena zaporedno in označena z oglatimi oklepaji [1] ter na koncu članka zbrana v seznamu literature. Vse opombe naj bodo označene z uporabo dvignjene številke[1].

Oblika članka

Besedilo naj bo pisano na listih formata A4, z dvojnim presledkom med vrstami in s 3 cm širokim robom, da je dovolj prostora za popravke lektorjev. Najbolje je, da pripravite besedilo v urejevalnilku Microsoft Word. Hkrati dostavite odtis članka na papirju, vključno z vsemi slikami in preglednicami ter identično kopijo v elektronski obliki.

Prosimo, da ne uporabljate urejevalnika LaTeX, saj program, s katerim pripravljamo Strojniški vestnik, ne uporablja njegovega formata. V urejevalniku LaTeX oblikujte grafe, preglednice in enačbe in jih stiskajte na kakovostnem laserskem tiskalniku, da jih bomo lahko presneli.

Enačbe naj bodo v besedilu postavljene v ločene vrstice in na desnem robu označene s tekočo številko v okroglih oklepajih

Enote in okrajšave

V besedilu, preglednicah in slikah uporabljajte le standardne označbe in okrajšave SI. Simbole fizikalnih veličin v besedilu pišite poševno (kurzivno), (npr. *v, T, n* itn.). Simbole enot, ki sestojijo iz črk, pa pokončno (npr. ms^{-1}, K, min, mm itn.).

Vse okrajšave naj bodo, ko se prvič pojavijo, napisane v celoti v slovenskem jeziku, npr. časovno spremenljiva geometrija (ČSG).

Papers submitted for publication should comprise:
- Title, Abstract, Main Body of Text and Figure Captions in Slovene and English,
- Bilingual Tables and Figures (graphs, drawings or photographs),
- List of references and
- Information about the authors.

Since 1992, the Journal of Mechanical Engineering has been published bilingually, in Slovenian and English. The two texts must be compatible both in terms of technical content and language. Papers should be as short as possible and should on average comprise 8 typed pages. In exceptional cases, at the request of the authors, speciality papers may be written only in Slovene, but must include an English abstract.

The format of the paper

The paper should be written in the following format:
- A Title, which adequately describes the content of the paper.
- An Abstract, which should be viewed as a miniversion of the paper and should not exceed 250 words. The Abstract should state the principal objectives and the scope of the investigation, the methodology employed, summarize the results and state the principal conclusions.
- An Introduction, which should provide a review of recent literature and sufficient background information to allow the results of the paper to be understood and evaluated.
- A Theory
- An Experimental section, which should provide details of the experimental set-up and the methods used for obtaining the results.
- A Results section, which should clearly and concisely present the data using figures and tables where appropriate.
- A Discussion section, which should describe the relationships and generalisations shown by the results and discuss the significance of the results making comparisons with previously published work. (Because of the nature of some studies it may be appropriate to combine the Results and Discussion sections into a single section to improve the clarity and make it easier for the reader.)
- Conclusions, which should present one or more conclusions that have been drawn from the results and subsequent discussion.
- References, which must be numbered consecutively in the text using square brackets [1] and collected together in a reference list at the end of the paper. Any footnotes should be indicated by the use of a superscript[1].

The layout of the text

Texts should be written in A4 format, with double spacing and margins of 3 cm to provide editors with space to write in their corrections. Microsoft Word for Windows is the preferred format for submission. One hard copy, including all figures, tables and illustrations and an identical electronic version of the manuscript must be submitted simultaneously.

Please do not use a LaTeX text editor, since this is not compatible with the publishing procedure of the Journal of Mechanical Engineering. Graphs, tables and equations in LaTeX may be supplied in good quality hard-copy format, so that they can be copied for inclusion in the Journal.

Equations should be on a separate line in the main body of the text and marked on the right-hand side of the page with numbers in round brackets.

Units and abbreviations

Only standard SI symbols and abbreviations should be used in the text, tables and figures. Symbols for physical quantities in the text should be written in Italics (e.g. *v, T, n,* etc.). Symbols for units that consist of letters should be in plain text (e.g. ms^{-1}, K, min, mm, etc.).

All abbreviations should be spelt out in full on first appearance, e.g., variable time geometry (VTG).

Slike

Slike morajo biti zaporedno oštevilčene in označene, v besedilu in podnaslovu, kot sl. 1, sl. 2 itn. Posnete naj bodo v kateremkoli od razširjenih formatov, npr. BMP, JPG, GIF. Za pripravo diagramov in risb priporočamo CDR format (CorelDraw), saj so slike v njem vektorske in jih lahko pri končni obdelavi preprosto povečujemo ali pomanjšujemo.

Pri označevanju osi v diagramih, kadar je le mogoče, uporabite označbe veličin (npr. *t, v, m* itn.), da ni potrebno dvojezično označevanje. V diagramih z več krivuljami, mora biti vsaka krivulja označena. Pomen oznake mora biti pojasnjen v podnapisu slike.

Vse označbe na slikah morajo biti dvojezične.

Za vse slike po fotografskih posnetkih je treba priložiti izvirne fotografije ali kakovostno narejen posnetek. V izjemnih primerih so lahko slike tudi barvne.

Preglednice

Preglednice morajo biti zaporedno oštevilčene in označene, v besedilu in podnaslovu, kot preglednica 1, preglednica 2 itn. V preglednicah ne uporabljajte izpisanih imen veličin, ampak samo ustrezne simbole, da se izognemo dvojezični podvojitvi imen. K fizikalnim veličinam, npr. *t* (pisano poševno), pripišite enote (pisano pokončno) v novo vrsto brez oklepajev.

Vsi podnaslovi preglednic morajo biti dvojezični.

Seznam literature

Vsa literatura mora biti navedena v seznamu na koncu članka v prikazani obliki po vrsti za revije, zbornike in knjige:

[1] Tarng, Y.S., Y.S. Wang (1994) A new adaptive controler for constant turning force. *Int J Adv Manuf Technol* 9(1994) London, pp. 211-216.

[2] Čuš, F., J. Balič (1996) Rationale Gestaltung der organisatorischen Abläufe im Werkzeugwesen. *Proceedings of International Conference on Computer Integration Manufacturing,* Zakopane, 14.-17. maj 1996.

[3] Oertli, P.C. (1977) Praktische Wirtschaftskybernetik. *Carl Hanser Verlag,* München.

Podatki o avtorjih

Članku priložite tudi podatke o avtorjih: imena, nazive, popolne poštne naslove, številke telefona in faksa ter naslove elektronske pošte.

Sprejem člankov in avtorske pravice

Uredništvo Strojniškega vestnika si pridržuje pravico do odločanja o sprejemu članka za objavo, strokovno oceno recenzentov in morebitnem predlogu za krajšanje ali izpopolnitev ter terminološke in jezikovne korekture.

Avtor mora predložiti pisno izjavo, da je besedilo njegovo izvirno delo in ni bilo v dani obliki še nikjer objavljeno. Z objavo preidejo avtorske pravice na Strojniški vestnik. Pri morebitnih kasnejših objavah mora biti SV naveden kot vir.

Rokopisi člankov ostanejo v arhivu SV.

Vsa nadaljnja pojasnila daje:

Uredništvo
STROJNIŠKEGA VESTNIKA
p.p. 197/IV
1001 Ljubljana
Telefon: (01) 4771-757
Telefaks: (01) 2518-567
E-mail: strojniski.vestnik@fs.uni-lj.si

Figures

Figures must be cited in consecutive numerical order in the text and referred to in both the text and the caption as Fig. 1, Fig. 2, etc. Figures may be saved in any common format, e.g. BMP, GIF, JPG. However, the use of CDR format (CorelDraw) is recommended for graphs and line drawings, since vector images can be easily reduced or enlarged during final processing of the paper.

When labelling axes, physical quantities, e.g. *t, v, m,* etc. should be used whenever possible to minimise the need to label the axes in two languages. Multi-curve graphs should have individual curves marked with a symbol, the meaning of the symbol should be explained in the figure caption.

All figure captions must be bilingual.

Good quality black-and-white photographs or scanned images should be supplied for illustrations. In certain circumstances, colour figures may be considered.

Tables

Tables must be cited in consecutive numerical order in the text and referred to in both the text and the caption as Table 1, Table 2, etc. The use of names for quantities in tables should be avoided if possible: corresponding symbols are preferred to minimise the need to use both Slovenian and English names. In addition to the physical quantity, e.g. *t* (in Italics), units (normal text), should be added in new line without brackets.

All table captions must be bilingual.

The list of references

References should be collected at the end of the paper in the following styles for journals, proceedings and books, respectively:

[1] Tarng, Y.S., Y.S. Wang (1994) A new adaptive controler for constant turning force. *Int J Adv Manuf Technol* 9(1994) London, pp. 211-216.

[2] Čuš, F., J. Balič (1996) Rationale Gestaltung der organisatorischen Abläufe im Werkzeugwesen. *Proceedings of International Conference on Computer Integration Manufacturing,* Zakopane, 14.-17. maj 1996.

[3] Oertli, P.C. (1977) Praktische Wirtschaftskybernetik. *Carl Hanser Verlag,* München.

Author information

The following information about the authors should be enclosed with the paper: names, complete postal addresses, telephone and fax numbers and E-mail addresses.

Acceptance of papers and copyright

The Editorial Committee of the Journal of Mechanical Engineering reserves the right to decide whether a paper is acceptable for publication, obtain professional reviews for submitted papers, and if necessary, require changes to the content, length or language.

Authors must also enclose a written statement that the paper is original unpublished work, and not under consideration for publication elsewhere. On publication, copyright for the paper shall pass to the Journal of Mechanical Engineering. The JME must be stated as a source in all later publications.

Papers will be kept in the archives of the JME.

You can obtain further information from:

Editorial Board of the
JOURNAL OF MECHANICAL ENGINEERING
P.O.Box 197/IV
1001 Ljubljana, Slovenia
Telephone: +386 (0)1 4771-757
Fax: +386 (0)1 2518-567
E-mail: strojniski.vestnik@fs.uni-lj.si